Energy Storage Materials 79 (2025) 104295

Contents lists available at ScienceDirect

Energy Storage Materials

journal homepage: www.elsevier.com/locate/ensm

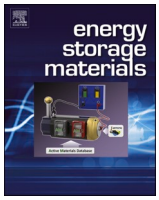

High-Entropy Approach *vs.* Traditional Doping Strategy for Layered Oxide Cathodes in Alkali-Metal-Ion Batteries: A Comparative Study

Yanjiao Ma [a,1,*], Han Du [a,1], Siyuan Zheng [a,1], Zihao Zhou [a], Hehe Zhang [a], Yuan Ma [b,*], Stefano Passerini [c,d,e,*], Yuping Wu [b,*]

[a] School of Energy and Mechanical Engineering, Nanjing Normal University, Nanjing 210023, China
[b] Confucius Energy Storage Lab, Key Laboratory of Energy Thermal Conversion and Control of Ministry of Education, School of Energy and Environment & Z Energy Storage Center, Southeast University, Nanjing 211189, Jiangsu, China
[c] Helmholtz Institute Ulm (HIU), Helmholtzstrasse 11, 89081 Ulm, Germany
[d] Karlsruhe Institute of Technology (KIT), 76021 Karlsruhe, Germany
[e] Austrian Institute of Technology (AIT) Transportation Technologies, Giefinggasse 4, 1210 Wien, Austria

ARTICLE INFO

Keywords:
Cathode materials
Layered oxides
Doping strategy
High-entropy approach

ABSTRACT

The traditional doping strategy has emerged as an effective method for addressing challenges such as irreversible phase transitions and poor cycling stability in transition metal layered oxides (TMLOs), making them promising cathode materials for alkali-ion batteries (AIBs). Recently, high-entropy approaches, a new class of modification strategies, have been gaining increasing attention. While these two methods – doping strategy and high-entropy – demonstrate some similarities, they also exhibit distinct differences. However, a systematic review of these approaches has not been performed yet, and their unique electrochemical outcomes are often confused. Herein, we present a comparative analysis and systematic discussion of the traditional doping strategy and the innovative high-entropy approaches. Using layered oxide cathodes as specific examples, we initially explore the effects of single-atom doping at various sites and the synergistic effects of multi-atom doping. Subsequently, we highlight five unique effects of materials modified through the high-entropy approaches: structure stabilization, high disorder characteristics, the entropy extension effect, cocktail effect and entropy-enhanced local regulation. These properties significantly enhance battery cycling performance, distinguishing the high-entropy method from the conventional doping. We also summarized its application in AIBs. Finally, a summary and outlook are provided, offering insights for the design and optimization of next-generation layered oxide cathode materials.

1. Introduction

With the growing adoption of electrical energy storage technologies, the development of a new generation of rechargeable batteries that are cost-efficient, possess high capacity, and offer long cycle life is of utmost importance. Advancing efficient cathode materials is crucial for the successful commercialization of secondary batteries. To date, researchers have explored a diverse array of cathode materials, including transition metal oxides,[1–6] poly-anionic compounds,[7–10] Prussian blue analogues,[11–16] and organic compounds [17–19]. Transition metal layered oxides (TMLOs) are considered very promising cathodes due to their high theoretical capacity, high working voltage and simplicity of synthesis [20–28].

Although TMLOs show great potential in alkali-metal-ion batteries (AIBs),[29–31] they suffer from two significant drawbacks. Firstly, the large ionic radii of alkali metal ions (Li^+, Na^+, K^+) cause transition metal layer slippage and substantial volume expansion/contraction during intercalation and deintercalation processes. This often leads to a series of phase transitions and even structural collapse. Additionally, TMLOs have poor air stability and may react with moisture in the air, resulting in performance degradation [30,32,33]. To address these issues, researchers typically modify TMLOs through doping strategy [34–40]. This involves doping heterogeneous elements into the transition metal (TM) layer, alkali metal (AM) layer, or oxygen (O) layer to achieve better structural stability. The doping strategy is also widely recognized as an essential method for improving the electrochemical performance

* Corresponding authors.
E-mail addresses: yanjiao.ma@njnu.edu.cn (Y. Ma), yuan.ma@seu.edu.cn (Y. Ma), stefano.passerini@ait.ac.at (S. Passerini), wuyp@seu.edu.cn (Y. Wu).
[1] These authors contributed equally to this work.

https://doi.org/10.1016/j.ensm.2025.104295
Received 23 February 2025; Received in revised form 2 April 2025; Accepted 29 April 2025
Available online 2 May 2025

of these cathode materials.

In recent years, a modification strategy known as the high-entropy, which involves the mixing of five or more elements within a crystal, has garnered significant attention from researchers [41–44]. The resulting multi-component layered cathodes offer superior performance compared to traditional materials due to their extensive compositional space [45]. With the emergence of high-performance high-entropy transition metal layered oxides (HE-TMLOs), high-entropy doping and entropy-tuning approaches are becoming effective strategies to reduce the inherent defects of TMLOs. In sodium-ion batteries (SIBs), Hu's team [46] synthesized high-entropy O3-$NaNi_{0.12}Cu_{0.12}Mg_{0.12}Fe_{0.15}Co_{0.15}Mn_{0.1}Ti_{0.1}Sn_{0.1}Sb_{0.04}O_2$, containing nine TM elements, achieving extended cycling stability and excellent rate performance. In lithium-ion batteries (LIBs), Xin's team [47] developed a zero-strain zero-cobalt layered cathode, $LiNi_{0.8}Mn_{0.13}Ti_{0.02}Mg_{0.02}Nb_{0.01}Mo_{0.02}O_2$, through the high-entropy doping. This Co-free, high-nickel material with inherent "zero strain" showcases significant commercialization potential. In potassium-ion batteries (PIBs), Lu's team [44] tuned the entropy of manganese-based layered oxides by varying the composition of the cathode materials. They synthesized a series of $K_{0.45}Mn_xCo_{(1-x)/4}Mg_{(1-x)/4}Cu_{(1-x)/4}Ti_{(1-x)/4}O_2$ (where x = 0.8, 0.6, and 0.4). The entropy-tuned $K_{0.45}Mn_{0.6}Co_{0.1}Mg_{0.1}Cu_{0.1}Ti_{0.1}O_2$ achieved high K^+ ion transport rates while mitigating the Jahn-Teller distortion of Mn^{3+} and reducing volumetric changes. They proposed universal high-entropy approaches, offering a novel solution for developing next-generation TMLOs cathode materials with high stability, high capacity, and low cost.

The emerging high-entropy approaches offer advantages over traditional doping strategies by simultaneously harnessing the benefits of both entropy tuning and doping effects [48–50]. While considering the influence of element doping, attention is also focused on the effect of entropy increasing on performance. By concurrently doping multiple elements into the materials, these elements can partially mimic the effects observed with single-element doping and exploit synergistic interactions among multiple elements to improve the performance of positive electrode materials through entropy tuning. The introduction of multiple elements increases configurational entropy within the lattice, lowers Gibbs free energy, and allows for diverse crystal structural changes, alterations in ion surroundings, and electron structure modifications [51,52]. This comprehensive modification of materials electrochemical properties serves to enhance structural stability.

This article primarily discusses the differences between doping strategy and high-entropy approach in TMLOs. Starting from the perspective of single/multi-atom doping in TMLOs, it elaborates on the influence of different doping elements and doping sites on performance, aiming to elucidate the relationship between compositional structure and electrochemical properties. From the perspective of the high-entropy approach, the article analyzes the effects achievable by current high-entropy materials, which differ from those of single/multi-atom doped materials. The effects of traditional doping strategy and high-entropy methods on battery performance have been summarized for the first time (see Fig. 1). The traditional doping strategy involves leveraging anionic redox reactions, lowering the energy barriers, establishing strong M (metal) - F bonds, and utilizing the pillar and pinning effects. In contrast, the high-entropy approach introduces unique effects such as the cocktail effect, structure stabilization, high degree of disorder, entropy extension and local regulation effect.

2. TMLOs in the AIBs

TMLOs represent a prominent class of cathode materials for advanced AIBs, encompassing LIBs, SIBs, and PIBs. These materials have been extensively studied and utilized due to their distinctive layered structure and excellent tunability. TMLOs are typically formulated as A_xTMO_2, where A represents Li, Na, or K [33,35]. AM and TM ions occupy lattice spaces between densely packed three-dimensional ABC stacking oxygen planes [53]. The layered structures are built up by edge-sharing TMO_6 octahedra, forming repeating layers between which alkali ions are positioned in the octahedral, prismatic or tetrahedral environment [5,54–59].

TMLOs are categorized based on their metal oxide layer arrangement and spatial organization of metal components. Delmas et al [60] introduced a nomenclature system using letters (P for prismatic, O for octahedral, T for tetrahedral) to denote AM ion polyhedral coordination environments, alongside numbers indicating the number of TMO_2 layers per unit cell. For example, the numbers 2 and 3 correspond to oxygen stacking sequences "AB BA" and "AB CA BC" respectively. Structural variations, indicated by primes (’), reflect distortions or significant deviations from the original crystallographic parameters. Current research predominantly focuses on TMLO phases such as P2, O2, P3, and O3 (Fig. 2**a-d**), which exhibit varying electrochemical performance due to different metal combinations and structural configurations [5,20,21,30]. O3 and P2 layered oxides are particularly prominent as positive electrode materials, with O-type structures offering higher theoretical specific capacities owing to greater AM content. However, their narrower tetrahedral diffusion paths may impose higher ion diffusion barriers compared to the broader channels in P-type structures [4,57]. Despite their promising attributes, TMLOs face challenges including poor capacity retention and structural stability. The large ionic radii of AM ions during extraction/insertion cycles often induce TM layer slippage and significant volume changes, leading to phase transitions or structural failures [24,30,55,59]. Moreover, TMLOs are susceptible to

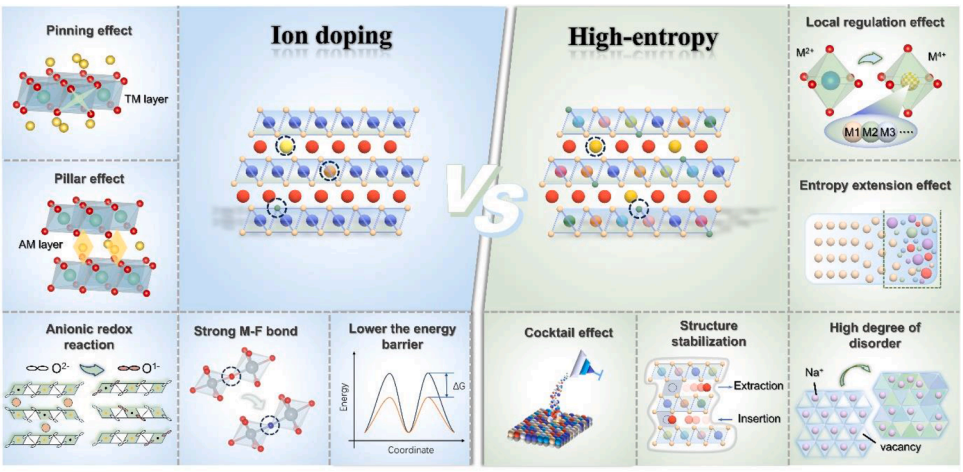

Fig. 1. Doping strategy *vs.* high-entropy approach in TMLOs.

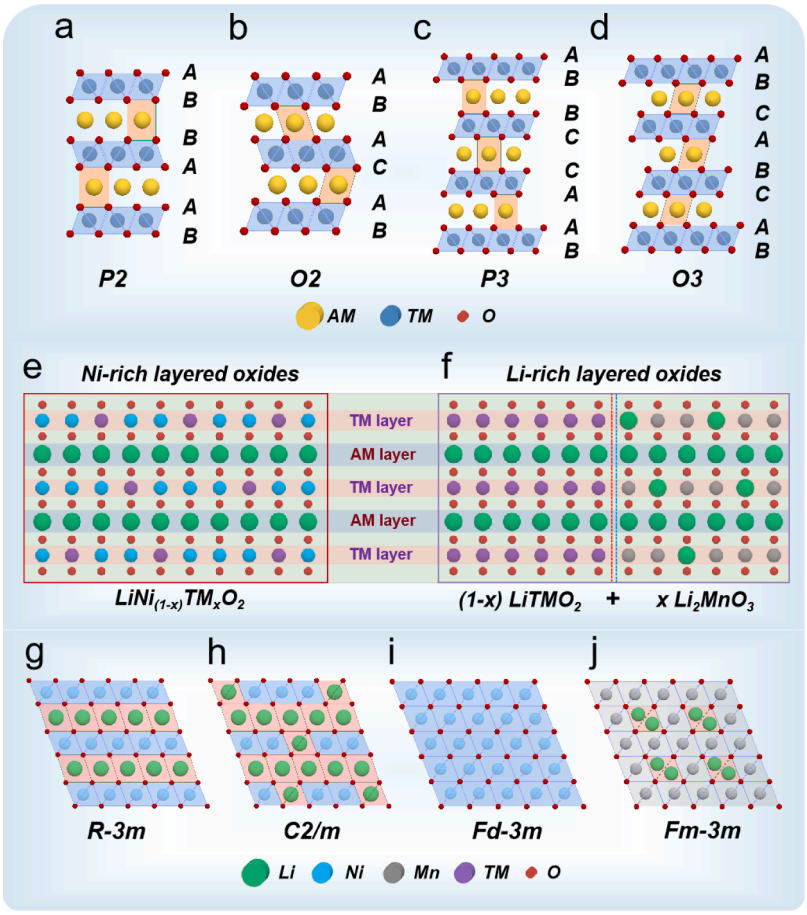

Fig. 2. (a-d) Schematic representation of the crystal structures for layered A_xTMO_2: (a) P2-type, (b) O2-type, (c) P3-type, and (d) O3-type stackings. (e) Schematic diagram of NRLOs structure. (f) Schematic diagram of LRLOs structure. (g-j) Crystal structure of layered materials in LIBs: (g) $LiNiO_2$, (h) Li_2MnO_3, (i) spinel $LiMn_2O_4$, and (j) NiO-type rock salt phases.

air and moisture-induced degradation, necessitating protective measures [23,30,60,61].

2.1. Li_xTMO_2 in LIBs

Currently, layered $LiCoO_2$ and various ternary materials, including a range of nickel manganese cobalt (NMC) compositions, have been commercialized for LIBs[62]. Notable examples include $LiNi_{1/3}Mn_{1/3}Co_{1/3}O_2$, (NMC-111), $LiNi_{0.5}Mn_{0.3}Co_{0.2}O_2$ (NMC-532), and $LiNi_{0.6}Co_{0.2}Mn_{0.2}O_2$ (NMC-622), among others [32,55,63–65]. Research on next-generation cathode materials is increasingly focusing on nickel-rich layered oxides (NRLOs) and lithium-rich layered oxides (LRLOs, i.e., Li_xTMO_2, ($1 \leq x \leq 1.2$)), due to their high specific capacity, energy density, and environmental friendliness [66–68]. Both NRLOs and LRLOs have a layered structure, typically composed of elements such as lithium, nickel, cobalt, manganese, and oxygen. TM ions and oxygen ions alternate in their arrangement, but there are certain differences in the distribution and arrangement of lithium-ions and TM ions, which determine their performance and applications in LIBs cathode materials [25,56,69–71].

NRLOs have rhombohedral crystal structure with an R-3m space group (Fig. 2**e**), which typically corresponds to an O3-type layered structure evolving from the $LiNiO_2$ phase through specific TM ion substitutions. Their chemical formula can be expressed as $LiNi_{1-x}TM_xO_2$ ($0 \leq x \leq 0.5$). The reversible capacity is mainly provided by the redox reactions of $Ni^{2+}/^{3+}/^{4+}$ [55,70]. On the other hand, LRLOs are expressed as (1-*x*) $LiTMO_2 \cdot xLi_2MnO_3$ (Fig. 2**f**), where TM can be Ni, Co or Mn as well as other TM dopants [72]. This composition features a layered structure, incorporating both $LiTMO_2$ (TM = Ni, Co, Mn, with an R-3m space group) (Fig. 2**g**) and Li_2MnO_3 (with a C/2m space group) (Fig. 2**h**) [24]. Both phases have similar structural features: all octahedral sites are occupied by oxygen, with the same oxygen-close-packed structure with a hexagonal close-packed pattern. Generally, LRLOs have higher Li-ion storage capacity because they are designed to accommodate more Li ions within their layered structure,[73] while NRLOs generally show more redox centers and higher operating voltages than NMC-111 and NMC-532, attributed to their elevated Ni content [55,70]. Those make NRLOs and LRLOs highly promising candidates for developing batteries with high energy density. Nonetheless, the commercialization of these materials faces significant challenges, especially concerning potential safety risks and processability in electrode manufacturing when the nickel content is 80% or higher [65,74]. Additionally, LRLOs face major hurdles such as low initial Coulombic efficiency, rapid voltage degradation, and poor rate capability [70,73].

The aforementioned drawbacks on NRLOs and LRLOs cathodes are mainly caused by structural instability, particularly at highly delithiated states and elevated temperatures [65,70,73]. *Ion mixing:* Due to the similarity in ionic radii between Li^+ (0.76 Å) and Ni^{2+} (0.69 Å), during charge and discharge processes of nickel-rich cathodes, Ni^{2+} ions can easily migrate into lithium layer, leading to the cation mixing, causing the original layered structure (R-3m) (Fig. 2**g**) to irreversibly transform into spinel phases (Fd-3m) (Fig. 2**i**) or electrochemically active NiO-type rock salt phases (Fm-3m) (Fig. 2**j**) on the electrode surface [25,61,75,76]. *Ion dissolution*: The presence of highly oxidized Ni^{4+} ions at the electrode/electrolyte interface may result in dissolution of TM ions and decomposition of organic electrolytes [76]. *Material thermal*

decomposition: Lithium-rich cathodes exhibit thermodynamic instability leading to microscopic defects when Li^+/Li voltage exceeds 4.6 V. Overcharged cathodes are prone to thermal decomposition, disrupting TM-O bonds and releasing oxygen from the main lattice [70,73]. *Trace contamination*: Residual lithium compounds, such as LiOH and Li_2CO_3 forming during preparation or storage in humid air, are spontaneously reduced from Ni^{3+} ions and enveloped into the particles' surface. Accumulation of Li_2CO_3 on the surface exacerbates adverse gas evolution significantly [75,76]. Currently, the phase transition from layered structure to the spinel/rock salt phases and material surface/interface degradation are widely recognized as significant barriers hindering the commercialization of NRLOs and LRLOs [70,73,74,76].

2.2. Na_xTMO_2 in SIBs

Current research on Na_xTMO_2 ($0 \leq x \leq 1$) primarily focuses on manganese-based and nickel-based P2 and O3 phases (Fig. 2**a, d**) [2,30]. Typically, during charging, the O3 phase transforms into the P3 phase, while the P2 phase transforms into the O2 phase. Conversely, during discharge, the opposite process occurs [5,30,77].

The significant difference in ionic radii between Na^+ and TM ions makes Na_xTMO_2 cathodes less prone to the mixing of AM and TM ions commonly observed in Li_xTMO_2 [78]. However, this also renders the structure more vulnerable to damage during the Na^+ extraction and insertion processes [1,30,78]. In the extraction of Na^+ ions, the O3 phase often undergoes more complex transitions compared to the P2 phase [77]. For instance, $NaNi_{0.5}Mn_{0.5}O_2$ undergoes a series of structural transformations during the charging process, such as O3 → (O3+O′3) P3 → P′3 → (P′3+P3″) → P3″ [79]. Generally, the O3 phase structured materials undergo an O3-P3 transition after roughly 25% Na^+ ion extraction,[80] while those with P2 phase typically experiences a single P2-O2 phase transition [1]. O3-structured materials initially possess a higher sodium content compared to those with P2 structure, leading to higher theoretical capacities [1,3]. However, in the P2 structure, sodium ions traverse a relatively wide planar square center, offering an open prismatic path with larger interlayer spacing and lower diffusion barriers. This characteristic generally results in superior rate performance of P2-structured materials [57,81].

The primary challenges facing Na_xTMO_2 include irreversible phase transitions and storage instability, leading to insufficient battery performance [30]. The former are particularly problematic as they can cause structural breakdown and rapid capacity degradation [2,3]. Therefore, suppressing or reducing these irreversible phase transitions is key to improving the electrochemical performance of SIBs layered oxides [35,54]. Another significant challenge is their hygroscopic nature when exposed to air, resulting in the formation of weakly electrochemically active NaOH or Na_2CO_3 on the surface of the active material, leading to decreased battery performance [30,82]. Additionally, the formed NaOH and Na_2CO_3 act as electrical insulators, hindering the conductivity of the material, and may react with the electrolyte [3,82].

2.3. K_xTMO_2 in PIBs

Current research on K_xTMO_2 ($0 \leq x \leq 1$) primarily focuses on potassium-deficient P2 and P3 phases (Fig. 2**a, c**) [33,59,83]. Compared to Li^+ and Na^+, the larger K^+ ions typically occupies the large prismatic sites rather than octahedral sites, resulting in a P-type structure [21,59].

Motivated by the implementation of Mn-based cathodes in LIBs, K_xMnO_2 has attracted noteworthy interest in PIBs. Layered K_xMnO_2 offers high capacity, low cost, and straightforward synthesis methods [33,59]. However, its production is influenced by the Jahn-Teller effect of Mn^{3+}. In manganese-based layered oxides, the mixed valence states of Mn^{3+} and Mn^{4+} play distinct roles: Mn^{4+} helps stabilize crystal structures by forming undistorted (ideal) MnO_6 octahedra, while high-spin Mn^{3+} with an electron configuration of $(t_{2g})^3(e_g)^1$ often causes Jahn-Teller distortion in the three-dimensional orbitals [21,23,33,83,84]. The alternating valence states of Mn result in recurring distortions and phase transitions, making it challenging to maintain structural integrity. Therefore, reducing the Jahn-Teller distortion of Mn^{3+} and enhancing the structural stability of these oxides are key to achieving long-term cycle stability [84,85].

K_xCoO_2 is another well-researched single-TM oxide [33]. The K^+ storage capacity of P2-$K_{0.41}CoO_2$ and P3-$K_{2/3}CoO_2$ in the 2.0-3.9 V range were reported by Hironaka and his colleagues [86]. X-ray diffraction (XRD) confirms that $K_{0.41}CoO_2$ retains its original P2 structure during reversible intercalation processes, albeit with different degrees of peak shifts and asymmetric peak evolution over a wide range of K^+ contents between 0.23 and 0.47 [86]. However, the cost of Co is a significant barrier to the commercialization of K_xCoO_2 cathodes [87].

3. Doping strategy in A_xTMO_2

Doping strategies involve the introduction of small amounts of alio-elements (typically 1-2 types) into the original material [34,36–38] These doping elements are distributed in trace amounts within the material's lattice, altering its physical and chemical properties to enhance electrochemical performance [88,89]. TMLOs present three unique types of doping sites: AM, TM, and O sites. Researchers commonly use doping with metal cations (such as Mg^{2+},[90–92] Cu^{2+}, [93–97] Zn^{2+},[98–101] Al^{3+},[36,102,103] Ti^{4+}, [100,104] B^{3+},[88, 105–107] etc.) and anions (such as F^- [108–115]) to address the issue of layered structural degradation. This diverse range of doping elements and sites offers substantial flexibility for material modification.

This section reviews the doping strategies employed in TMLOs for AIBs, including bulk doping and surface doping. The discussion begins with single-atom doping at TM, AM, or O sites in the bulk phase and progresses to multi-atom doping, typically involving two heterogeneous elements. By summarizing and discussing the effects of numerous elements at these three doping sites, the positive impacts of doping strategies in leveraging ARR, lowering the energy barriers, establishing strong M-F bonds, and utilizing the pillar and pinning effects, are highlighted (Fig. 3). Subsequently, the critical role of surface doping in suppressing surface/interface side reactions is explored, offering an additional pathway to enhance the stability and performance of TMLOs.

3.1. Single-atom doping in A_xTMO_2

Single-atom doping primarily focuses on the characteristics of the doping element and the effects of different doping sites on the electrochemical properties of materials [35,40]. The doping of various elements at different sites results in distinct modification effects [35,101, 111,113,116]. For example, doping Li at AM or TM sites in Na_xTMO_2 (see Fig. 4**a**) will produce significantly different modification effects [117,118].

3.1.1. Doping at TM layer

Doping in the TM layer is the most commonly used method in doping strategies because the TM sites can be occupied by various elements (such as Li, Mg, Zn, Cu, Ca, Cr, Al, Ni, Co, Fe, Mn, V, Ti, Sn, Mo, Zr, W, etc.) [38,119–127]. When heterogeneous metal ions are doped into the TM sites, they typically exert a strong influence on the original metal ions and oxygen ions.

Doping high-valence cations (such as Ti^{4+},[128] Sn^{4+},[129–131] W^{6+},[132] Mo^{6+},[133,134] etc.) into the TM layer often results in the formation of strong TM-O bonds, which may suppress oxygen vacancy formation and even induce a "pinning effect" that stabilizes the layered structure. In LIBs, Sun et al [134] investigated the effects of different dopants (Mg^{2+}, Al^{3+}, Ti^{4+}, Ta^{5+}, and Mo^{6+}) on the oxidation state of $LiNi_{0.91}Co_{0.09}O_2$ and its electrochemical, morphological, and structural properties. They showed that cathodes doped with high oxidation state dopants outperformed undoped cathodes as well as those doped with low oxidation state dopants. In particular, $LiNi_{0.91}Co_{0.09}O_2$ cathodes

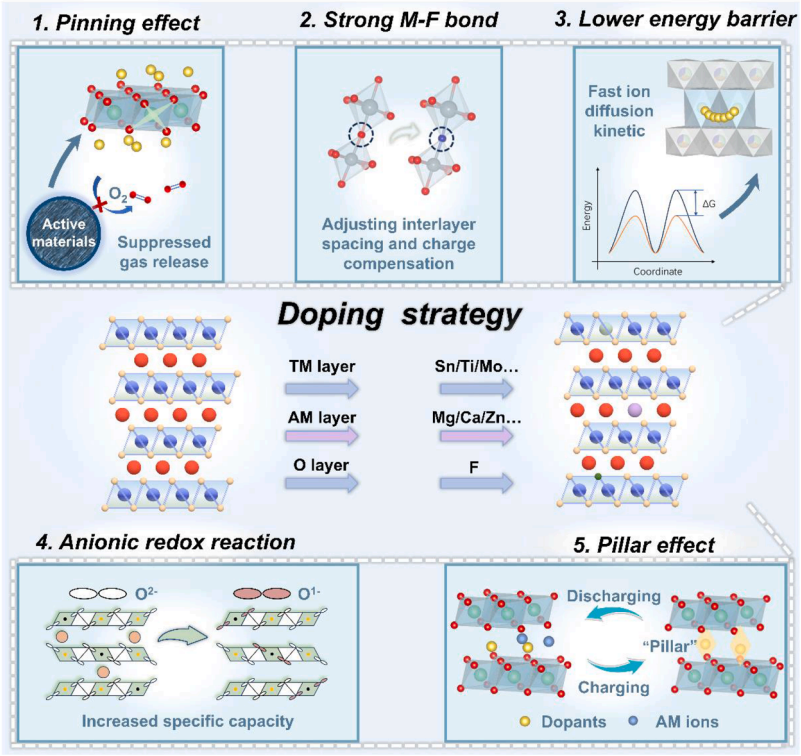

Fig. 3. Schematic of traditional doping methods at different sites in layered oxides and their corresponding effects.

doped with Ta^{5+} and Mo^{6+} exhibited 81.5% capacity retention after 3000 cycles at 200 mA g^{-1}. Bao et al [135] synthesized Yb-doped $Li_{1.2}Mn_{0.54}Ni_{0.13}Co_{0.13-x}Yb_xO_2$ cathodes via sol-gel method. XRD and scanning transmission electron microscopy (STEM) results indicated that Yb ions occupied TM sites at appropriate doping levels ($x < 0.005$), increasing the spacing between Li layers, stabilizing the oxygen framework, and suppressing phase transitions due to Yb's larger ionic radius and strong binding energy. Cheng et al [136] doped Ti into the TM layer of $LiNi_{0.6}Co_{0.2}Mn_{0.2}O_2$, synthesizing $LiNi_{0.6}Co_{0.2}Mn_{0.18}Ti_{0.02}O_2$. The strong Ti-O bonds and absence of unpaired electrons enhance the structural and electrode-electrolyte interface stability. Ti doping also suppresses undesirable H2-H3 phase transitions, minimizing mechanical degradation. Non-*in-situ* TEM and X-ray photoelectron spectroscopy analysis indicated that Ti doping inhibits the release of interfacial oxygen and reduced undesirable interface reactions. In SIBs, Yang et al [128] successfully doped Ti^{4+} into $Na_{2/3}Fe_{1/3}Mn_{2/3}O_2$, synthesizing P2-$Na_{2/3}Fe_{1/3}Mn_{0.57}Ti_{0.1}O_2$ without any phase transitions during low-voltage charge and discharge processes. Ti^{4+} doping suppresses phase transitions caused by the Jahn-Teller effect and promotes sodium ion transfer kinetics, thereby enhancing structural stability. In PIBs, Han et al [133] doped Mo^{6+} and Co^{3+} into P3-$K_{0.45}MnO_2$, introducing [Mn-Co-Mo]O_6 octahedra. By incorporating Mo^{6+}, which has a smaller ionic radius and higher oxidation state, a pinning effect was established in the TM layer (Fig. 4**c**). This induces a second-order Jahn-Teller effect (pseudo JTE) in the adjacent MnO_6 octahedra, which helps prevent uneven elongation of Mn-O bonds, reduces structural instability within the cathode materials, and enhances long-term cycling stability.

Doping low-valence cations (such as Mg^{2+},[137–139] Zn^{2+}, Cu^{2+}, [96,97] etc.) into the TM layer may potentially suppress the expansion/contraction of TMO_6 octahedra and help maintain the integrity of the TMO_2 layer. Additionally, this doping plays a significant role in mitigating the Jahn-Teller effect associated with Mn. Liu et al [96] demonstrated that doping Cu^{2+} into $Na_{2/3}MnO_2$ reduces the deformation of MnO_6 octahedra, maintains the integrity of the TMO_2 layer, facilitates Na ion transport, and delays the P2-P'2 phase transition. Similarly, Gao et al [141] found that Cu doping into Na_xTMO_2 (TM = Fe, Mn) inhibits the $Mn^{4+/3+}$ redox process, leading to the formation of a small amount of inactive Mn, which lowers the average Mn valence and improves cycling stability. Additionally, Chen et al [142] prepared a series of $Na_yLi_{0.1}Cu_xMn_{0.9-x}O_2$ compounds, and theoretical calculations indicated that with increasing Cu content, electron aggregation around O atoms increases, resulting in strong covalent bonds between Cu and O, leading to a more stable structure. Clément et al [139] introduced Mg into P2-$Na_{2/3}MnO_2$, which reduces the number of Mn^{3+} Jahn-Teller centers and delays the sliding of the oxygen layers, resulting in a higher reversible capacity and smoother charge-discharge curves. Subsequently, Zhang et al [99] reported on Zn-doped $Na_{0.833}Li_{0.25}Mn_{0.75}O_2$, finding that Zn doping led to lower formation energy, a more stable ground state, and fewer spinodal decomposition regions, enabling the material to maintain a phase-stable charge-discharge process while reducing the number of Mn^{3+}. Xiao et al [84] proposed that adjusting the average oxidation state of Mn could mitigate structural degradation caused by the Jahn-Teller effect in K_xTMO_2. Their studies revealed that the introduction of Ti^{4+} reduces the oxidation state of Mn, while Mg^{2+} increases it, with Mg-doped $K_{0.5}Mn_{0.6}Co_{0.2}Fe_{0.1}Mg_{0.1}O_2$ exhibiting the highest oxidation state for Mn. The results indicate that, compared to $K_{0.5}Mn_{0.7}Co_{0.2}Fe_{0.1}O_2$, which undergoes harmful phase transitions from P3 to O3 due to the Jahn-Teller effect, $K_{0.5}Mn_{0.6}Co_{0.2}Fe_{0.1}Mg_{0.1}O_2$ demonstrates highly reversible single-phase structural evolution during K^+ extraction/insertion. After 150 cycles at 100 mA g^{-1}, it retains 91% of its initial capacity, outperforming both the original and Ti-doped materials.

During charging and discharging, TMLOs undergo anionic (O^{2-}) redox reaction (ARR) at high cutoff voltages, typically resulting in lattice oxygen depletion and the release of oxygen (O_2). Doping with low-valence cations (such as Li^+,[117,143,144] Mg^{2+},[145,146] Zn^{2+},[98, 147] etc.) can enhance the cycling stability of cathode materials at high voltages and improve the reversibility of ARR, thereby increasing the reversible capacity of the battery. In particular, the doping of Li^+ in Na_xTMO_2 plays a significant role in enhancing the capacity by triggering

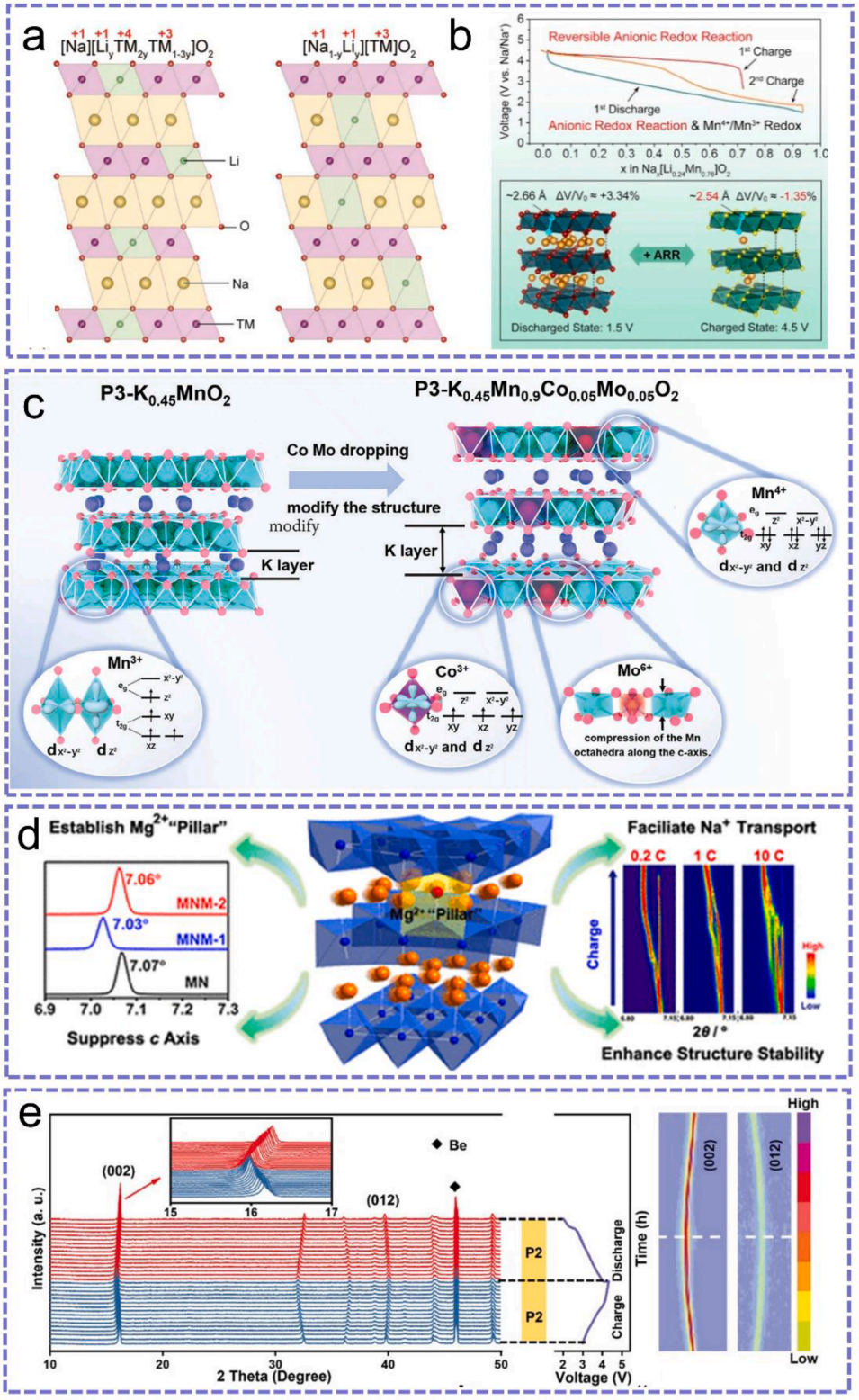

Fig. 4. (a) Schematic diagram of the two potential substitution sites for Li in the O3-type layered structure. Reproduced with permission [118]. Copyright 2018, Royal Society of Chemistry. (b) Schematic diagram illustrating the role of ARR in enhancing reversible specific capacity in a P2-type cathode. Reproduced with permission [143]. Copyright 2018, Elsevier. (c) Diagram illustrating the Pinning Effect: The electronic configurations of Mn, Mo and Co with possible crystal octahedra structure. Reproduced with permission [133]. Copyright 2024, Wiley-VCH. (d) Diagram illustrating the Pillar Effect: Mg ions in the Na layer serve as "pillars" to facilitate the layered structure. Reproduced with permission [149]. Copyright 2019, American Chemical Society. (e) Synergistic effect inhibiting material phase transition: *In-situ* XRD patterns of LMNM during the first cycle at 2-4.35 V (0.2 C) and Contour plots of (002) and (012) diffraction peaks. Reproduced with permission [153]. Copyright 2023, Wiley-VCH.

ARR. For example, Wang et al [117] reported an O3-type cathode, $NaLi_{1/3}Mn_{2/3}O_2$, with ARR, exhibiting a high reversible capacity of 190 mAh g^{-1} and almost no voltage decay after 40 cycles. The introduction of Li^+ into the TM layer promotes the redox reactions of anionic O^{2-} and leads to densification of the electrode through intralayer migration of transition metal cations after the first oxygen release, effectively suppressing voltage decay. Similarly, Nazar et al [148] reported P2-$Na_{0.6}Li_{0.2}Mn_{0.8}O_2$, providing approximately 190 mAh g^{-1} after 100 cycles in the voltage range of 2.0-4.6 V. Rong et al [143] revealed the role of ARR in stabilizing the structure of P2-$Na_{0.72}Li_{0.24}Mn_{0.76}O_2$ cathode (Fig. 4**b**), which demonstrated an initial charge capacity of about 210 mAh g^{-1}. Even after complete Na^+ removal, the P2 structure maintained minimal volume changes (1.35%). These studies collectively demonstrate the critical role of Li^+ doping in activating ARR to significantly boost the specific capacity of materials.

3.1.2. Doping at AM layer

Doping ions like Mg,[85,90,149] Zn,[150] Ca,[122,151] etc. into AM layer may enhance its affinity for surrounding O ions. These ions could potentially act as "pillar ions", contributing to a stabilizing "pillar effect" that supports the AM layer during the insertion and extraction of AM ions (Li^+, Na^+, K^+). In LIBs, Choi et al [90] achieved *in-situ* electrochemical doping of Mg^{2+} at Li sites by assembling a Li-deficient Mn-based cathode material with Mg metal in half-cell configuration. They synthesized $[Li_{1-x}Mg_y]Mn_{1-z}M_zO_2$ (M = Co and Ni), in which the introduction of Mg^{2+} at Li sites effectively reduces cation mixing during cycling, leading to enhanced capacity retention over 200 cycles. In SIBs, Wang et al [149] introduced Mg ions into the Na layer of P2-$Na_{0.7}Mn_{0.6}Ni_{0.4}O_2$, where Mg ions in the sodium layer act as "pillars" to stabilize the layered structure, particularly during high-voltage charging (Fig. 4**d**). Additionally, Mg ions in the AM layers can destroy the Mn/Ni charge ordering and Na^+/vacancy ordering, facilitating Na-ion diffusion and helping to smooth the voltage profiles. Peng and colleagues [152] synthesized Zn-doped P2-$[Na_{0.67}Zn_{0.05}]Ni_{0.18}Cu_{0.1}Mn_{0.67}O_2$ and discovered that Zn ion doping at the AM site forms an O^{2-}-Zn^{2+}-O^{2-} "pillar", strengthening electrostatic cohesion between adjacent transition metal layers, which prevents the cracking of active material along the a-b plane and inhibits the formation of the O2 phase during deep desodiation. In PIBs, Luo et al [85] introduced Mg^{2+} into the K layer of P3-$K_{0.5}MnO_2$, which pushes Mn to a higher oxidation state significantly suppressing the Jahn-Teller effect. When the Mg content exceeds 0.1 equivalents per formula unit, Mg^{2+} enters the K layer, resulting in smoother charge-discharge curves. This demonstrates that Mg doping in the K layer effectively stabilizes the AM layer during K ion deintercalation, reducing phase transitions caused by slab gliding.

Doping heterogenous alkali metal elements (Li^+,[118,154] K^+,[155,156] Na^+ [157,158]) into the AM layer is believed to stabilize the layered structure during electrochemical reactions and potentially enhance the diffusion kinetics of AM ions by lowering the AM migration energy barrier. For instance, Li et al [157] introduced Na doping into the Li layer of Ni-rich $LiNi_{0.6}Co_{0.2}Mn_{0.2}O_2$ and observed crystal structure changes and lattice distortions with picometer precision using aberration-corrected STEM. DFT and Modified Planck-Nernst-Poisson coupled Frumkin-Butler-Volmer (an electrochemical model) [157,159] were employed to reveal the relationship between activation energy and charge transfer resistance at multiple scales. Doping with Na^+ ions reduced the activation energy barrier from 1.10 eV to 1.05 eV and decreased the interface resistance from 297 Ω to 134 Ω, demonstrating enhanced diffusion kinetics of Li^+ and electrochemical reaction kinetics with Na^+ doping. Li et al [160] introduced K into Li layer of Li-rich $Li_{1.20}Mn_{0.54}Co_{0.13}Ni_{0.13}O_2$, demonstrating that *in-situ* K doping stabilizes the host layered structure by preventing the formation of spinel structure during cycling. The doped K^+ fixed in the Li layer blocked Mn migration pathways, thereby inhibiting spinel phase growth. The large radius of K^+ increases the resistance to spinel phase growth, thereby reducing voltage decay caused by phase transitions. Additionally, Wang et al [118] reported that Li doping into the Na layer of O3-$Na_xFe_yMn_{1-y}O_2$ ($0 \leq x, y \leq 1$) stabilized the layered structure and facilitated Na insertion by lowering the Na migration energy barrier. This effect was validated through various experimental and computational methods, demonstrating the impact of heterogenous alkali metal doping on structural stability and ion diffusion.

3.1.3. Doping at O layer

Doping non-redox-active cations at AM/TM sites may potentially impact the initial specific capacity, while incorporating anions into the O layer could potentially influence the average oxidation state of redox-active centers and adjust interlayer spacing. Among various anionic dopants (such as F, S, Cl, etc.), F is considered the most promising candidate [161,162].

The F^- doping can reinforce the layered structure by forming stronger metal-F bonds and regulate the interlayer spacing. In LIBs, Wang et al [163] introduced F doping into the O layer of $LiNi_{0.8}Co_{0.15}Al_{0.05}O_2$, resulting in $LiNi_{0.8}Co_{0.15}Al_{0.05}O_{1.96}F_{0.04}$ with enhanced M-F bonds and wider interlayer spacing along the c-axis. This stabilized the host structure and enhanced the rate capability. Similarly, Sun's group [164] synthesized $LiNi_{0.80}Co_{0.05}Mn_{0.15}O_{2-x}F_x$ with varying concentrations of F^- doping, increases the capacity retention (78% of its capacity after 8000 cycles), whereas the undoped $LiNi_{0.80}Co_{0.05}Mn_{0.15}O_2$ cathode retained only 64.6% of its initial capacity. The F doping improved structural stability, reducing microcrack formation and enabling 100% depth of discharge (DOD) cycling. This is a significant improvement over typical cathodes that are limited to 60–80% DOD to prevent degradation. In SIBs, Zhang et al [111] synthesized $NaNi_{1/3}Fe_{1/3}Mn_{1/3}O_{2-x}F_x$ cathode materials, showing that F-doping modified the binding energy of oxygen and the Mn^{3+}/Mn^{4+} ratio, suppressing the Jahn-Teller effect of Mn^{3+} and consequently enhance the electrochemical performance. Similarly, Chen et al [109] synthesized F-doped P2-$Na_{0.6}Mn_{0.95}Ni_{0.05}O_{2-x}F_x$ (x = 0, 0.02, 0.05, 0.08), finding that F^- doping adjusted lattice parameters and aided charge compensation, enhancing the redox activity of Ni^{2+}/Ni^{3+}. In PIBs, Xu et al [89] synthesized F-doped P2-$K_{2/3}Mn_{7/9}Ni_{1/9}Ti_{1/9}O_{17/9}F_{1/9}$, observing that F^- incorporation increased interlayer spacing and facilitated K^+ ions transport without severe structural damage. F^- doping also raised the concentration of redox-active Mn ions by lowering the average manganese oxidation state, enabling a reversible capacity of 132.5 mAh g^{-1} with 0.53 K^+ reversibly (de)intercalated in the structure.

Overall, the diversity of doping sites and dopant elements plays a crucial role in enhancing the design flexibility of layered materials, serving as an effective strategy to mitigate inherent structural and electrochemical limitations. We have systematically summarized the applications of typical element doping in A_xTMO_2 (Table 1) and established correlations between dopant elements, doping sites, and the five key modification effects in layered cathodes (Fig. 5), providing valuable insights to guide researchers in selecting optimal doping elements for material design.

In addition, different doping concentrations of the same doping element significantly influence electrochemical properties. For layered oxide cathodes, the dopant content is typically kept below 5% of the total cations. While a small amount of doping maintains the original phase of the crystal structure, it can induce substantial modifications in the crystal structure, electronic properties, nanomorphology, and surface stability, ultimately impacting the performance of AIBs [165]. Clément et al [139] conducted an in-depth study on the effects of different concentrations of Mg doping on the electrochemical performance and structural stability of P2-$Na_{2/3}MnO_2$. They synthesized three $Na_{2/3}Mn_{1-y}Mg_yO_2$ compounds (y = 0.0, 0.05, 0.1) and found that the compound with 5% Mg doping exhibited excellent electrochemical performance, with a very high rate capability. Chen et al. [142] developed a series of $Na_yLi_{0.1}Cu_xMn_{0.9-x}O_2$ cathode materials by introducing Cu^{2+} into the transition metal layer. Theoretical calculations indicated that as the Cu content increased, electron aggregation around the O

Table 1
Summary of the electrochemical performance of commonly doped elements in layered cathodes for AIBs.

Cathode	Voltage range [V]	Initial capacity [mAh g^{-1}]	Cycle retention	Rate performance [mAh g^{-1}]	Ref
Ti doped materials					
$Na_{2/3}Fe_{1/3}Mn_{0.57}Ti_{0.1}O_2$	1.5-4.3	173	76% after 50 cycles/ 0.2C	52/ 3C	[128]
$LiNi_{0.6}Co_{0.2}Mn_{0.18}Ti_{0.02}O_2$	3-4.5	193	91.8% after 150 cycles/ 0.5C	118/ 10C	[136]
Sn doped materials					
$Na_{0.67}Ni_{0.3}3Mn_{0.57}Sn_{0.1}O_2$	2.0-4.3	155.2	~65% after 30 cycles/ 0.3C	99.7 / 3C	[129]
Sn doped $LiNi_{0.6}Co_{0.2}Mn_{0.2}O_2$	3.0-4.5	~180	88.31% after 100 cycles/ 1C	136.2/5C	[130]
$NaNi_{0.5}Sn_{0.5}O_2$	1.5- 4.2	100	~75% after 70 cycles/ 0.1C	/	[131]
Mo doped materials					
$K_{0.45}Mn_{0.9}Co_{0.05}Mo_{0.05}O_2$	1.5-4	96	59.6% after 2000 cycles/ 5C	77.3/ 5C	[133]
Mo doped $LiNi_{0.91}Co_{0.09}O_2$	2.7-4.3	~230	94.9% after 100 cycles/ 0.5C	/	[134]
Mg doped materials					
Mg doped $LiNi_{0.90}Mn_{0.05}Co_{0.05}O_2$	2.9-4.3	~187	/	158/ 3C	[137]
$Na_{0.9}Mn_{0.60}Ni_{0.35}Mg_{0.05}O_2$	2-4	179	81% after 100 cycles/ 0.1C	102.5/ 5C	[138]
$Na_{2/3}Mn_{0.95}Mg_{0.5}O_2$	1.5-4	~175	~100% after 50 cycles/ 3C	106/ 28.6C	[139]
$Na_{0.67}Ni_{0.23}Mn_{0.67}Mg_{0.1}O_2$	2-4.5	~125	81.7% after 100 cycles/ 0.1C	/	[146]
$K_{0.5}Mg_{0.15}[Mn_{0.8}Mg_{0.05}]O_2$	1.4-4	102	48.2% after 400 cycles/ 1C	54.3/ 5C	[85]
Zn doped materials					
$Na_{0.44}Mn_{0.995}Zn_{0.005}O_2$	2-4	100	~75% after 10 cycles/ 0.14C	/	[140]
Zn doped $Na_{0.833}Li_{0.25}Mn0_{.75}O_2$	1.5-4.6	166	96.9% after 200 cycles/ 0.2C	/	[99]
$Na_{2/3}Mn_{7/9}Zn_{2/9}O_2$	1.5-4.5	195	75% after 50 cycles/ 1C	/	[98]
$Na_{2/3}Zn_{1/4}Mn_{3/4}O_2$	1.5-4.5	~200	67% after 50 cycles/ 0.2C	~150/ 2C	[147]
Cu doped materials					
$Na_{0.66}Mn_{0.8}Cu_{0.2}O_2$	1.5-4.4	142	~90% after 100 cycles/ 0.5C	79.9/ 5 C	[96]
$Na_{0.67}Mn_{0.6}Ni_{0.2}Co_{0.1}Cu_{0.1}O_2$	1.9-4	131.3	86.7% after 200 cycles/ 0.1C	65/ 15C	[97]
$Na_{0.8}Cu_{0.3}Fe_{0.2}Mn_{0.5}O_2$	2.5-4.2	112.6	67.1% after 200 cycles/ 0.1C	/	[141]
$Na_{0.7}Li_{0.1}Cu_{0.2}Mn_{0.7}O_2$	1.5-4.5	160	84.3% after 100 cycles/ 1C	102.7/ 5C	[142]
Li doped materials					
$NaLi_{1/3}Mn_{2/3}O_2$	1.5-4.5	~200	/	/	[117]
$Na_{0.72}Li_{0.24}Mn_{0.76}O_2$	1.5-4.5	270	~75% after 30 cycles/ 0.05C	/	[143]
$Na_{0.6}Li_{0.2}Mn_{0.8}O_2$	3.5-4.5	80	~42% after 60 cycles/ 2C	72/2C	[144]
F doped materials					
$LiNi_{0.8}Co_{0.15}Al_{0.0}5O_{1.96}F_{0.04}$	2.8-4.3	157.8	98.3% after 100 cycles/ 2C	~150/ 5C	[163]
F doped $LiNi_{0.80}Co_{0.05}Mn_{0.15}O_2$	2.7-4.3	216	78% after 8000 cycles/ 1C	/	[164]
F doped $NaNi_{1/3}Fe_{1/3}Mn_{1/3}O_2$	2-4	~120	~89% after 70 cycles/ 1C	/	[111]
Other doped materials					
W doped $LiNi_{0.92}Co_{0.04}Mn_{0.04}O_2$	2.8-4.3	210.83	93.97% after 100 cycles/ 0.5C	159.11/ 5C	[132]
K doped $Na_{0.7}MnO_2$	1.8-4.3	240.5	98.2% after 100 cycles/ 0.5C	/	[155]
Na doped $LiNi_{0.6}Co_{0.2}Mn_{0.2}O_2$	2.7-4.3	179	90.8% after 100 cycles/ 0.2C	108/5C	[157]
Ca doped $NaNi_{1/3}Fe_{1/3}Mn_{1/3}O_2$	2-4	116.3	91.8% after 200 cycles/ 1C	86.2/10C	[151]
Yb doped $Li_{1.2}Mn_{0.54}Ni_{0.13}Co_{0.13}O_2$	2-4.8	294.5	84.4% after 100 cycles/ 1C	~150/ 5C	[135]

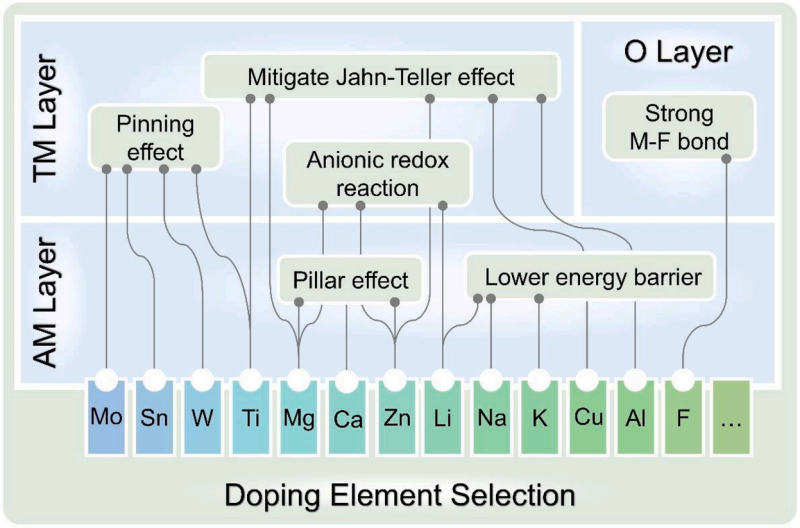

Fig. 5. Schematic illustration summarizing the doping of various elements at different sites in layered cathode materials and their modification effects.

atom intensified, resulting in stronger covalent bonding between Cu and O, which in turn stabilized the structure.

However, the effect of doping is not linear, as excessive doping concentrations can lead to detrimental effects on the material's performance. For example, F doping can enhance rate performance, but excessively high concentrations may reduce the achievable discharge capacity [166]. Improper doping levels can negatively impact key properties such as electronic conductivity, cation mixing, and alkali-ion transfer, ultimately leading to performance degradation at high current density rates or operating voltages [167]. Wang et al. [146] doped Mg

into P2-$Na_{0.67}Ni_{0.33}Mn_{0.67}O_2$, synthesizing P2-$Na_{0.67}Ni_{0.33-x}Mn_{0.67}Mg_xO_2$ cathode materials. Randomly distributed Mg dopants tend to segregate into the Na layer, forming high-density precipitates that serve as 3D network pillars. This structural reinforcement strengthens the material, suppresses cracking, and significantly enhances cycling stability. Increasing the Mg concentration from 5% to 10% further improves stability but slightly reduces the initial discharge capacity. Additionally, excessive Mg segregation into the Na layer may hinder ion transport, leading to a decline in rate capability. Feng et al [135] synthesized a series of trace Yb-doped lithium-rich cathode materials, $Li_{1.2}Mn_{0.54}Ni_{0.13}Co_{0.13-x}Yb_xO_2$ ($0 \leq x \leq 0.050$). The results showed that when Yb^{3+} was doped at low concentrations ($x \leq 0.005$), it enhanced the Yb-O bond energy, expanding the lithium layer spacing and stabilizing the oxygen stacking. However, when the doping concentration exceeded the critical threshold ($x > 0.005$), the charge transfer impedance increased, leading to a dramatic deterioration in electrochemical performance. These findings collectively suggest the presence of a concentration threshold effect, where the optimal doping concentration is crucial for achieving the desired electrochemical and structural stability in electrode materials.

Dopants may primarily concentrate near the surface of the layered oxides or establish a concentration gradient from the core to the surface. When the doping concentration is higher at the surface, this modification functions similarly to a coating, predominantly influencing surface properties without altering the core characteristics [167]. This particular doping approach—surface doping—is also significantly influenced by the concentration of dopant elements. For further details on surface doping, please refer to Section 3.3.

3.2. Multi-atom doping in A_xTMO_2

Compared to single-atom doping, multi-atom doping involves incorporating multiple heterogeneous elements (typically two or three) into TMLOs [108,110,156,158]. This approach aims to harness the advantages of different single-atom dopants and utilize the "synergistic effect" among these elements, potentially effective in suppressing irreversible phase transitions and stabilizing the structure. Currently, the application of co-doping strategies is primarily focusing on the dual-element doping, with a few cases involving the three-element doping [34,40,168,169].

3.2.1. Multi-atom doping in A_xTMO_2 with cations

In LIBs, Wang et al [170] demonstrated Mg and Ti co-doping to inhibit the transition of the layered structure of $LiNiO_2$ to a disordered spinel/rock-salt structure and prevent the formation of internal cracks, thereby delaying the structural degradation of the layered material. Feng et al [102] introduced Al and Zr into $LiNi_{0.6}Co_{0.2}Mn_{0.2}O_2$, resulting in the formation of a protective Li_2ZrO_3 coating suppressing interface reactions and enhancing the cycling performance (capacity retention of 92.1% after 100 cycles at 50°C). In comparison, single Al and Zr doping resulted in lower capacity retention, 85.4% and 87.1%, respectively, although improving with respect to the pristine material (76.3%). Sun's group [164] reported a multi-doping strategy for $LiCoO_2$, where Al was doped into Co sites and Nb/W into Li sites. In this material, Al doping helps stabilizing the structure at high voltage, while Nb/W doping increases interlayer spacing and enhanced Li^+ diffusion. Overall, the dual-site doping improves the cycling stability of the material, resulting in a delivered capacity of 142.1 mAh g^{-1} at 15C and a capacity retention of 60.4% after 1000 cycles at 10C up to 4.5 V. Similarly, Zhang et al [171] achieved stable cycling of $LiCoO_2$ at 4.6 V through trace co-doping with Ti, Mg, and Al. The presence of Mg and Al reduces high-voltage phase transitions by altering phase behavior during the (de)lithiation process, while Ti modifies the microstructure of the particles and suppresses oxygen reactivity at high voltages. The synergistic effects of these doping elements significantly enhance the electrochemical performance.

In SIBs, Fu et al [172] found that co-doping Mg^{2+} and Ca^{2+} in $Na_{0.67}Ni_{0.33}Mn_{0.67}O_2$ could reduce O-type stacking in high-voltage regions. DFT studies revealed that Mg^{2+} and Ca^{2+} hindered high-voltage reactions, such as Ni-O bonding issues, enhancing structural stability under these conditions. Anilkumar and Nair [173] reported the synergistic effect of Li and Cu co-doping in the TM layer in reducing Na^+/vacancy ordering and P2-O2 phase transition in P2-$Na_{0.67}Ni_{0.33}Mn_{0.67}O_2$. The presence of Li and strong bonding between Cu-O inhibited irreversible P2-O2 phase transition, preventing the formation of O2/OP4 phase upon charging to 4.2 V. Shen et al [153] synthesized a quasi-zero-strain P2-$Na_{0.75}Li_{0.15}Mg_{0.05}Ni_{0.1}Mn_{0.7}O_2$ (LMNM) cathode by co-doping Li and Mg into P2-$Na_{2/3}Ni_{1/3}Mn_{2/3}O_2$. *In-situ* XRD results indicated that the synergistic effect of Li and Mg suppressed the slip of the P2-O2 transition (Fig. 4**e**), leading to a minimal volume change of just 0.49%. After 500 cycles at 5C rate, the capacity retention was maintained at 83.9%.

In PIBs, Zhong et al [22] extended this approach by substituting Mn^{3+} ions with Co^{3+} and Fe^{3+} ions in the TM layers, creating a double-doped P3-$K_{0.5}Mn_{0.7}Co_{0.2}Fe_{0.1}O_2$ material. This substitution reduced structural degradation induced by the Jahn-Teller effect of Mn^{3+}. The smaller ionic radii of Co^{3+} and Fe^{3+} ions resulted in thinner TMO_2 layers and increased separation between neighboring layers, facilitating potassium ion diffusion and buffering volume changes during cycling. The structure's alteration also slows down the phase transition from P3 to O3, enhancing the structural resilience of the material. Furthermore, the increased layer separation also stabilizes the material by mitigating O^{2-} ion release during cycling.

3.2.2. Multi-atom doping in A_xTMO_2 with cations and anions

In an effort to combine the benefits of both cation and anion doping, Guo et al [174] synthesized $Li_{1.2}Ni_{0.13}Co_{0.13-x}Mn_{0.54}Al_xO_{2(1-y)}F_{2y}$ co-doped with Al and F. This co-doping alleviated the layered-to-spinel phase transition, reducing capacity and voltage decay (after 150 cycles at 0.5 C the discharge capacity was 217 mAh g^{-1} with 88.21% retention and the average discharge voltage decay was 0.4019 mV. Furthermore, with increased electronic and ionic conductivity, this co-doping method improved rate capability, providing a discharge capacity of 157 mAh g^{-1} at 10 C. The thermal stability was also enhanced, as evidenced by the less intense exothermic peak (221 J g^{-1} at 273°C) compared with the undoped material (755 J g^{-1} at 210°C). Similarly, Chae et al [108] synthesized the co-doped compound P2-$Na_{0.46}Mn_{0.93}Al_{0.07}O_{1.79}F_{0.21}$, where the incorporation of Al in the TM layer stabilized the layered structure by affecting the Jahn-Teller distortion of Mn^{3+}. Meanwhile, the substitution of F reduced the Na^+ diffusion energy barrier by altering the bonding energy between anions and cations and increasing the interlayer spacing.

3.3. Surface doping in A_xTMO_2

Surface doping involves the introduction of specific elements onto the surface or near-surface regions of a material, typically within a few to tens of nanometers in depth, to enhance the physical and chemical properties of the surface or interface [39,61,76,100]. Unlike bulk doping, where elements are uniformly distributed throughout the material, surface doping focuses on optimizing surface performance while preserving the internal structure, thus minimizing capacity loss. This approach has gained significant attention for its effectiveness in mitigating interfacial side reactions in lithium-based layered oxides, making it a prominent research area in recent years [40,72,175,176].

In NRLOs, Kong et al [177] modified $LiNi_{0.8}Co_{0.2}O_2$ with surface gradient doping of Ti, achieving a clean surface free of any residual deposits. TEM analysis revealed a about 6 nm disordered layered phase at the particle surface, while the rhombohedral structure remained intact in the core. This disordered phase on the particle surface enhanced rate capacity and cycling stability. Sun's group [178] modified the $LiNi_{0.9}Co_{0.05}Mn_{0.05}O_2$ cathode using the non-metallic element B

doping to alter its surface microstructure. B doping preferentially reduced the surface energy of the (003) plane, creating a highly textured microstructure. This alleviated internal strain during delithiation, enhanced Li migration, and reduced microcracks.

In LRLOs, Liu et al [179] employed Nb^{5+} surface doping on $Li_{1.2}Mn_{0.54}Ni_{0.13}Co_{0.13}O_2$ to suppress TM migration and oxygen vacancies. Nb^{5+} ions localized near the Li layers formed strong Nb-O bonds, which stabilized the layered structure, inhibited the transition from layered to spinel phases at the surface, and reduced surface oxygen evolution, thereby improving structural reversibility and discharge voltage stability. Building on this, Cheng et al [100] developed a dual-gradient surface doping strategy using Zn and Ti. Zn content decreased from the interface to the particle interior, while Ti content increased to stabilize at a constant level. Zn ions could incorporate into both the Li and TM layers, further enhancing surface stability.

From these studies, it is clear that both bulk doping and surface doping can achieve significant modifications, albeit with distinct focuses. Bulk doping targets the overall structural stability and evolution, whereas surface doping concentrates on mitigating surface side reactions and preventing microcrack formation. Each approach offers unique advantages, allowing for tailored optimization to meet the specific requirements of different layered cathode materials.

4. From doping to high-entropy approaches

The doping strategy entails incorporating a small quantity of foreign elements (typically one or two) into the base material to modify its properties. The amount of doping elements is typically minimal, usually comprising only a few atomic percent [36,109,132,134,146,171]. In contrast, the high-entropy approaches are emerging material design strategies that incorporates multiple elements — typically five or more — into the material's lattice, resulting in the formation of multi-component high-entropy materials or entropy-stabilized compounds [180–184].

The high-entropy concept was first demonstrated in high-entropy alloys. In 2004, Yeh et al [185] and Cantor et al [186] introduced a pioneering concept in their papers, describing a new class of alloys composed of several elements in almost equiatomic proportions. These alloys were subsequently found to exhibit enhanced mechanical properties and finely tuned catalytic activity, highlighting their promising applications in engineering and catalysis [187,188]. In 2015, the high-entropy concept was first applied to multi-component oxides, such as the $Cu_{0.2}Co_{0.2}Ni_{0.2}Mg_{0.2}Zn_{0.2}O$,[189] demonstrating the entropy stabilization effect in oxide compounds. Since then, the high-entropy concept has rapidly expanded to other materials [181,190,191]. Recently, high-entropy materials have garnered significant attention from researchers due to their potential in electrochemical energy storage [182,192–195].

4.1. Basic concepts of high-entropy materials

"High-entropy" is a term created to distinguish materials with complex compositions from those with simpler compositions. The so-called "high-entropy" refers to the mixing entropy of the system, including configurational, vibrational, electronic, and magnetic entropy among others [196,197]. Although all these factors contribute to the total mixing entropy, the complexity of chemical bonds, physical and mechanical properties, and structure makes it difficult to quantify entropy values other than configurational entropy in ceramic systems [180]. Therefore, while acknowledging the importance of other entropy values, we categorize materials primarily based on configurational entropy: [198] materials are defined as high-entropy if their ΔS_{config} exceeds the critical threshold value of high-entropy (1.5R), as "medium-entropy" if their ΔS_{config} between 1R and 1.5R, and as "low-entropy" if their ΔS_{config} is less than 1R. The specific formula for calculating configurational entropy is as follows:

For single-phase solid solutions with N elements uniformly distributed, the system's configurational entropy can be approximately expressed by the following equation: [197]

$$\Delta S_{config} = -R\sum_{i=1}^{N} c_i lnc_i \tag{1}$$

where R represents the gas constant, N denotes the number of components, and c_i signifies the mole fraction of component i. When the mole ratios of each element are equal, the configurational entropy of the system reaches its maximum value (Fig. 6**a**): [182]

$$\Delta S_{config} = RlnN \tag{2}$$

In reality, the presence of multiple sublattice compositions in A_xTMO_2 systems complicates the calculation of configurational entropy. Therefore, their configurational entropy can be calculated using the following formula: [48,51,199,200]

$$\Delta S_{config} = -R\left[\sum_{a=1}^{L} x_a lnx_{a\,AM-site} + \sum_{b=1}^{N} y_b lny_{b\,TM-site} + \left(R\sum_{c=1}^{M} z_c lnz_c\right)_{O-site}\right] \tag{3}$$

where x_a, y_b, and z_c are the mole fractions of the elements that occupy the AM layer, TM layer, and O layer, respectively. Meanwhile, L, N, and M are the number of cations present on AM sites, TM sites, and O sites, respectively.

In addition to the definition based on configurational entropy values, high-entropy materials can also be defined based on their composition. Materials are typically labeled as "high-entropy" if they consist of five or more main elements, each having an atomic percentage ranging from 5% to 35% [190].

As the high-entropy strategy advanced, the family of high-entropy materials gradually expanded to ceramic system, including oxides, [196,201] borides,[202,203] oxyfluorides,[162] carbides,[204,205] nitrides,[206,207] and other materials,[183,208–213] experiencing sustained growth in popularity. Currently, high-entropy alloys and high-entropy ceramics with various structures have garnered significant attention in the field of electrochemical energy storage and conversion (Fig. 6**c, d**) [190].

Compared to conventional materials, multi-component disordered high-entropy materials typically exhibit distinct characteristics, which can be summarized into four main classes: entropy stabilization, sluggish diffusion, lattice distortion, and the cocktail effect [180,210,215,216].

Entropy stabilization effect: The concept of entropy stabilization was first introduced by Rost et al. in alloy systems [189]. They observed that the four-component material could not achieve a single-phase structure at the same transition temperature (T) of the five-component system. Additionally, when the component ratios deviated from equimolar proportions, the single-phase transition temperature for five-component systems increased accordingly. Therefore, in Rost's experiments,[189] the entropy stabilization effect was shown to reduce the synthesis temperature required for forming single-phase solid solutions, thereby promoting their formation. As illustrated by this work, [189] the conclusion regarding entropy-stabilized phases/structures requires extensive experimental data for validation, and it significantly differs from the structural stability observed in some high-entropy materials, which will be discussed in detail in section 4.3.1.

Sluggish diffusion effect: In high-entropy alloys, the limited number of vacancies restricts the cooperative diffusion of solute atoms to new phase nucleation sites [215]. The lower atomic diffusion efficiency results in a significantly slower phase transition rate for high-entropy alloys compared to traditional alloys [217]. Consequently, component segregation frequently occurs within high-entropy alloys, often resulting in precipitates on the sub-10-nanometer scale [218]. In HE-TMLOs, this

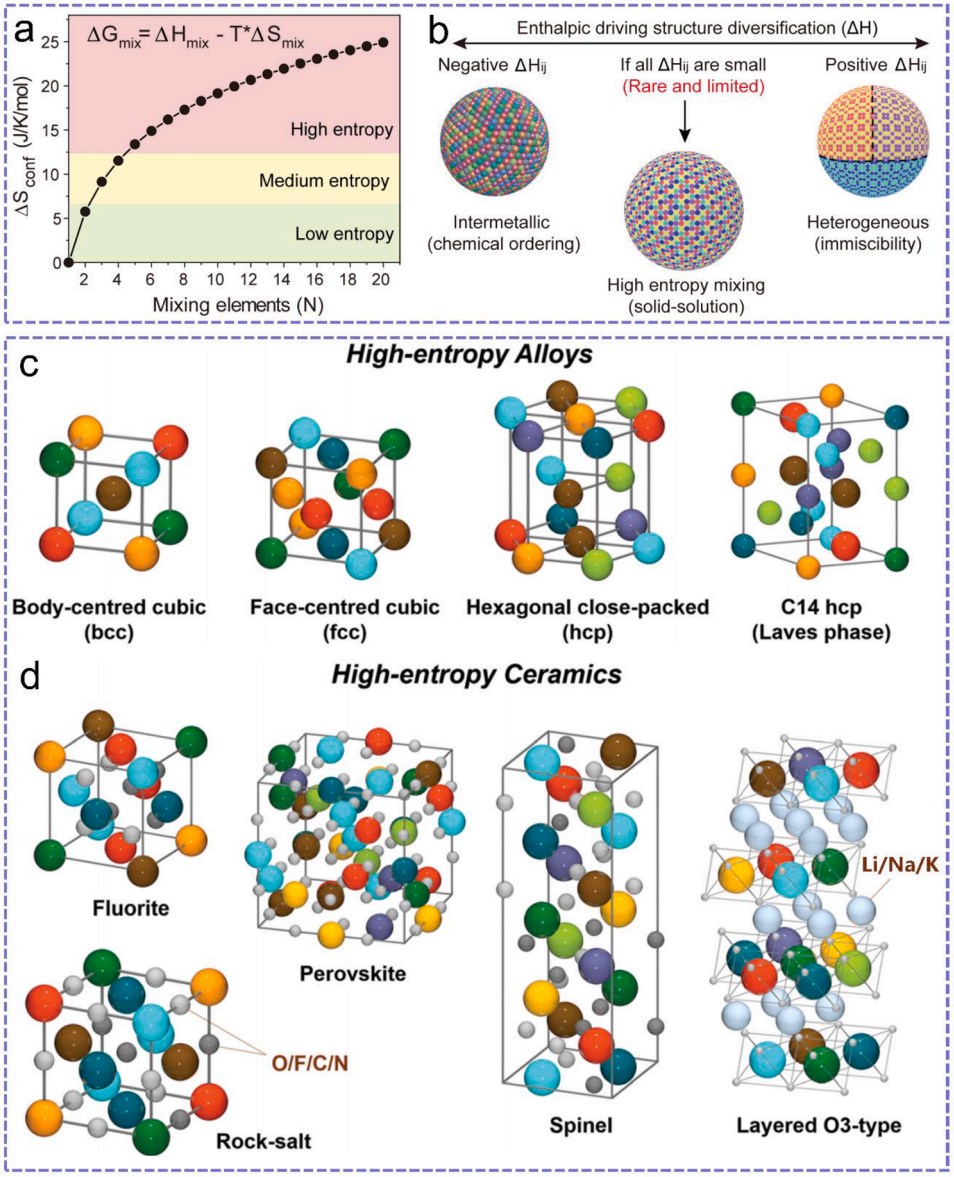

Fig. 6. Thermodynamic analysis of high-entropy mixing considers both entropy (a) and enthalpy (b). Reproduced with permission [214]. Copyright 2022, American Association for the Advancement of Science. (c-d) The crystal structures of high-entropy materials used in energy-related fields: (c) high-entropy alloys (d) high-entropy ceramics. Reproduced with permission [190]. Copyright 2021, Royal Society of Chemistry.

segregation may occur near the material's surface, forming a high-entropy region that inhibits interfacial side reactions and enhances structural stability.

Lattice distortion effect: Lattice distortion occurs due to variations in atomic sizes and bond energies between different elements [190]. The degree of this distortion is dependent upon the types of atoms occupying specific positions and their local environment [197]. Recent research has indicated that the complex elemental composition of HE-TMLOs can result in differences in local coordination environments. The variations may lead to the strengthening of individual TM-O bonds, resulting in a pinning effect that suppresses oxygen loss [47,219–221] Additionally, the local electronic environment could be adjusted, thereby influencing ion transport kinetics [222]. The enhancing process is probably associated with lattice distortion, and the specific mechanisms will be explored in the subsequent sections.

Cocktail effect: The cocktail effect refers to the enhancement of overall performance resulting from the mixing of various elements [223]. This phenomenon commonly occurs as a consequence of the synergistic effect among multiple elements. Any changes in the type or concentration of elements can alter their subtle interactions, thereby indirectly impacting the microstructure [180]. Therefore, in the electrochemical applications of high-entropy materials, the performance can be tailored by optimizing the combination of elements and the stoichiometric ratios of the components.

4.2. *High-entropy approaches in TMLOs*

With the gradual development of the high-entropy concept, the creation of compositionally complex material systems has emerged as a new trend [48–50,181,184,191,193,195,201]. This development has also given rise to various other modification approaches, such as entropy-tuning and high-entropy (compositionally complex) doping [47,219–221,224,225]. Similar to traditional doping, high-entropy strategies involve the introduction of multiple elements into different lattice sites, modifying the intrinsic physical and chemical properties of the material. In layered oxides, doping typically occurs at the AM sites,

TM sites, and O sites. However, in most reported high-entropy layered oxides, the incorporated elements predominantly occupy the TM sublattice, where the high-entropy effect plays a critical role in stabilizing the layered framework and regulating electrochemical properties. Future studies may explore the feasibility of extending high-entropy strategies to AM and O sites, which could introduce additional degrees of tunability in material design. While many published studies present high-entropy approaches as an extension of conventional multi-element doping, it is important to emphasize that as the number of incorporated elements increases, the interactions among them become more complex and pronounced. Additionally, the rise in elemental diversity leads to a corresponding increase in configurational entropy (degree of disorder) within the material system. Therefore, while acknowledging the similarities between high-entropy strategies and conventional multi-element doping, it remains reasonable to explore high-entropy approaches as a distinct and novel modification method.

To prevent potential confusion surrounding the high-entropy concept, this article categorizes high-entropy strategies into three main types (see Section 4.3.3 for additional types, such as entropy-extension coatings) and explores their similarities and differences (Fig. 7):

High-Entropy Structure: A high-entropy structure refers to a material system where the configurational entropy is greater than or equal to the high-entropy threshold (1.5R). In such materials, five or more elements can coexist at equal or near-equal molar ratios (or with element concentrations between 5% and 35%), sharing the same lattice site and forming a unique high-entropy configuration [41,46,226–228]. This configuration typically exhibits enhanced structural stability compared to simpler compositional systems [41,46,227]. Moreover, the coexistence of multiple elements creates a relatively disordered atomic arrangement, which significantly influences ion diffusion kinetics [229]. It is worth noting that the high-entropy concept is still in its early exploratory stage, with most current studies on high-entropy structures focusing on the TM sites. In the future, the development of multi-site high-entropy structures will become a new focal point in the design of high-entropy materials.

High-Entropy Doping: Unlike traditional multi-element doping, high-entropy doping adheres to strict standards regarding both the variety of elements introduced and their stoichiometric ratios. In terms of element variety, high-entropy doping typically involves the introduction of four or more foreign elements into a base model [47,221,224,225,230,231]. Generally, these elements share the same lattice site; however, in some cases, certain ions may escape and migrate to other sites during synthesis [221]. The number of elements introduced in traditional multi-element doping is usually fewer (up to three),[66,70,168,175] and the doping sites are more flexible,[35] including single-site doping [116] and doping across multiple sites [119]. Regarding stoichiometric ratios, high-entropy doping involves elements that are present in limited concentrations (each $\leq$ 5%) but maintain equal or near-equal molar ratios, ensuring a relatively uniform distribution of element concentrations [219,225,232]. In contrast, traditional multi-element doping does not impose strict requirements on the concentrations of the added elements, and in some cases, individual elements may be present at relatively high levels [131,233].

The differences in the number of elements and their concentration result in distinct focuses for these two modification strategies in regulating the electrochemical performance of batteries. Multi-element doping tends to focus on selecting and optimizing the concentration of each element based on its specific contributions to material properties. In contrast, high-entropy doping places greater emphasis on the choice of element types [47,219,221]. This approach aims to optimize the combination of elements and fine-tune their interactions, ultimately enhancing the overall performance of the material.

Entropy-Tuning: Entropy-tuning, similar to high-entropy structures, aims to enhance the disorder and configurational entropy of a material system, focusing on achieving a higher degree of disorder [44,52,150,234]. This approach typically involves a dominant element constituting over 50% of the composition, which influences the configurational entropy values to generally fall within the range of 1R to 1.5R [44,52,235]. By precisely adjusting element concentrations, entropy tuning seeks to optimize this configurational entropy. While materials modified through this method can show significant increases in disorder, the predominance of the main element prevents them from reaching the high-entropy threshold [236–238]. Nevertheless, entropy-tuning strategies are valuable for improving cycling stability and other performance aspects in battery materials [49,238].

As discussed above, these high-entropy approaches indeed have some fundamental differences. However, they all demonstrate

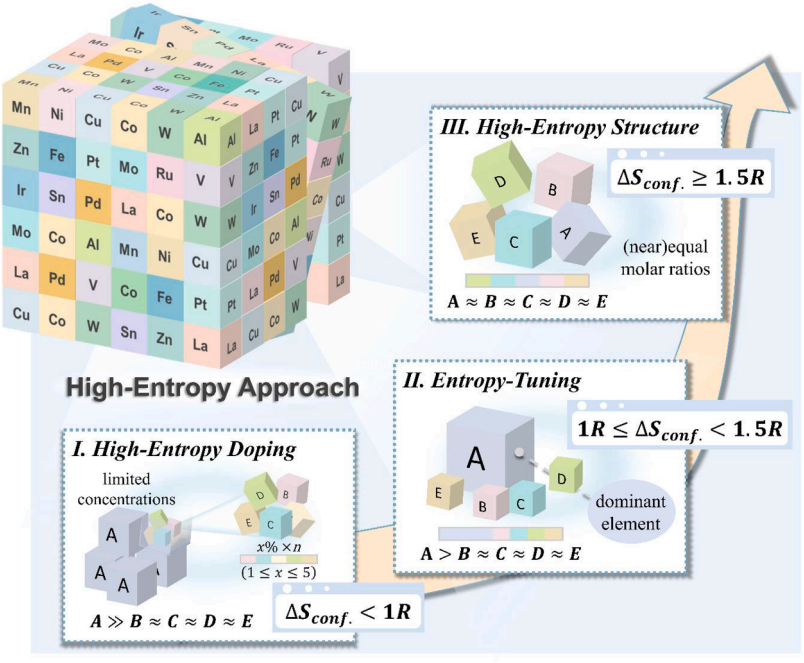

Fig. 7. Main classifications of high-entropy approaches.

significant potential in enhancing the electrochemical performance of materials. To better understand the underlying mechanisms of these modification strategies and to further establish the relationship between configurational entropy and enhanced material properties, this paper summarizes several distinct effects of high-entropy approaches observed in TMLOs: structural stabilization, high disorder characteristics, entropy-enhanced local regulation effect, the cocktail effect — synergy of multi-elements, and entropy extension effect. Detailed discussions can be found in Section 4.3.

4.3. The distinct effects of high-entropy approaches

HE-TMLOs, entropy-tuned and high-entropy doped cathodes often exhibit improved structural stability and ion diffusion kinetics compared to traditional materials, resulting in enhanced cycling stability and rate performance. Additionally, these materials typically exhibit higher disorder, a more complex local environment, and more effective elemental synergy than conventionally doped materials. These inherent characteristics are closely tied to their performance improvements.

In light of this, the following sections will systematically summarize the five distinct properties of TMLOs optimized through high-entropy approaches, including structure stabilization, high disorder characteristics, cocktail effect — synergy of multi-elements, entropy extension and local regulation effect (Fig. 8). Furthermore, relevant case studies will be explored to delve into how these properties influence the electrochemical performance of these materials.

4.3.1. Structure stabilization

In high-entropy materials, the interactions between elements often result in enhanced comprehensive properties, such as structural/phase stability. Most studies attribute these phenomena to the entropy stabilization effect. However, it is important to note that entropy stabilization only occurs under specific conditions and requires substantial experimental data to support its validity.

The equation (4) (Gibbs-Helmholtz equation) represents the change in Gibbs free energy due to the mixing in a high-entropy system [184, 192,239–242].

$$\Delta G_{mix} = \Delta H_{mix} - T\Delta S_{mix} \tag{4}$$

where $\Delta G_{mix}$is the change of Gibbs free energy, ΔH_{mix} is the change of enthalpy, ΔS_{mix} is the change of entropy, and T is the temperature. The Gibbs-Helmholtz equation demonstrates a competition between the $-T\Delta S_{mix}$ term and the ΔH_{mix} term (Fig. 6**a, b**). The formation of a single-phase solid solution will be promoted when the usually negative term $-T\Delta S_{mix}$, driven by ΔS_{mix}, overcompensates for the usually positive ΔH_{mix}, resulting in a more negative ΔG_{mix}. However, it is important to note that various factors, such as defects, can influence phase stability. Entropy stabilization only occurs when entropy plays a crucial role in the thermodynamic landscape and governs the structure and phase behavior [180]. Currently, the phenomenon of neat entropy stabilization has been confirmed exclusively for individual materials [189].

In layered oxide materials, phase transition behavior is driven by a combination of factors. During the charge and discharge processes, changes in electronic structure and chemical environment, along with lattice distortions occurring during the insertion and extraction of alkali metal ions, contribute to the instability of the original phase, thereby altering the material's phase transition characteristic [2,54]. As discussed in the previous sections, traditional element doping typically involves adding extra alkali metal ions (e.g., Li^+, Na^+, K^+) to the AM layer to stabilize the host structure,[154–158] while elements like Mg^{2+},[90] Zn^{2+},[150] and Ca^{2+} [151] may also be selected as dopants to create a unique pillar effect that ensures the integrity of the interlayer structure during cycling. Additionally, in the TM layer, some electrochemically inert elements (e.g., Ti^{4+},[128] Sn^{4+} [116]), which do not participate in redox reactions, are often used to stabilize the material's structure. The high-entropy strategy builds on these traditional doping approaches while introducing additional structural stabilization through the formation of high-entropy configurations [180]. This approach shows significant potential in alleviating lattice strain during ion insertion and extraction and in suppressing the occurrence of irreversible phase

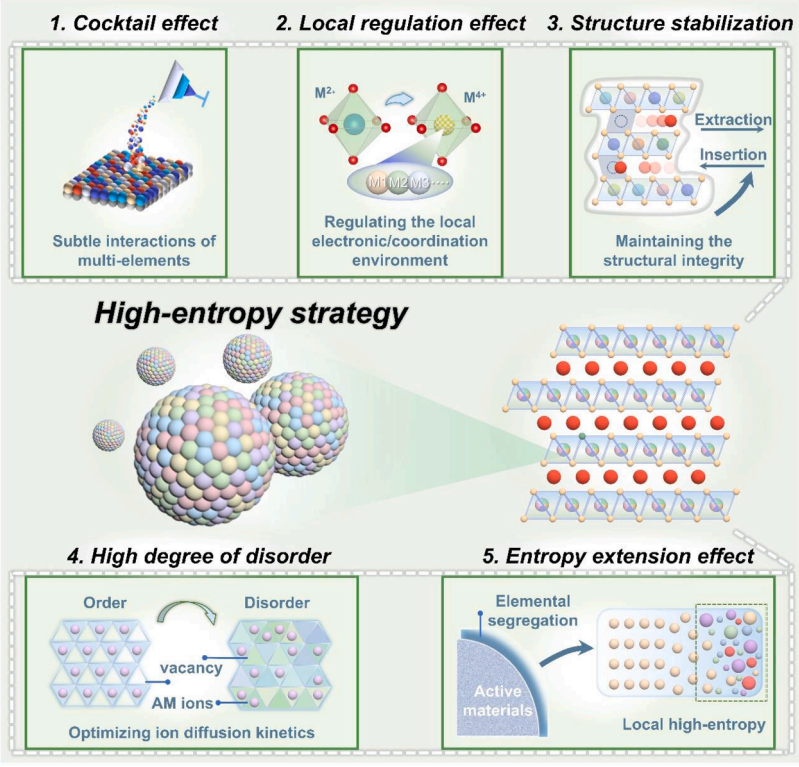

Fig. 8. The distinct effects of high-entropy approaches in TMLOs.

transitions [193,243]. Although it cannot be conclusively stated that these high-entropy materials are entropy-stabilized, their beneficial effects on structural stability are evident, even if the underlying mechanisms remain elusive [180]. These effects significantly improve the cycling stability of high-entropy materials by enhancing the reversibility of redox reactions [190]. For instance, Zhao et al [46] utilized a high-entropy strategy to design an O3-type cathode material, $NaNi_{0.12}Cu_{0.12}Mg_{0.12}Fe_{0.15}Co_{0.15}Mn_{0.1}Ti_{0.1}Sn_{0.1}Sb_{0.04}O_2$, which unique high-entropy configuration modifies the material's phase characteristics endowing it with excellent long-term cycling stability, maintaining 83% of its capacity retention after 500 cycles.

From a microscopic perspective, the interactions between multiple atoms or ions - including Coulombic attractions/repulsions,[244] electrostatic forces,[245] and van der Waals forces [246] - can, to some extent, drive the phase transition behavior of materials. In practical material design, these interactions can be altered by adjusting the combinations of elements to regulate phase transitions and enhance structural stability [131,247]. This conclusion has been corroborated by various studies utilizing traditional element doping methods. For example, Guo et al [248] successfully adjusted the interactions between transition metals and oxygen through a Cu/Ti co-doping strategy, resulting in the synthesized $NaNi_{0.45}Cu_{0.05}Mn_{0.4}Ti_{0.1}O_2$ effectively suppressing charge ordering and complex phase transitions during cycling, while improving air stability. In contrast, under high-entropy conditions, the presence of various transition metals complicates these interactions, which may balance or synergize with one another, significantly affecting the interlayer structural characteristics of layered oxides (including interlayer spacing and structural stability) and subsequently altering the material's phase transition properties.

In addition to the diverse elemental composition and subtle micro-level interactions between atoms or ions, the stoichiometry of elements plays a crucial role in determining the structural stability of materials [190,199]. In high-entropy materials, five or more elements are typically present in equimolar or near-equimolar ratios, a feature not commonly observed in traditional elemental doping [243]. For instance, some electrochemically inert elements, such as Mg^{2+}, can reach equal or near-equimolar concentrations (theoretically up to 0.2 for five-component high-entropy materials) [183,209]. This not only significantly enhances the stability of materials, but also prevents the phase separation issues typically seen in traditional doping when the concentration of inert elements exceeds 0.1 [249]. The precise control of stoichiometry is therefore essential for maintaining the structural integrity and electrochemical performance of high-entropy materials, offering a distinct advantage over conventional materials [199].

4.3.2. High disorder characteristics

In layered oxides, disorder is closely associated with various chemical interactions, such as size effects [233] and electrostatic interactions. As a critical material design parameter, the disorder can be modulated by manipulating chemical parameters to improve material properties [250]. In high-entropy oxides, the introduction of multiple transition metals further increases the configurational entropy of the system, often leading to a more disordered internal environment. This disorder significantly impacts both the micro- and macro-level properties of the materials, thereby enhancing their electrochemical performance.

During electrochemical cycling, the extraction of sodium ions results in the formation of vacancies and the oxidation of TMs. Both of these processes thermodynamically drive the in-plane rearrangement of the remaining sodium ions and vacancies, leading to a local transition from order to disorder (Na^+/vacancy ordering-disordering) and even triggering irreversible phase transitions [251]. Studies have shown that a high-entropy strategy can effectively suppress Na^+/vacancy ordering, thereby mitigating these transitions. For example, Ding et al [41] designed an O3-type high-entropy layered oxide, $NaNi_{0.25}Mg_{0.05}Cu_{0.1}Fe_{0.2}Mn_{0.2}Ti_{0.1}Sn_{0.1}O_2$ (HEO424). The high-entropy configuration of HEO424 effectively reduced Na^+/vacancy ordering, and fewer phase transitions (including the Na^+/vacancies order-disorder transition), were detected in this material. These characteristics endowed HEO424 with excellent long-term cycling stability, achieving a capacity retention of 75% after 500 cycles.

Research has shown that the atomic arrangement in the TM layer is affected by the type and number of elements present [233,252]. A more disordered arrangement of TMs can suppress Na^+/vacancy ordering, thereby optimizing ion diffusion. For instance, Wang et al [233] introduced Cr^{3+} and Ti^{4+} into Na_xTMO_2, successfully inhibiting Na^+/vacancy ordering. The improved sodium-ion diffusion kinetics resulted in the designed P2-type cathode material, $Na_{0.6}[Cr_{0.6}Ti_{0.4}]O_2$, exhibiting excellent rate performance. In HE-TMLO, the introduction of multiple TM elements leads to a more disordered atomic arrangement in the TM layers, which further preventing Na^+/vacancy ordering. Wang et al [237] designed a P2-type entropy-turned cathode with a complex atomic arrangement, $Na_{0.65}Mn_{0.65}Cu_{0.2}Li_{0.06}Mg_{0.015}Ti_{0.015}Al_{0.015}Zr_{0.015}Y_{0.015}La_{0.015}O_2$ (Mn-Cu-HEO). Benefiting from the reduced Na^+/vacancy ordering during desodiation/sodiation processes, Mn-Cu-HEO exhibits excellent cyclic stability, with 87.2% capacity retention after 500 cycles.

4.3.3. Entropy extension effect

During the surface doping/coating modification process of layered oxides, certain dopants (elements) have a tendency to undergo self-segregation, which may be attributed to their solubility and the high temperature heating involved in the synthetic processes. This results in the enrichment of the material's surface or coating layer [253–259]. The rise in the quantity of elements (compositionally disorder) results in an escalation of the entropy value within this specific area, which is referred to as the entropy extension effect. Such effect can alter the interfacial properties of electrode materials, significantly suppressing side reactions like oxygen evolution.

For instance, Tan et al [253] utilized the entropy extension effect to construct a high-entropy region with a disordered rock salt structure on the near-surface of $LiCoO_2$ (LCO) particles. This complex surface effectively mitigated oxygen evolution and Co ion dissolution, preventing cathode electrolyte interface formation and near-surface structure degradation. As a result, the modified LCO achieved a capacity retention of 86.3% after 800 cycles within the voltage range of 2.8 to 4.6 V, and when the lower voltage limit was adjusted to 3.0 V, the capacity retention was 72.0% even after 2000 cycles.

This entropy extension effect also occurs during the surface modification of cathode materials, leading to the formation of localized high-entropy regions in specific areas (such as the material's outer surface coating). Amine and colleagues [254] applied a mixture of $Nb_{12}WO_3$ and ZrO_2 nanoparticles onto the surface of $LiNi_{0.9}Co_{0.05}Mn_{0.05}O_2$ (NCM90) cathode material. They observed that some transition metal elements (Ni, Co, Mn) from NCM90 migrated to the surface layer and reacted with the nanoparticle mixture during heating, resulting in the formation of a new phase aligned along the original particle's layered direction. This epitaxial high-entropy coating significantly mitigated lattice dislocations/strain and oxygen release issues in NCM90. Compared to the unmodified NCM90, the material with the epitaxial high-entropy coating retained 96% of its capacity after 200 cycles at a 1C rate.

It is important to clarify that the entropy extension effect, while being a high-entropy approach, is not part of the mainstream high-entropy strategies discussed in Section 4.2, such as high-entropy structure, high-entropy doping, and entropy-tuning. Instead, it represents a distinct surface modification method where partial element segregation leads to the formation of high-entropy regions at the material's surface [253,255–259]. While this approach shares some common traits with high-entropy strategies—such as the incorporation of multiple elements and an increase in configurational entropy—it does not rely on site-specific doping within the material's bulk phase. Given the variability in elemental composition and doping sites in the spontaneously

formed coating, it is not appropriate to categorize this as a typical high-entropy doping strategy. However, it is undeniable that, as the number of elements increases, the resulting compositionally disordered phase plays a significant role in suppressing surface side reactions and enhancing electrochemical performance. Therefore, despite its differences from the primary high-entropy strategies outlined in Section 4.2, the entropy extension effect remains an important phenomenon in optimizing the electrochemical properties of layered oxides and is included in the discussion due to its significant impact on performance improvement.

This intriguing self-segregation behavior has actually been observed in high-entropy alloys, where the introduction of multiple elements can cause lattice distortion, leading to irregular fluctuations in lattice potential energy [215,260]. Vacancies in low potential energy act as potential wells, making it easier for atoms to diffuse into these positions. Consequently, the probability of atoms in low potential energy positions jumping out is significantly lower than that of atoms in high potential energy positions, hindering the diffusion process and reducing the diffusion rate [215]. Moreover, the range of potential energy fluctuations is proportional to the number of potential wells; larger fluctuations create more potential wells, resulting in higher energy barriers and activation energies. A similar vacancy filling diffusion mechanism occurs in high-entropy oxides, where slow diffusion kinetics within the material significantly reduce the rates of atomic diffusion and phase transitions,[199] potentially leading to element enrichment in specific areas and promoting the formation of localized high entropy.

4.3.4. Cocktail effect — Synergy of multi-elements

The synergistic effects of multiple elements, arising from their subtle interactions during mixing, are one of the key factors contributing to the overall performance enhancement of HE-TMLO [180,190]. These interactions are influenced by the types of elements introduced and their concentration, leading to changes in material properties. This characteristic endows HE-TMLOs with highly tunable properties, allowing for the customization of material performance based on the desired functional characteristics during the design process.

Drawing from the design experience of traditional layered oxides, electrochemically active elements (such as Ni, Fe, and Co) in the TM layer can serve as redox centers to contribute to capacity, while electrochemically inert elements (such as Zn, Ti, and Sn) can act as interlayer sliding inhibitors to stabilize the host structure. Additionally, the introduction of F at oxygen sites aids in charge compensation and helps maintain structural integrity. For example, Wang et al [200] meticulously selected elements to design a six-component O3-type layered oxide cathode material, $NaNi_{0.2}Fe_{0.2}Mn_{0.35}Cu_{0.05}Zn_{0.1}Sn_{0.1}O_2$. In this material, Ni, Fe, and Cu act as charge compensators, while the other elements serve as interlayer slipping inhibitors, effectively suppressing irreversible phase transitions and structural degradation. Benefiting from the synergistic effects of multiple elements, this material exhibits enhanced electrochemical performance, maintaining a reversible specific capacity of 128 $mAh{\bullet}g^{-1}$ at a current density of 0.1C and achieving 87% capacity retention after 500 cycles at a current density of 3C.

It is worth noting that this effect, as a positive outcome of elemental mixing, can sometimes be observed in traditionally doped materials. However, in high-entropy materials, where at least five major elements are used to enhance material properties, the synergistic interactions induced by the "cocktail effect" are much more pronounced and complex [48,215]. As such, the cocktail effect-driven synergy has been regarded as one of the most distinctive features of high-entropy materials. Furthermore, the cocktail effect can occasionally deviate from simple mixing rules, providing a framework to explain the factors and mechanisms responsible for these deviations [215]. This also accounts for the unexpected performance characteristics often observed in high-entropy materials following the mixing of multiple elements, thereby offering potential application value [180,190,214].

4.3.5. Entropy-enhanced local regulation effect

The local environment of electrode materials is a critical factor in determining their electrochemical performance and structural stability. Unlike conventional materials with single or limited components, high-entropy materials, which typically consist of five or more elements, form a highly mixed, multicomponent structure where these elements are uniformly distributed in the lattice. This creates a more complex and diverse local environment compared to traditional single or binary electrode materials [180]. Such a varied local environment exhibits strong regulatory characteristics, playing a crucial role in tailoring the electronic structure and coordination environment of the material, thereby significantly influencing the properties of layered oxides.

In practical design, adjusting the elemental composition can modify the electronic local environment of high-entropy oxides, thereby altering the density of states (DOS) and the distribution of electrons near the Fermi level [222]. This adjustment can facilitate Na^+ diffusion and improve the rate performance of batteries. Wang et al [222] employed this strategy to design an O3-type layered oxide, $Na_{0.9}Ni_{0.2}Fe_{0.2}Co_{0.2}Mn_{0.2}Ti_{0.15}Cu_{0.05}O_2$ (NaNFCMTC-1). The study showed that the high-entropy strategy effectively regulated the local electronic structure of the TM layers in NaNFCMTC-1, enhancing the TMO_2 framework and expanding the sodium ion diffusion channels. This leads to increased reversibility of TM redox reactions, a smoother transition from O3 to P3 phase, and a lower energy barrier for Na^+ migration.

Moreover, studies have shown that entropy-tuned oxides exhibit a stable local coordination environment, which significantly aids in maintaining the structural integrity and fixing oxygen during ion intercalation and deintercalation [47,180,219,220,261,262]. For instance, Xin and colleagues employed high-entropy doping to modify NMC811 and NMC532, designing cobalt-free cathode materials, $LiNi_{0.8}Mn_{0.13}Ti_{0.02}Mg_{0.02}Nb_{0.01}Mo_{0.02}O_2$ [47] and $LiNi_{0.5}Mn_{0.43}Ti_{0.02}Mg_{0.02}Nb_{0.01}Mo_{0.02}O_2$ [220]. The results from various characterizations indicated that these materials maintain a stable local coordination environment throughout the cycling process, effectively mitigating the structural degradation and oxygen loss commonly observed in traditional Ni-rich cathode materials. Additionally, they exhibit enhanced thermal stability and smaller volume changes.

5. Applications of high-entropy approaches in A_xTMO_2

The following sections will delve into how high-entropy approaches applied across different battery chemistries, including Li-ion, Na-ion, and K-ion batteries, offer new perspectives for battery design and innovation.

5.1. Applications of high-entropy approaches in Li_xTMO_2

In the early exploration of high-entropy lithium-containing cathodes, researchers focused on nearly equimolar high-entropy transition metal layered oxides (HE-TMLOs) (see Table 2). In 2020, Breitung's group [263] synthesized a series of equimolar single-phase HE-TMLOs using aerosol spray pyrolysis and high-temperature annealing. Advanced characterization techniques, including XRD, TEM, XPS, ICP-OES, and Mössbauer spectroscopy, confirmed the formation of uniform single-phase layered solid-solution structures capable of lithium storage, even under certain degrees of Li/TM mixing. This work highlighted the relevance of Hume-Rothery's second rule for solid-solution formation, which specifies that ionic radii differences should not exceed 15%, and elements should have similar crystal structures, valence electrons, and electronegativity [263]. However, as research progressed, it became evident that equimolar HE-TMLOs exhibit suboptimal performance in terms of discharge capacity, cycling stability, and production costs compared to commercial cathodes. For example, Chen et al [264] reported that $LiNi_{0.2}Co_{0.2}Mn_{0.2}Fe_{0.2}Al_{0.2}O_2$, initially studied by Breitung's group,[263] showed rapid capacity decay due to the formation of a spinel M_3O_4 phase on the surface, caused by the migration of TM ions.

Table 2
Summary of exploration of HE-TMLOs in layered cathodes for LIBs.

Cathode	Voltage range [V]	Initial capacity [mAh g^{-1}]	Entropy value	Ref
$Li(NiCoMnAlZn)_1O_2$	3-4.5	60	1.61R	[263]
$Li(NiCoMnAlFe)_1O_2$	3-4.5	45	1.61R	[263]
$LiNa(NiCoMnAlFe)_1O_2$	3-4.5	100	1.75R	[263]
$LiNi_{0.47}Co_{0.2}Mn_{0.18}Mg_{0.04}Al_{0.04}Cr_{0.02}Ti_{0.02}V_{0.015}Cu_{0.015}O_2$	/	/	1.53R	[263]
$LiNi_{0.46}Co_{0.2}Mn_{0.2}Mg_{0.04}Al_{0.04}Cr_{0.015}Ti_{0.015}Zr_{0.015}Cu_{0.015}O_2$	/	/	1.51R	[263]
$LiNi_{0.2}Mn_{0.2}Co_{0.2}Fe_{0.2}Ti_{0.2}O_2$	2.6−4.4	160	1.61R	[266]
$LiNi_{0.2}Co_{0.2}Mn_{0.2}Fe_{0.2}Al_{0.2}O_2$	2.8−4.5	70	1.61R	[264]
$Li_{1.2}Ni_{0.15}Co_{0.15}Al_{0.1}Fe_{0.15}Mn_{0.25}O_{1.7}F_{0.3}$	2.8−4.5	85.4	1.98R	[265]

To address this, Chen et al [265] partially substituted O^{2-} with F^-, creating $Li_{1.2}Ni_{0.15}Co_{0.15}Fe_{0.15}Al_{0.1}Mn_{0.25}O_{1.7}F_{0.3}$, which achieved a discharge capacity of 85.4 mAh g^{-1} with a retention rate of 71.5% after 100 cycles. While this was a marked improvement, these materials still lagged behind commercialized cathodes in terms of practicality.

Recognizing these limitations, the focus in LIB research shifted toward NRLOs and LRLOs, which are more promising for achieving high energy density. These materials require high concentrations of Ni and Li, making near-equimolar strategies impractical. To achieve this compositional enrichment, researchers have increasingly turned to high-entropy doping and entropy-induced modifications.

High-entropy doping and entropy tuning have emerged as effective strategies to balance high capacity and stability while reducing or eliminating cobalt usage [47,220,221,232]. Although these approaches do not meet the strict high-entropy threshold of 1.5R, the intricate interactions among elements during the mixing process significantly influence material properties. These interactions enhance performance and structural stability, demonstrating the potential of entropy-informed approaches to optimize cathode materials for future LIBs. Table 3 summarizes recent advancements in these strategies.

To enhance the cycling and thermal stability of NRLOs while reducing cobalt dependence, Xin's team [220] employed high-entropy doping strategy to modify the commercial NMC-532, resulting in the successful synthesis of cobalt-free, entropy-tuned cathode, $LiNi_{0.5}Mn_{0.43}Ti_{0.02}Mg_{0.02}Nb_{0.01}Mo_{0.02}O_2$ (HE-N50). Fourier-transformed extended X-ray absorption fine structures (FT-EXAFS) analysis was conducted to compare the lattice parameter changes of HE-N50 and NMC-532 before and after long-term cycling. The results revealed that while NMC-532 experiences significant changes in TM-O and TM-TM coordination numbers and distances, HE-N50, benefiting from its stable local coordination environment, maintains consistent interatomic peaks with minimal lattice parameter changes. This highlights the crucial role of the local coordination environment in suppressing lattice distortions and enhancing cycling stability. HE-N50 also demonstrated high specific energy (Fig. 9**a, b**) and excellent cycling stability (Fig. 9**c**), retaining 95% of its capacity after 1000 cycles at 1C in the 2.8-4.3 V voltage range in pouch-type cells [220]. Additionally, through a high-entropy doping strategy, Xin's team [47] designed $LiNi_{0.8}Mn_{0.13}Ti_{0.02}Mg_{0.02}Nb_{0.01}Mo_{0.02}O_2$ (HE-LNMO), which also shows promising performance. The XANES (Fig. 9**d, f**) and FT-EXAFS (Fig. 9**e**) analyses of HE-LNMO and $LiNi_{0.8}Mn_{0.1}Co_{0.1}O_2$ (NMC-811) revealed that the highly stable local coordination environment is in HE-LNMO is attributed to the combined "pinning effect" of high-valence Ti, Nb, and Mo. This effect localizes oxygen vacancies around these dopants, thereby reducing oxygen loss around the Ni redox centers. In this material, Ni and Mn had similar TM-O bond lengths while Ti, Nb and Mo had significantly shorter TM-O bonds resulting from stronger electrostatic interactions. Minimal changes in dopant-oxygen bonds after cycling confirmed that oxygen vacancies or defects were effectively "trapped" around the dopants, preventing crack formation through vacancy aggregation. This pinning effect inhibits lattice deformation (such as dislocation nucleation and slip) and the formation of nano/microcracks, resulting in improved capacity retention in HE-LNMO. After 100 cycles at 2.5 - 4.4 V (vs. Li/Li^+), the capacity retention rate was 98.5%, and after 50 cycles at 2.5 - 4.5 V (vs. Li/Li^+), it was 98%. In contrast, NMC-811 showed capacity retention rates of only 87.1% and 85.8% under the same conditions. The volume strain during operation dropped to 0.3%, well below the critical zero-strain threshold (1%) [47]. This significant reduction in lattice strain contributed to an ultra-stable lattice structure capable of resisting chemical-mechanical cracking and lattice defects during prolonged cycling. Additionally, the cooperative pinning effect of multiple dopants significantly reduced oxygen loss and the detrimental rock-salt phase conversion, leading to enhanced structural stability under harsh cycling and thermal conditions. Specifically, HE-LNMO exhibited superior thermal stability (Fig. 9**g, h**), retaining 96.6% of its capacity after 50 cycles at 50°C, compared to 90.3% for the commercial NMC-811 [47].

Transitioning from NRLOs to LRLOs, researchers have increasingly explored high-entropy strategies to tackle challenges such as capacity degradation and voltage fade during cycling. In this context, Song et al [219] employed a high-entropy approach to synthesize a Li-rich $Li_{1.0}Li_{0.15}Mn_{0.50}Ni_{0.15}Co_{0.10}Fe_{0.025}Cu_{0.025}Al_{0.025}Mg_{0.025}O_2$ (E-LRM), where the octahedral TM sites are occupied by eight elements. Co^{3+}, Ni^{2+}, Fe^{3+}, and Cu^{2+} serve as electrochemically active centers for charge compensation, while Li^+, Mg^{2+}, and Al^{3+} form "Li-O-Li", "Li-O-Mg", and

Table 3
Summary of high-entropy doped and entropy-tuned layered cathodes for LIBs.

Cathode	Voltage range [V]	Initial capacity [mAh g^{-1}]	Cycle retention	Rate performance [mAh g^{-1}]	Entropy value	Ref
$LiNi_{0.5}Mn_{0.43}Ti_{0.02}Mg_{0.02}Nb_{0.01}Mo_{0.02}O_2$	2.7-4.5	185	~95% after 100 cycles/ 1/3C	~50 /5C	0.99R	[220]
$LiNi_{0.8}Mn_{0.13}Ti_{0.02}Mg_{0.02}Nb_{0.01}Mo_{0.02}O_2$	2.5-4.3	210.1	85% after 1000 cycles/ 1/3C	/	0.73R	[47]
$LiNi_{0.88}Mn_{0.03}Mg_{0.02}Fe_{0.02}Ti_{0.02}Mo_{0.02}Nb_{0.01}O_2$	2.8-4.5	~200	89.5% after 300 cycles/ 1C	~150 /20C	0.57R	[221]
$LiNi_{0.8}Mn_{0.12}Al_{0.02}Ti_{0.02}Cr_{0.02}Fe_{0.02}O_2$	2.5-4.5	203.2	80.06% after 300 cycles/ 0.5C	~140 /5C	0.75R	[232]
$LiNi_{0.9}Mn_{0.05}Zr_{0.01}Nb_{0.01}Ti_{0.01}Al_{0.01}Mg_{0.01}O_2$	2.7-4.3V	206.35	76% after 100 cycles/ 1C	~110/5C	0.47	[267]
$Li_{1.0}(Li_{0.15}Mn_{0.50}Ni_{0.15}Co_{0.10}Fe_{0.025}Cu_{0.025}Al_{0.025}Mg_{0.025})O_2$	2.1-4.8V	~260	93% after 100 cycles/ 0.1C	~190 /2C	/	[219]

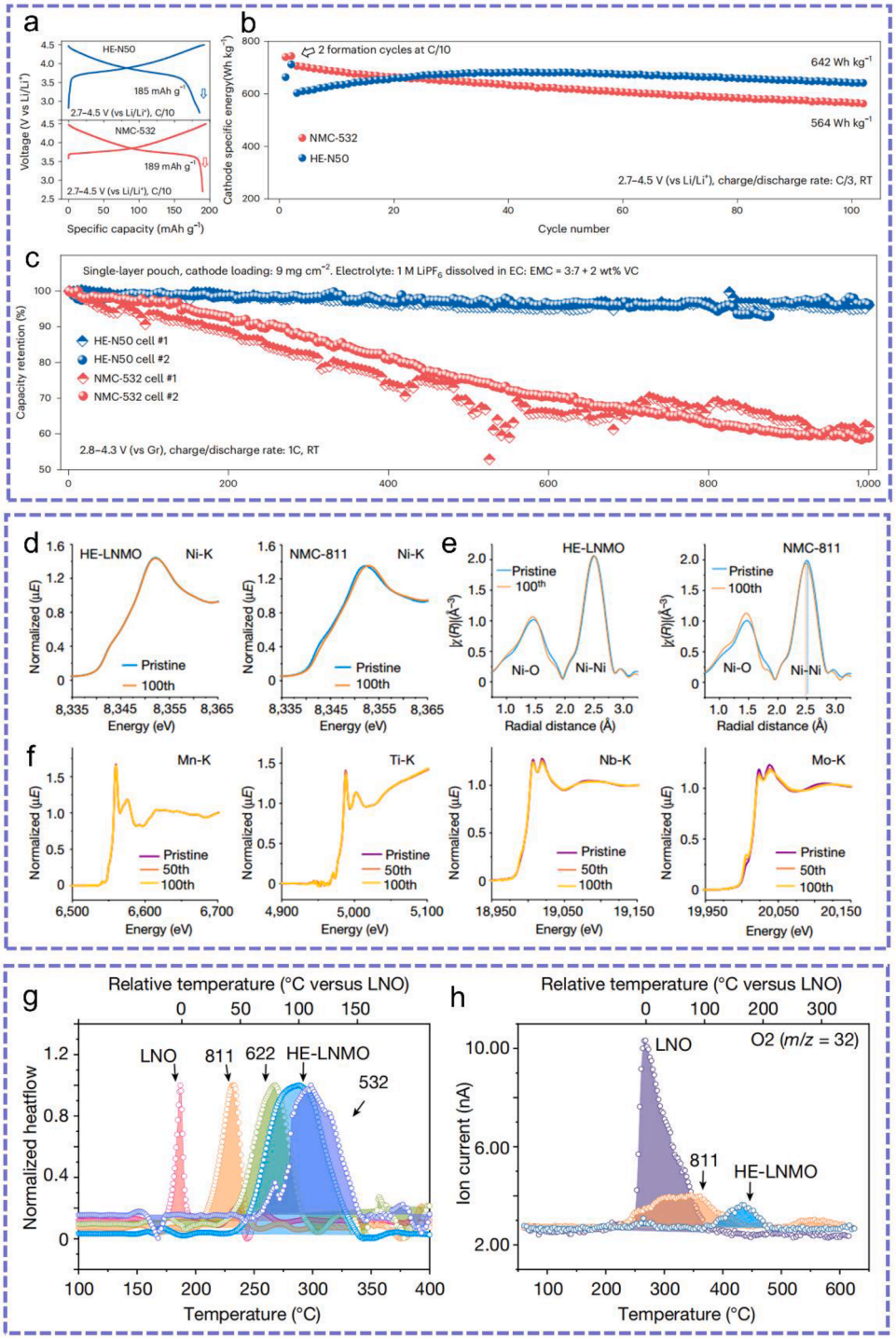

Fig. 9. (a-c) Comparison of the electrochemical performance of HE-N50 and NMC-532: [220]. (a) Second charge and discharge profiles at 0.1C rate. (b) Specific energy (based on cathode) in half cells. (c) Long-term cycling performance in single-layer pouch cells. Reproduced with permission [220]. Copyright 2023, Springer Nature. (d-f) The local coordinate environment stability of HE-LNMO: (d) Ni-K edge XANES spectrum of pristine and cycled HE-LNMO and NMC-811. (e) FT-EXAFS of pristine and cycled HE-LNMO and NMC-811. (f) XANES of Mn-K, Ti-K, Nb-K and Mo-K edges of HE-LNMO after different cycles. (g-h) Comparison of the thermal stability of HE-LNMO with other nickel-rich materials: (g) DSC profile of delithiated $LiNiO_2$ (LNO), NMC-811, NMC-622, HE-LNMO and NMC-532. (h) TGA–MS of $LiNiO_2$ (LNO), NMC-811 and HE-LNMO. Reproduced with permission [47]. Copyright 2022, Springer Nature.

"Li-O-Al" configurations, regulating the charge compensation behavior of anionic oxygen and stabilizing the crystal structure. XANES spectra revealed that the TM electronic structure of E-LRM remained stable throughout cycling, with minimal changes between the first and the 100th discharge. When comparing the FT-EXAFS spectra, E-LRM showed milder changes in Mn, Co, and Ni coordination compared to the significant variations observed in traditional Li-rich materials ($Li_{1.20}Mn_{0.54}Ni_{0.13}Co_{0.13}O_2$, T-LRM). First-principles calculations indicated that E-LRM's diverse combination of TMO_6 octahedra and local structural diversity contributed to better adaptability to structural changes, reducing capacity loss and voltage fade. Under a current density of 0.1 C, E-LRM delivered a capacity of around 260 mAh g^{-1} after

100 cycles, with a capacity retention of about 93%, while T-LRM shows a rapid capacity drop to around 150 mAh g^{-1}, retaining only 51% of its initial capacity. Within a voltage range of 2.1-4.6 V and at a current density of 1C, E-LRM maintains 96.2% voltage retention after 200 cycles, with a voltage fade of only 160 mV. The per-cycle voltage fade is less than 0.02%, approximately 0.8 mV per cycle, much lower than the 442 mV observed in T-LRM.

Taken as a whole, the exploration of high-entropy strategies in layered oxide cathodes for LIBs has undergone a clear transition—from the initial focus on nearly equimolar HE-TMLOs to more practical and performance-driven approaches. Although equimolar HE-TMLOs demonstrated the feasibility of stabilizing multi-component solid-solution structures, their limited discharge capacity, poor long-term cycling stability, and high synthesis cost have significantly restricted their commercial relevance. In contrast, NRLOs and LRLOs, known for their high energy densities, represent more promising candidates for practical

Table 4
Summary of layered cathodes with high-entropy configuration or entropy-tuned in SIBs.

Initial phase	Cathode	Voltage range [V]	Initial capacity [mAh g^{-1}]	Cycle retention	Rate performance [mAh g^{-1}]	Entropy value	Ref
O3	$NaNi_{0.3}Cu_{0.1}Fe_{0.2}Mn_{0.3}Ti_{0.1}O_2$	2.0-4.0	141.5	85% after 500 cycles/ 1C	120/ 5C	1.50R	[261]
O3	$NaMn_{0.2}Fe_{0.2}Co_{0.2}Ni_{0.2}Ti_{0.2}O_2$	1.5-4.2	180	97% after 100 cycles/ 0.1C	173/ 5C	1.61R	[268]
O3	$NaCu_{0.1}Ni_{0.3}Fe_{0.2}Mn_{0.2}Ti_{0.2}O_2$	2.0-3.9	130	87% after 100 cycles/ 0.1C	85/ 5C	1.56R	[269]
O3	$NaFe_{0.2}Cu_{0.1}Ni_{0.2}Mn_{0.3}Ti_{0.2}O_2$	2.0-4.1	121	83.8% after 200 cycles/ 2C	70.2/ 5C	1.56R	[270]
O3	$Na_{2/3}Li_{1/6}Fe_{1/6}Co_{1/6}Ni_{1/6}Mn_{1/3}O_2$	2.0-4.5	171.2	89.3% after 90 cycles/ 1C	78/ 10C	1.56R	[227]
O3	$NaLi_{0.1}Ni_{0.3}Fe_{0.1}Mn_{0.25}Ti_{0.25}O_2$	2.0-4.0	123	77% after 400 cycles/ 2C	78/ 5C	1.51R	[271]
O3	$Na_{0.8}Ni_{0.2}Fe_{0.2}Co_{0.2}Mn_{0.2}Ti_{0.2}O_2$	2.0-4.0	107	90% after 100 cycles/ 0.05C	94.1/ 5C	1.61R	[226]
O3	$NaFe_{0.2}Co_{0.2}Ni_{0.2}Ti_{0.2}Sn_{0.1}Li_{0.1}O_2$	2.0-4.2	130.6	72% after 100 cycles/ 0.1C	80.8/ 2C	1.75R	[272]
O3	$NaMg_{0.08}Cu_{0.12}Ni_{0.2}Fe_{0.2}Mn_{0.2}Ti_{0.2}O_2$	2-4.3	131	84% after 200 cycles/ 1C	110.3/ 5C	1.74R	[273]
O3	$NaNi_{0.2}Fe_{0.2}Mn_{0.35}Cu_{0.05}Zn_{0.1}Sn_{0.1}O_2$	0.5-4.0	128	87% after 500 cycles/ 3C	64.3/ 2C	1.62R	[200]
O3	$Na_{0.94}Ni_{0.29}Cu_{0.1}Fe_{0.16}Mn_{0.3}Ti0_{.15}O_2$	2.0-4.0	122	79% after 300 cycles/ 0.5C	68/ 4C	1.53R	[274]
O3	$Na_{0.9}Ni_{0.2}Fe_{0.2}Co_{0.2}Mn_{0.2}Ti_{0.15}Cu_{0.05}O_2$	2.2-4.1	117.8	79.4% after 2000 cycles/ 5C	98.6/ 10C	1.72R	[222]
O3	$NaNi_{0.25}Mg_{0.05}Cu_{0.1}Fe_{0.2}Mn_{0.2}Ti_{0.1}Sn_{0.1}O_2$	2.0-4.0	130.8	75% after 500 cycles/ 1C	108/ 5C	1.83R	[41]
O3	$Na_{0.83}Li_{0.1}Ni_{0.25}Co_{0.2}Mn_{0.15}Ti_{0.15}Sn_{0.15}O_{2-\delta}$	2.0-4.2	109.4	87.2% after 200 cycles/ 2C	83.3/ 10C	1.75R	[228]
O3	$Na_{0.95}Li_{0.07}Cu_{0.11}Ni_{0.11}Fe_{0.3}Mn_{0.41}O_{1.97}F_{0.03}$	1.5-4.0	138.6	73.1% after 302 cycles/ 1C	109/ 10C	1.48R	[236]
O3	$NaNi_{0.1}Mn_{0.15}Co_{0.2}Cu_{0.1}Fe_{0.1}Li_{0.1}Ti_{0.15}Sn_{0.1}O_2$	2.0-4.1	115	82.7% after 1000 cycles/ 8C	~100/ 4C	2.04R	[275]
O3	$Na_{0.9}Li_{0.1}Ni_{0.4}Fe_{0.2}Mn_{0.44}Ti_{0.04}Mg_{0.02}O_{1.9}F_{0.1}$	2.0-4.0	105	90% after 200 cycles/ 0.5C	80/ 3C	1.61R	[234]
O3	$NaNi_{0.12}Cu_{0.12}Mg_{0.12}Fe_{0.15}Co_{0.15}Mn_{0.1}Ti_{0.1}Sn_{0.1}Sb_{0.04}O_2$	2.0-3.9	110	83% after 500 cycles/ 3C	86/ 5C	2.15R	[46]
P2	$Na_{0.67}Mn_{0.6}Cu_{0.08}Ni_{0.09}Fe_{0.18}Ti_{0.05}O_2$	2.0-4.5	146	97.1% after 50 cycles/ 2C	62.5/ 10C	1.18R	[235]
P2	$Na_{0.6}Ti_{0.2}Mn_{0.2}Co_{0.2}Ni_{0.2}Ru_{0.2}O_2$	1.5-4.5	174	40.9% after 400 cycles/ 0.1C	68/ 86C	1.61R	[229]
P2	$Na_{0.73}Ni_{0.21}Mn_{0.6}Li_{0.06}Cu_{0.06}Ti_{0.07}O_2$	2.0-4.5	128.12	79.21% after 500 cycles/ 5C	85.6/ 10C	1.16R	[42]
P2	$Na_{0.85}Li_{0.08}Mg_{0.04}Ni_{0.22}Al_{0.04}Mn_{0.62}O_2$	2.0-4.3	110	87% after 100 cycles/ 8C	91/ 8C	1.09R	[238]
P2	$Na_{0.75}Mn_{0.55}Ni_{0.25}Co_{0.05}Fe_{0.10}Zr_{0.05}O_2$	1.5-4.2	143	74% after 100 cycles/ 2C	53/ 10C	1.21R	[276]
P2	$[Na_{0.67}Zn_{0.05}]Ni_{0.22}Cu_{0.06}Mn_{0.66}Ti_{0.01}O_2$	2.0-4.3	146.1	92.7% after 100 cycles/ 1C	91.54/ 10C	1.07R	[150]
P2	$Na_{0.62}Mn_{0.67}Ni_{0.23}Cu_{0.05}Mg_{0.07}Ti_{0.01}O_2$	2.0-4.2	148	75.4% after 2000 cycles/ 10C	82.6/ 10C	0.99R	[52]
P2	$Na_{0.67}Mn_{0.45}Ni_{0.18}Co_{0.18}Ti_{0.1}Mg_{0.03}Al_{0.04}Fe_{0.02}O_2$	1.5-4.6	113	91.8% after 50 cycles/ 0.5C	/	1.52R	[277]
P2	$Na_{0.65}Mn_{0.65}Cu_{0.2}Li_{0.06}Mg_{0.015}Ti_{0.015}Al_{0.015}Zr_{0.015}Y_{0.015}La_{0.015}O_2$	2.0-4.5	115	87.2% after 500 cycles/ 10C	55.5/ 10C	1.15R	[237]
P2	$Na_{0.667}Mn_{0.667}Ni_{0.167}Co_{0.117}Ti_{0.01}Mg_{0.01}Cu_{0.01}Mo_{0.01}Nb_{0.01}O_2$	1.5-4.5	166.9	76.4% after 100 cycles/ 1C	111/ 5C	1.05R	[225]
P2/O3	$Na_{0.7}Mn_{0.4}Ni_{0.3}Cu_{0.1}Fe_{0.1}Ti_{0.1}O_{1.95}F_{0.1}$	2.0-4.3	118.4	88.9% after 200 cycles/ 2C	86.7/ 8C	1.61R	[278]
P2/O3	$Na_{0.75}Ni_{0.33}Mn_{0.4}Cu_{0.1}Ti_{0.13}Sn_{0.05}O_2$	2.0-4.5	150	68.4% after 300 cycles/ 1C	88.7/ 7.5C	1.38R	[279]
P2/O3	$Na_{0.85}Li_{0.05}Ni_{0.25}Cu_{0.025}Mg_{0.025}Fe_{0.05}Al_{0.05}Mn_{0.5}Ti_{0.05}O_2$	2.0-4.2	122	90% after 1000 cycles/ 10C	81.8/ 10C	1.48R	[280]

applications, yet they suffer from severe degradation during cycling.

Recent progress has shown that high-entropy doping and entropy tuning strategies offer an effective path forward. By selectively introducing multiple dopant elements in non-equimolar proportions, these approaches enable the retention of high capacity while improving structural integrity and suppressing degradation mechanisms. These developments highlight a critical shift in the role of entropy—from a purely structural concept to a versatile design tool capable of addressing key performance limitations in advanced layered cathode materials.

5.2. Applications of high-entropy approaches in Na_xTMO_2

Na_xTMO_2, featuring multiple key redox centers (Ni, Co, Mn, Fe) and complex phase transitions, has become a prominent area of application for the high-entropy approaches. This resulted in the development of several high-performance layered cathodes, as summarized in Table 4.

5.2.1. High-entropy O3-Na_xTMO_2 cathodes

In 2019, Hu's team pioneered the introduction of high-entropy concept into O3-Na_xTMO_2. They reported a material with the composition of $NaNi_{0.12}Cu_{0.12}Mg_{0.12}Fe_{0.15}Co_{0.15}Mn_{0.1}Ti_{0.1}Sn_{0.1}Sb_{0.04}O_2$, which contains nine elements in the TM layer (Fig. 10**a**). This material exhibited delayed unfavorable phase transitions and an extended O3-P3 phase transition. The O3 phase region provided approximately 60% reversible specific capacity (Fig. 10**b**), significantly surpassing other layered materials. The proposed mechanism highlights the crucial role of the high-entropy configuration and chemical disorder in the TMO_2 layers. This structure allows for better accommodation of local structural changes induced by electroactive TM cations during Na^+ (de) insertion and reduces Na^+ interactions within the NaO_2 layers. As a result, the material offers significantly improved rate performance and cycling stability as a cathode material for SIBs. Following this success, their team further reported high-entropy configurations that enhanced the framework structure of $NaNi_{0.25}Mg_{0.05}Cu_{0.1}Fe_{0.2}Mn_{0.2}Ti_{0.1}Sn_{0.1}O_2$ (HEO-424) [41] and modified the electronic structure of $Na_{0.95}Li_{0.07}Cu_{0.11}Ni_{0.11}Fe_{0.3}Mn_{0.41}O_{1.97}F_{0.03}$ (LCNFMF) [236], reinforcing the potential of high-entropy strategies for improving the electrochemical properties and stability of layered materials.

More recently, Hu's team conducted a comparative study between O3-$NaNi_{0.3}Cu_{0.1}Fe_{0.2}Mn_{0.3}Ti_{0.1}O_2$ (NCFMT) and O3-$NaNi_{0.3}Cu_{0.1}Fe_{0.2}Mn_{0.3}Sn_{0.1}O_2$ (NCFMS),[261] both of which have the same configurational entropy. Both materials exhibit a distinct layered structure, composed of alternating Na and TM layers. Elemental mapping confirmed that all five elements are uniformly and randomly distributed within the projected atomic columns in each sample (Fig. 10**c**). However, NCFMS displayed planar strain due to lattice distortions caused by mismatches in ionic size, mass, and valence electron configuration. The inherited strain in the TMO_2 layers, along with the accumulated lattice strain during repeated TM redox cycles, led to thermodynamically driven metal ion migration. This results in elemental segregation and crack formation within the NCFMS cathode particles, both internally and on the surface. In contrast, NCFMT, with better mechanochemical compatibility among the 3d TMs, does not exhibit the degradation mechanisms observed in NCFMS, thereby enhancing the cycling stability of both half-cells and full cells. In half-cells with a Na metal anode, it exhibited outstanding rate performance within a voltage range of 2.0-4.0V, delivering a specific capacity of 120 mAh g^{-1} at 5C and retaining 85% of its capacity after 500 cycles at 1C at 25°C. At 45°C, it showed a discharge capacity of 106 mAh g^{-1}, retaining 80% capacity after 500 cycles. Full cells, with a hard carbon anode, delivered an energy density of 269 Wh kg^{-1} (based on the total mass of active materials) at 0.1C (14 mA g^{-1}), retaining 80% of its initial capacity after more than 600 cycles (see Fig. 10**d, e**). Even at a higher cutoff voltage range of 0.5-4.15V, it maintained excellent rate performance and good capacity retention (Fig. 10**f, g**). This work highlights the critical impact of elemental compatibility within the TM layers on structural integrity and underscores the importance of element selection.

Additionally, Cui's team [200] reported a zero-strain O3-$NaNi_{0.2}Fe_{0.2}Mn_{0.35}Cu_{0.05}Zn_{0.1}Sn_{0.1}O_2$. In this high-entropy structure, Ni, Fe, and Cu serve as charge compensators, while Mn, Zn, and Sn stabilize their valence states and act as inhibitors of interlayer sliding by enhancing charge localization. Those lead to a significant improvement in the cycling performance of the material. Recent studies have shown that the high-entropy approach continues to enhance structural stability even at high cutoff voltages (above 4.2V). For example, Yao et al [227] reported an O3-$Na_{2/3}Li_{1/6}Fe_{1/6}Co_{1/6}Ni_{1/6}Mn_{1/3}O_2$ material, capable of operating over a broad voltage window (2.0-4.5 V), with minimal impact from phase transitions and oxygen redox reactions (as shown in Fig. 10**h**). This material exhibits a high reversible capacity of 171.2 mAh g^{-1} at 0.1C and retains 89.3% of its initial capacity after 90 cycles at 1C.

The aforementioned studies show that the high-entropy configuration in layered materials can effectively enhance structural stability during cycling. However, the inherently slow sodium-ion dynamics, significant voltage hysteresis, and poor air stability continue to impede the practical application of O3-Na_xTMO_2. The work of Wang [222], Joshi [234], and Dang [270] offers new insights for overcoming these challenges. To address the sluggish sodium-ion dynamics and notable voltage hysteresis in the O3-Na_xTMO_2, Wang et al [222] applied a high-entropy tailoring strategy, synthesizing O3-$Na_{0.9}Ni_{0.2}Fe_{0.2}Co_{0.2}Mn_{0.2}Ti_{0.15}Cu_{0.05}O_2$. The high-entropy configuration within the transition metal slabs modulates the electronic structure, strengthen the TMO_2 framework, and widen the sodium ion diffusion channels. This leads to higher reversibility of TM redox, a more gradual phase transition from O3 to P3, and a lower Na^+ migration barriers (0.17 eV), resulting in faster sodium-ion diffusion rate during (de)intercalation processes ($\approx 10^{-10}$ cm^2 s^{-1}). Consequently, the material exhibits suppressed voltage hysteresis (< 0.09 V), enhanced rate capability, and prolonged cycling stability. In particular, the material exhibits a reversible specific capacity of 106.1 mAh g^{-1} at 5C, retaining 79.4% of its capacity after 2000 cycles, and superior rate performance with a reversible specific capacity of 98.6 mAh g^{-1} at 10 C. The study offers valuable guidance for the development of high-rate, high-energy TMLOs cathodes by reducing voltage hysteresis and promoting Na^+ diffusion. To achieve better air and water stability, Joshi et al [234] reported on O3-$Na_{0.9}Li_{0.1}Ni_{0.4}Fe_{0.2}Mn_{0.44}Ti_{0.04}Mg_{0.02}O_{1.9}F_{0.1}$, where the presence of F at the oxygen site reduced oxygen loss during cycling, and the introduction of Li accelerated the Na^+ insertion/extraction kinetics. The cocktail effect and the establishment of a high-entropy configuration suppressed the degradation of the layered structure, thereby improving both cycling stability and diffusion kinetics while also enhancing air stability. Additionally, Dang et al [270] synthesized O3-$NaFe_{0.2}Cu_{0.1}Ni_{0.2}Mn_{0.3}Ti_{0.2}O_2$, which exhibited excellent water resistance, offering a capacity of 105.2 mAh g^{-1} after 2 hours of soaking and maintaining 83% capacity retention after 200 cycles at 1C.

5.2.2. Entropy-tuned P2-Na_xTMO_2 cathodes

Inspired by the significant improvements in structural stability exhibited by HE-TMLOs in the electrochemical field, entropy-tuning strategies have rapidly found application in P2-Na_xTMO_2 systems. In 2022, Fu et al [52] tuned P2-$Na_{0.62}Mn_{0.67}Ni_{0.37}O_2$ by adjusting its configurational entropy and ionic diffusion structure, leading to the development of P2-$Na_{0.62}Mn_{0.67}Ni_{0.23}Cu_{0.05}Mg_{0.07}Ti_{0.01}O_2$ (CuMgTi-571). This entropy-tuned material features more {010} active facets, better structural and thermal stability, and faster anionic redox kinetics (Fig. 11**a**). As a result, CuMgTi-571 exhibited excellent capacity retention rates (87% after 500 cycles at 120 mA g^{-1} and 75% after 2000 cycles at 1200 mA g^{-1}). Similarly, the entropy-tuned P2-[$Na_{0.67}Zn_{0.05}$]$Ni_{0.22}Cu_{0.06}Mn_{0.66}Ti_{0.01}O_2$ [150] exhibits an impressive high practical capacity of 91.54 mAh g^{-1} at 10 C and maintaining near 100% capacity retention over 500 cycles. More recently, Zhou's team [235] developed a P2-$Na_{0.67}Mn_{0.6}Cu_{0.08}Ni_{0.09}Fe_{0.18}Ti_{0.05}$ (MCNFT) material, which

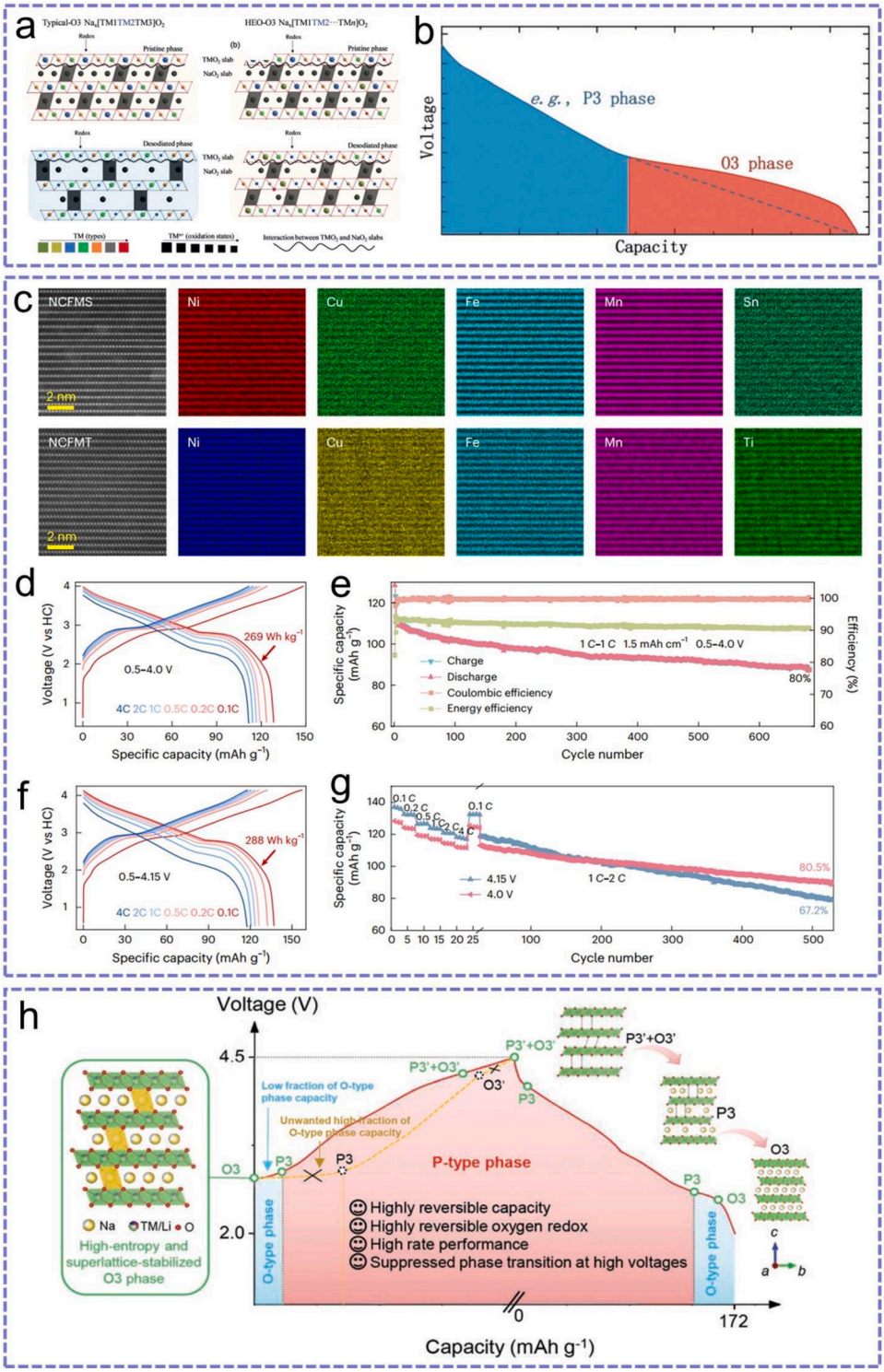

Fig. 10. (a-b) Structure evolution and delayed phase transition of $NaNi_{0.12}Cu_{0.12}Mg_{0.12}Fe_{0.15}Co_{0.15}Mn_{0.1}Ti_{0.1}Sn_{0.1}Sb_{0.04}O_2$: (a) Corresponding crystal structure evolution of this HE-TMLOs cathode. (b) Discharge curves of the representative O3-type Na-ion cathodes. Reproduced with permission [46]. Copyright 2020, Wiley-VCH. (c-g) Atomic-level layered structures of NCFMS and NCFMT and full-cell performance of NCFMT//HC in different voltage ranges: (c) Atomic EDS mapping of element distributions in the NCFMS and NCFMT, including the corresponding HAADF-STEM image of the lattice structure along the {110} zone axes. (d) Charge-discharge profile at 0.1 C, 0.2 C, 0.5 C, 1 C, 2 C and 4 C within a voltage range of 0.5-4.0 V. (e) Cycling performance at a current rate of 1 C and a cutoff potential of 4.0 V. (f) Charge-discharge profile at 0.1 C, 0.2 C, 0.5 C, 1 C, 2 C and 4 C within a voltage range of 0.5-4.15 V. (g) Rate capability at cutoff potentials of 4.0 and 4.15 V. Reproduced with permission [261]. Copyright 2024, Springer Nature. (h) A schematic representation of the charge/discharge behavior of high-entropy and superlattice-stabilized $Na_{2/3}Li_{1/6}Fe_{1/6}Co_{1/6}Ni_{1/6}Mn_{1/3}O_2$. Reproduced with permission [227]. Copyright 2022, Wiley-VCH.

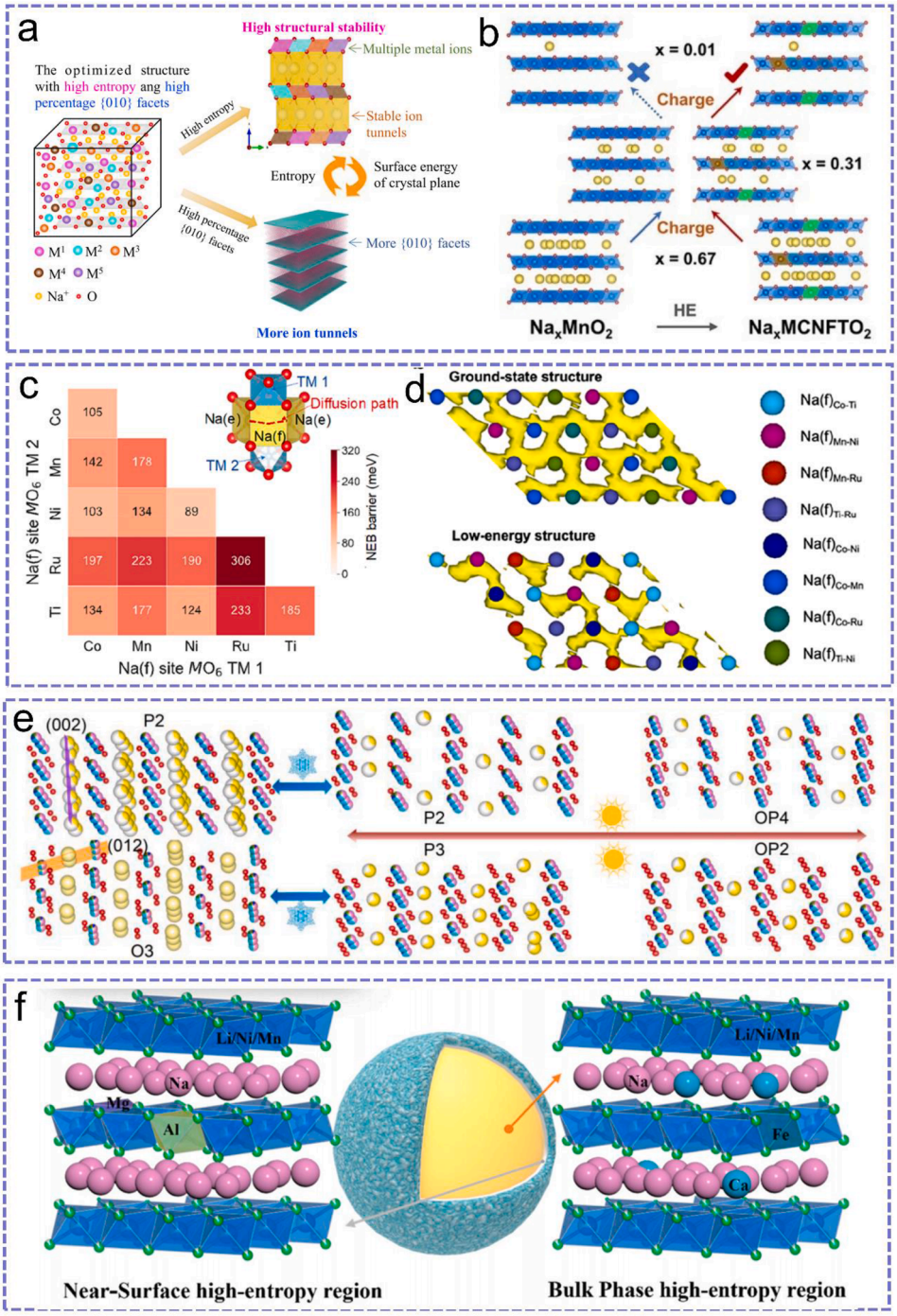

Fig. 11. (a) Design strategy for optimized P2-type cathode structures involves high-entropy layered cathodes with multiple cations, which can provide enhanced structural stability and stable ion-diffusion channels. Reproduced with permission [52]. Copyright 2022, Springer Nature. (b) Schematic diagram of Na^+ migration in NMO (left) and MCNFT (right). Reproduced with permission [235]. Copyright 2024, Wiley-VCH. (c-d) Percolating network of low-barrier pathways enabling rapid, large-scale Na diffusion, contributing to the high rate performance observed: (c) Single Na hopping migration barriers (meV) for Na(e)-Na(f)-Na(e) across various Na (f) site compositions at the fully charged state. (d) Isosurfaces showing the probability density distribution (P) of Na ions (yellow) at $P = P_{max/32}$ for P2-TMCNR at 1000 K, based on AIMD trajectories for both the ground-state structure and a low-energy configuration with $Na(f)_{Ti-Ru}$ sites. Reproduced with permission [229]. Copyright 2020, American Chemical Society. (e) Schematic diagram of structural evolution of P2/O3-NaMnNiCuFeTiOF. Reproduced with permission [278]. Copyright 2023, Elsevier. (f) Elements for near-surface and bulk phase high-entropy region. Reproduced with permission [127]. Copyright 2023, Elsevier.

demonstrated high stability in deeply desodiated states (Fig. 11**b**). It achieved a charge capacity of 158.1 mAh g^{-1}, corresponding to 0.61 Na^+, with an initial Coulombic efficiency of up to 98.2%, significantly surpassing the 57.7% (corresponding to 0.36 Na^+) of $Na_{0.67}MnO_2$. Additionally, the MCNFT material exhibited superior cycling stability compared to $Na_{0.67}MnO_2$ (NMO).

The aforementioned studies highlight the significant impact of entropy-tuned P2 materials on Na^+ diffusion kinetics. Therefore, understanding how the TM layer influences Na^+ diffusion pathways in the AM layer could provide valuable insights into identifying optimal element combinations for enhancing performance. To investigate the impact of disordered TM elements on Na^+ in P2-Na_xTMO_2, Yang et al

[229] conducted a series of analyses the Na^+ migration pathways in the designed P2-$Na_{0.6}Ti_{0.2}Mn_{0.2}Co_{0.2}Ni_{0.2}Ru_{0.2}O_2$ (P2-TMCNR) using the climbing-image nudged elastic-band calculation and ab-initio molecular dynamics simulations. Their findings revealed that the optimal transition metal composition can create a percolation network with low-energy barrier pathways. Fig. 11**c** presents the Na migration barriers of various $Na(f)_{M-M'}$, showing that the lowest migration barriers occur when Na(f) sites share faces with NiO_6 and/or CoO_6. Specifically, $Na(f)_{Ni-Ni}$ sites have the lowest barriers of 89 meV, while $Na(f)_{Ni-Co}$ and $Na(f)_{Co-Co}$ sites have slightly higher values, ranging from 103 to 105 meV. In contrast, Na(f) sites containing Ti and Mn have intermediate diffusion barriers, whereas those with Ru display significantly higher migration barriers, making Ti-Ru combinations the least favorable for Na^+ diffusion (Fig. 11**d**). The disordered distribution of cations in the TM layer helps reduce Na^+/vacancies ordering. Computational evaluations revealed that P2-TMCNR forms a percolation network with low-energy barrier diffusion pathways, enabling the material to achieve a specific capacity of 68 mAh g^{-1} (with an active material mass loading of 1−2 mg/cm^2) at a very high current density of 86C (15000 mA g^{-1}).

5.2.3. P2/O3 multiphase and gradient doping cathodes

Combining high-entropy design with phase engineering offers a promising route for enhancing layered cathodes in SIBs. In 2024, Li et al [279] reported that a five-component high-entropy multiphase cathode (Ni/Mn/Cu/Ti/Sn) demonstrates enhanced structural stability due to the synergistic effect of multiple cations at TM sites. This design enlarges the lattice while maintaining capacity, with the high-entropy P2/O3 phases effectively suppressing harmful phase transitions at high voltages, thus improving cycling performance. The cathode showed a capacity retention of 77.3 mAh g^{-1} after 300 cycles and a rate performance of 88.7 mAh g^{-1} at 750 mA g^{-1}, outperforming both low-entropy P2/O3 cathodes and single-phase HE-O3 cathodes. Further investigation refined the TM content in 43 different high-entropy multiphase structures, revealing that weighted average ionic radius (WAIR) is crucial in determining phase compositions. When WAIR ranges between 0.583 and 0.637 Å, multiphase cathodes containing P2 and O3 are formed, with the proportion of the O3 phase increasing with WAIR. The disordered distribution of Mn, Cu, Ti, and Sn in the TMO_2 layer helps suppress undesirable O3→P3 and P2→O2 phase transitions, while the varied lattice orientations of P2 and O3 phases prevent interlayer sliding, contributing to enhanced stability. Additionally, these materials exhibit superior air stability and mechanical strength, demonstrating the combined advantages of high-entropy and multiphase structures in cathode materials.

Mu et al [280] developed a biphasic high-entropy cathode composed of eight elements: $Na_{0.85}Li_{0.05}Ni_{0.25}Cu_{0.025}Mg_{0.025}Fe_{0.05}Al_{0.05}Mn_{0.5}Ti_{0.05}O_2$ cathode. Compared to its single-phase analogue, this biphasic high-entropy cathode exhibited high initial Columbic efficiency (95.4%), and delivered a capacity of 128.4 mAh g^{-1} at 40 mA g^{-1} (~90% capacity retention after 300 cycles). The synergy between O3 and P2 phases helps present sliding of the TM layer during Na^+ extraction/insertion, thus improving the structural stability.

Cheng et al [278] explored the effect of P2/O3 ratios on battery performance by designing a high-entropy cathode material, $Na_{0.7}Mn_{0.4}Ni_{0.3}Cu_{0.1}Fe_{0.1}Ti0_{.1}O_{1.95}F_{0.1}$, synthesized under varying synthesis temperature. *In-situ* XRD analysis revealed that sintering temperature significantly influences phase generation. At 500°C, a pure P3 phase is formed, while at temperatures above 640°C, a P2/O3 biphasic structure emerges (see Fig. 11**e**). The material sintered at 900°C exhibited the highest capacity of 131.5 mAh g^{-1} with an initial Coulombic efficiency of 97.6% and superior cycling stability. The unique P2/O3 two-phase structure facilitated the migration of Na^+, and the high-entropy doping can effectively inhibit the Jahn-Teller effect of Mn^{3+}, thus suppressing the destructive sliding of the TM layer and contributing to improved structural stability.

Furthermore, gradient doping in conjunction with the high-entropy design enhances cathode- electrolyte interface. Feng et al [127] developed gradient-doped high-entropy cathode, $Na_{0.79}Li_{0.13}Ni_{0.20}SS_{0.1}Mn_{0.57}O_2$ by doping steel slag(SS) with available elements such as Mg, Al, Si, Fe, and Ca (Fig. 11**f**). The surface high-entropy region acts as an artificial cathode-electrolyte interface layer, preventing impurity formation and reducing side reactions during cycling. The Na-O-Mg configuration in the near-surface high-entropy region continuously stimulates anionic redox activity, while differential electrochemical mass spectrometry (DEMS) indicates that the high-strength Al-O bond achieves zero oxygen release. Additionally, the Ca^{2+} in the bulk high-entropy region disrupts the Na^+/vacancy ordered transition, improving the kinetic performance, delivering a capacity of 90 mAh g^{-1} at 1000 mA g^{-1}.

Taken together, the application of high-entropy strategies in Na_xTMO_2 layered cathodes has demonstrated remarkable potential in addressing key limitations of SIB systems. The successful implementation of these strategies in lithium-ion layered oxides has naturally motivated their extension to sodium-ion systems, which share similar ion storage mechanisms. In particular, O3-type layered oxides, while capable of accommodating a large number of Na^+ ions, often suffer from complex phase transitions during charge/discharge, leading to severe structural degradation and capacity fading. The introduction of high-entropy configurations has been shown to effectively suppress these irreversible transitions, thereby enhancing structural integrity and cycling stability.

At the same time, entropy-tuning strategies have demonstrated great promise in improving the structural robustness and Na^+ diffusion kinetics of P2-type layered oxides, ultimately contributing to superior electrochemical performance. From the pioneering development of equimolar HE-TMLOs to more compositionally refined entropy-tuned and gradient-doped cathodes, researchers have made significant progress in improving rate capability, voltage hysteresis, and long-term cycling performance. These advances highlight the critical role of compositional complexity in stabilizing the layered framework under high-voltage and extended cycling conditions.

Nevertheless, challenges such as sluggish sodium-ion transport, oxygen redox instability, and poor tolerance to air and moisture remain significant barriers to practical application. Future work should focus on the rational integration of high-entropy configurations with phase engineering, interface design, and advanced computational tools to deepen our understanding of structure–property relationships. Ultimately, fine-tuning elemental combinations and spatial distributions within the layered lattice will be essential to fully unlock the potential of high-entropy strategies in next-generation, high-energy SIBs.

5.3. Applications of high-entropy approaches in K_xTMO_2

Inspired by entropy stabilization strategies, high-entropy approaches are increasingly being utilized to enhance the cycling stability of cost-effective Mn-based K_xTMO_2. In 2023, Li et al [44] introduced entropy tuning by altering the composition to address the challenges faced by K_xTMO_2. Specifically, in their study of low-entropy and high-entropy variants of $K_{0.45}Mn_xCo_{(1-x)/4}Mg_{(1-x)/4}Cu_{(1-x)/4}Ti_{(1-x)/4}O_2$, they found that $K_{0.45}Mn_{0.6}Co_{0.1}Mg_{0.1}Cu_{0.1}Ti_{0.1}O_2$ exhibits superior electrochemical performance in PIBs. By utilizing entropy tuning to suppress the Jahn-Teller distortion of Mn^{3+}, $K_{0.45}Mn_{0.6}Co_{0.1}Mg_{0.1}Cu_{0.1}Ti_{0.1}O_2$ achieves high K^+ ion transport rates and mitigates volume changes while maintaining high specific capacity. In full cells, the $K_{0.45}Mn_{0.6}Co_{0.1}Mg_{0.1}Cu_{0.1}Ti_{0.1}O_2$ cathode exhibits a capacity of 100 mAh g^{-1} at 50 mA g^{-1}, providing superior rate capability (65.8 mAh g^{-1} at 500 mA g^{-1}) and cycle stability (67.8 mAh g^{-1} after 350 cycles at 100 mA g^{-1}). Similarly, Chu et al [281] successfully synthesized $K_{0.45}Mn_{0.60}Ni_{0.075}Fe_{0.075}Co_{0.075}Ti_{0.10}Cu_{0.05}Mg_{0.025}O_2$ (HE-$K_{0.45}$MO). This material exhibited semimetal oxide characteristics with a narrow bandgap of 0.19 eV. The increased entropy also reduces the surface energy of the {010} active planes, resulting in a 2.6-fold increase in exposure of the

{010} planes compared to that of the low-entropy $K_{0.45}MnO_2$ ($K_{0.45}MO$). Additionally, high-entropy suppresses the space charge ordering during the K^+ (de)intercalation process and enhances the transition metal-oxygen covalent interaction in HE-$K_{0.45}MO$, thereby inhibiting phase transitions within 1.5 - 4.2 V voltage range. Furthermore, HE-$K_{0.45}MO$ exhibited superior electrochemical stability, with an average capacity fade of 0.2% after 200 cycles, compared to 0.41% for low-entropy KMO. Additionally, Cai et al [230] employed a high-entropy approach to modify $K_{0.6}MnO_2$, synthesizing a series of $K_xNi_{0.05}Fe_{0.05}Mg_{0.05}Ti_{0.05}Mn_yO_2$ (x/y = 3:6, 4:6, 5:6, 6:6, and 7:6) materials. Benefiting from the stabilized high-entropy structure and the solid-solution K^+ ion storage mechanism, the designed $K_{0.5}(NiFeMgTi)_{0.05}Mn_{0.75}O_2$ (HE-KMO4/6) and $K_{0.6}(NiFeMgTi)_{0.05}Mn_{0.725}O_2$ (HE-KMO5/6) demonstrated superior performance, especially when compared to many previously reported doped K_xTMO_2 layered materials (Fig. 12**a**).

To extend the high-entropy approach beyond traditional PIBs, recent research has explored its application in aqueous PIBs. Building on this, Zeng et al [224] synthesized $K_{0.27}Mn_{0.9}Fe_{0.02}Co_{0.02}Ni_{0.02}Zn_{0.02}Mg_{0.02}O_2$ (HE-KMO), featuring a locally disordered structure that demonstrated significantly improved cycling performance in aqueous PIBs compared to the bare KMO sample (Fig. 12**b, c**). Fig. 12**d** illustrates the potassium

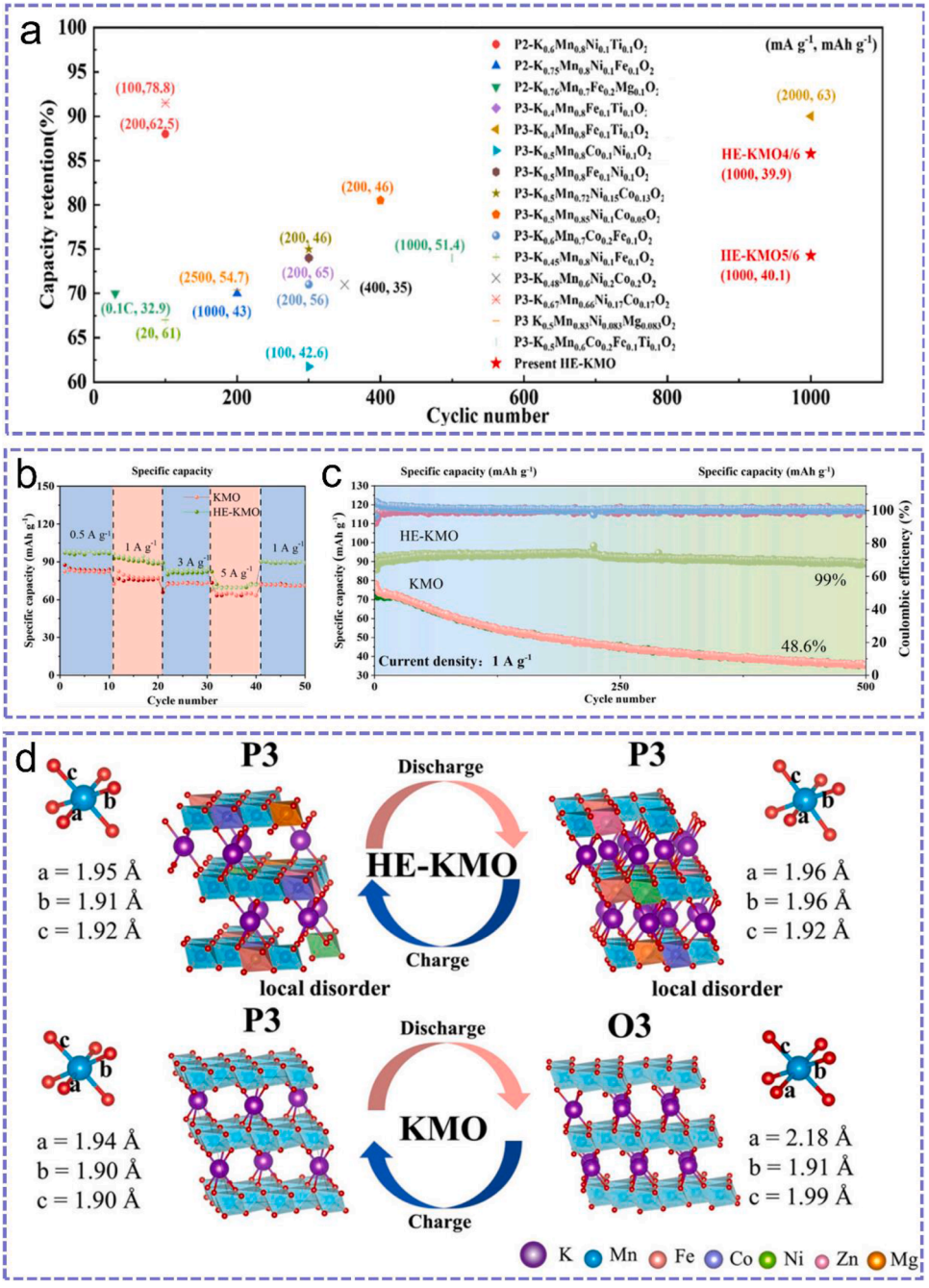

Fig. 12. (a) Comparison of the cyclic retention ratio and rate capability of HE-KMO5/6 and HE-KMO4/6 with other previously reported K_xTMO_2 layered cathodes for PIBs, which have been doped with two or three types of metal ions. Reproduced with permission [230]. Copyright 2023, American Chemical Society. (b-d) Electrochemical performance and structural evolution for KMO and HE-KMO: (b) Rate capability of KMO and HE-KMO from 0.5 to 5000 mA g^{-1}. (c) KMO and HE-KMO cycling stability for 500 cycles at 1000 mA g^{-1}. (d) Schematic diagrams of K^+ intercalation and deintercalation in HE-KMO and KMO, as well as the changes in MO_6 octahedral structure parameters by theoretical calculations. Reproduced with permission [224]. Copyright 2024, Elsevier.

ion intercalation and deintercalation mechanisms in both HE-KMO and KMO. Using *in-situ* XRD, theoretical calculations, and Raman spectroscopy, it was shown that the disordered local environment effectively reduced transport barriers, suppressed phase transitions, and enhanced the stability of HE-KMO during charge-discharge cycles.

Taken together, manganese-based K_xTMO_2 layered oxides are among the most developed cathode systems for PIBs, offering relatively high theoretical capacities. However, the large ionic radius of K^+ leads to severe lattice strain during repeated (de)intercalation, often resulting in structural collapse and rapid capacity fading. High-entropy strategies—particularly high-entropy doping—have emerged as a promising solution to this challenge. Although still in the early stages of exploration, these approaches have demonstrated the ability to suppress irreversible phase transitions, reduce Jahn–Teller distortion, and improve K^+ transport kinetics. Recent studies have reported substantial improvements in structural integrity, rate capability, and cycling stability across both organic and aqueous systems. These findings highlight the potential of entropy-informed design to enhance the electrochemical performance and durability of K_xTMO_2 cathodes, paving the way for more practical and long-lasting PIB technologies.

5.4. Comparison of two methods in enhancing material performance

Traditional doping and high-entropy strategies are two widely used methods to enhance the performance of layered oxide cathodes. Traditional doping typically involves introducing one or two elements at low concentrations to adjust specific properties such as electronic structure, ion transport, or phase stability. It is well-established, with clear mechanisms and controllable effects, making it suitable for fine-tuning material performance. In contrast, high-entropy strategies introduce multiple elements to increase compositional complexity, aiming to regulate the overall structural and electrochemical behavior through synergistic interactions. This approach is still under development but shows potential for improving long-term stability and enabling broader performance optimization.

To illustrate the differences between these methods, we summarized the electrochemical performance of representative materials before and after traditional doping and high-entropy modification (Table 5). Both

Table 5
Summary of the electrochemical performances of layered oxide cathodes before and after traditional doping and high-entropy modification.

Cathode	Voltage range [V]	Initial capacity [mAh g^{-1}]	Cycle retention	Rate performance [mAh g^{-1}]	Ref
$LiNi_{0.6}Co_{0.2}Mn_{0.2}O_2$	2.7-4.3	168	67.5% after 100 cycles /0.1C	105.8 /5C	[157]
Na doped $LiNi_{0.6}Co_{0.2}Mn_{0.2}O_2$	2.7-4.3	179	90.8 % after 100 cycles /0.1C	90 /5C	[157]
$LiNi_{0.6}Co_{0.2}Mn_{0.18}Ti_{0.02}O_2$	3-4.5	197	91.8 after 150 cycles /0.5C	118 /10C	[136]
$LiNa(NiCoMnAlFe)_1O_2$	3-4.5	~100	~70% after 20 cycles /0.2C	/	[263]
$LiNi_{0.2}Mn_{0.2}Co_{0.2}Fe_{0.2}Ti_{0.2}O_2$	2.5-4.4	160	~78% after 50 cycles /0.2C	/	[282]
$Li_{1.2}Ni_{0.2}Mn_{0.6}O_2$	2-4.8	~180	~83% after 200 cycles /0.5C	/	[283]
$Li_{1.20}Mn_{0.54}Ni_{0.13}Co_{0.13}O_2$	2-4.8	302	81% after 30 cycles /0.1C	142.3 /5C	[160]
K doped $Li_{1.20}Mn_{0.54}Ni_{0.13}Co_{0.13}O_2$	2-4.8	315	85% after 110 cycles /0.1C	197 /5C	[160]
$Li_{1.2}Ni_{0.13}Co_{0.13-x}Mn_{0.54}Al_xO_{2(1-y)}F_{2y}$	2-4.8	217	88.21% after 150 cycles / 0.5C	157 /10C	[174]
$Li_{1.0}(Li_{0.15}Mn_{0.50}Ni_{0.15}Co_{0.10}Fe_{0.025}Cu_{0.025}Al_{0.025}Mg_{0.025})O_2$	2.1-4.8	~260	93% after 100 cycles/ 0.1C	~200 /2.5C	[219]
$Na_{2/3}MnO_2$	1.5-4.4	150	~53% after 100 cycles/ 0.5C	~50/ 5 C	[96]
$Na_{0.66}Mn_{0.8}Cu_{0.2}O_2$	1.5-4.4	142	~90% after 100 cycles/ 0.5C	79.9/ 5 C	[96]
$Na_{2/3}Mn_{0.95}Mg_{0.5}O_2$	1.5-4	~175	~100% after 50 cycles/ 3C	106/ 28.6C	[139]
$Na_{0.62}Ca_{0.025}Ni_{0.28}Mg_{0.05}Mn_{0.67}O_2$	2.2-4.35	~130	83% after 100 cycles /0.5C	66.7/ 5C	[172]
$Na_{0.667}Mn_{0.667}Ni_{0.167}Co_{0.117}Ti_{0.01}Mg_{0.01}Cu_{0.01}Mo_{0.01}Nb_{0.01}O_2$	1.5-4.5	166.9	76.4% after 100 cycles/ 1C	111/ 5C	[278]
$NaNi_{1/3}Fe_{1/3}Mn_{1/3}O_2$	2-4	122	67% after 200 cycles/ 1C	83.2/10C	[151]
$Na_{0.9}Ca_{0.05}Ni_{1/3}Fe_{1/3}Mn_{1/3}O_2$	2-4	116.3	91.8% after 200 cycles/ 1C	86.2/10C	[151]
$NaNi_{1/3}Fe_{1/3}Mn_{1/3}O_{1.99}F_{0.01}$	2-4	~120	~89% after 70 cycles/ 1C	/	[111]
$NaNi_{0.12}Cu_{0.12}Mg_{0.12}Fe_{0.15}Co_{0.15}Mn_{0.1}Ti_{0.1}Sn_{0.1}Sb_{0.04}O_2$	2.0-3.9	110	83% after 500 cycles/ 3C	86/ 5C	[46]
$NaNi_{0.25}Mg_{0.05}Cu_{0.1}Fe_{0.2}Mn_{0.2}Ti_{0.1}Sn_{0.1}O_2$	2.0-4.0	130.8	75% after 500 cycles/ 1C	108/ 5C	[41]
$K_{0.45}MnO_2$	1.5-4	68	80% after 100 cycles/ 5C	~50 /5C	[133]
$K_{0.45}Mn_{0.9}Co_{0.05}Mo_{0.05}O_2$	1.5-4	96	59.6% after 2000 cycles/ 5C	77.3/ 5C	[133]
$K_{0.45}Mn_{0.6}Co_{0.1}Mg_{0.1}Cu_{0.1}Ti_{0.1}O_2$	1.5-4	100	67.8% after 350 cycles/ 1C	65.8 /5C	[44]
$K_{0.45}Mn_{0.60}Ni_{0.075}Fe_{0.075}Co_{0.075}Ti_{0.10}Cu_{0.05}Mg_{0.025}O_2$	1.5-4.2	106.8	60.4% after 200 cycles/ 1C	39.6 /5C	[281]
$K_{0.5}MnO_2$	1.4-4	136.6	18.4% after 400 cycles/ 1C	1.2 /5C	[85]
$K_{0.5}Mn_{0.7}Co_{0.2}Fe_{0.1}O_2$	1.7-3.9	104	71% after 300 cycles /2C	58 /10C	[22]
$K_{0.5}Mg_{0.15}[Mn_{0.8}Mg_{0.05}]O_2$	1.4-4	102	48.2% after 400 cycles/ 1C	54.3 /5C	[85]
$K_{0.6}Ni_{0.05}Fe_{0.05}Mg_{0.05}Ti_{0.05}Mn_{0.0725}O_2$	1.5-4	80	86% after 3000 cycles /50C	~40 /20C	[230]

methods can enhance performance, although trade-offs such as slight capacity loss may occur depending on the system. Their respective strengths and limitations are further discussed in Section 6.1.

6. Summary and outlook

In conclusion, while doping has long been a cornerstone of material modification, providing targeted enhancements to the structural and electrochemical properties of A_xTMO_2, the emerging high-entropy approaches present promising alternative strategies with the potential for transformative impact. By introducing multiple elements into the crystal lattice, high-entropy strategies not only expand the compositional possibilities, but also significantly enhance material stability and performance. This comparative analysis underscores the complementary nature of these approaches, highlighting the precision and reliability of traditional doping against the innovative potential of high-entropy approaches. Moving forward, the integration of these strategies, supported by advanced computational tools and novel synthesis techniques, holds great promise for the development of next-generation materials in energy storage applications.

6.1. Advantages and limitations comparison

Traditional doping and high-entropy approach each present unique advantages and limitations. Doping strategies offer precise control over the type, concentration, and location of dopant elements within TMLOs, allowing for targeted modification of material properties. For example: (1) High-valence ion doping — introducing high-valence ions (such as Ti^{4+}, Sn^{4+}, Mo^{6+}) into the TM layer can enhance anion attraction, potentially creating a pinning effect that mitigates oxygen loss and improves material stability; (2) Low-valence ion doping — doping low-valence ions (such as Li^{+}, Mg^{2+}, Zn^{2+}) in the TM layer may enhance the reversibility of ARR, leading to higher reversible capacity at elevated cutoff voltages; (3) Heteroalkali metal doping — incorporating heteroalkali metal ions (such as Li^{+}, Na^{+}, K^{+}) into the AM layer can lower the migration energy barrier of the original AM ions, thereby increasing the ion diffusion coefficient; (4) Non-alkali metal doping — doping non-alkali metal ions (such as Mg^{2+}, Ca^{2+}, Zn^{2+}) into the AM layer may create a pillar effect, stabilizing the layered structure during ion insertion and extraction processes and preventing structural collapse; (5) Anion doping — introducing anions such as F^{-} into oxygen sites can form strong M-F bonds, providing charge compensation while regulating interlayer spacing.

Conventional ion doping techniques have been extensively studied and widely applied in layered oxides, making them a well-established and mature strategy for tuning material properties. Over the years, researchers have developed precise control over dopant selection, concentration, and distribution, enabling systematic optimization of electrochemical performance, structural stability, and ionic conductivity. While these well-established strategies benefit from clear design rules and empirical guidelines, making them reliable and predictable present certain limitations. The amount of dopant introduced is typically small; too little may lead to inconspicuous effects, while too much can sometimes introduce impurities, compromising material purity and performance. Additionally, although doping techniques are relatively mature, they still rely heavily on experimental exploration to optimize concentrations and configurations, which can increase the complexity and time required for development. Moreover, under operational conditions, dopants may migrate or segregate, leading to potential degradation in performance. These challenges, while significant, should be viewed within the context of the overall maturity and established success of doping methods in improving material properties.

In contrast, the high-entropy approaches introduce multiple elements into the material's crystal lattice, resulting in high-entropy or entropy-turned materials with enhanced structural stability and electrochemical performance. This method significantly broadens the compositional range, allowing for more comprehensive control over material properties through the complex interactions of multiple elements. HE-TMLOs and entropy-turned layered materials often exhibit five key advantages: (1) Structure stabilization — Enhancing structural stability through interactions between elements under high-entropy effects, leading to superior phase stability during repeated ion insertion and extraction processes; (2) High disorder characteristics — Introducing ions of varying sizes and electronegativities not only increases the configurational entropy of the system but also contributes to greater disorder within the internal environment. This disorder impacts both micro- and macro-level properties, ultimately improving electrochemical performance; (3) Entropy extension effect — During surface doping or coating modifications, some elements tend to segregate, creating local high-entropy regions. These regions can significantly suppress side reactions at the electrode material's interface, thereby enhancing stability; (4) Cocktail effect—Synergy of multi-elements — The synergistic effects of multiple elements enhance the overall performance of HE-TMLOs. By carefully selecting and balancing the elements, their interactions can be optimized to suppress irreversible phase transitions and improve electrochemical performance; (5) local regulation effect — Adjusting the elemental composition in HEOs can modify their local electronic and coordination environments, which optimizes electrochemical performance. These strategies help maintain a stable local coordination environment, reducing structural degradation and oxygen loss. Despite these significant benefits, the design complexity of high-entropy materials is considerably greater than that of traditional doping strategies. The expanded design space introduces challenges in predicting phase behavior, structural stability, and performance outcomes, often requiring advanced computational tools and extensive experimental validation. Additionally, the synthesis of high-entropy materials typically demands more intense conditions, such as higher temperatures and longer durations, which increase energy consumption and complicate scalability[45,189]. The practical application of high-entropy approaches, especially in large-scale production, remains challenging due to these factors. The lack of well-defined design rules and the need for high precision in controlling the elemental composition further complicate the reproducibility and consistency of high-entropy materials in commercial applications.

Furthermore, while the high-entropy approach introduces additional entropy gain to the system, the incorporation of multiple elemental species results in greater disorder compared to conventional doping strategies. This heightened disorder can complicate atomic and molecular interactions, where even minor variations in concentration or elemental composition may significantly impact the final regulatory outcome. Additionally, challenges commonly encountered in conventional doping, such as elemental segregation and compatibility issues, may be further exacerbated in high-entropy systems. Therefore, substantial future research efforts should be directed toward establishing rational design principles to guide material design and parameter optimization for both conventional doping and high-entropy strategies.

6.2. Future Development

Looking forward, both traditional doping and high-entropy approaches offer promising avenues for further research and innovation, particularly with the optimization of element modulation, synthesis methods, and mechanistic understanding (Fig. 13).

6.2.1. Element modulation

Designing a rational elemental composition is crucial for tailoring the functional properties of materials. Whether employing conventional doping strategies or high-entropy approaches, material design typically involves substituting one or more elements based on a selected reference model. Generally, electrochemically active elements (e.g., Co, Mn, Ni, Fe) serve as redox centers in layered oxides, contributing to the system's capacity, whereas electrochemically inert elements (e.g., Zn, Ti) do not

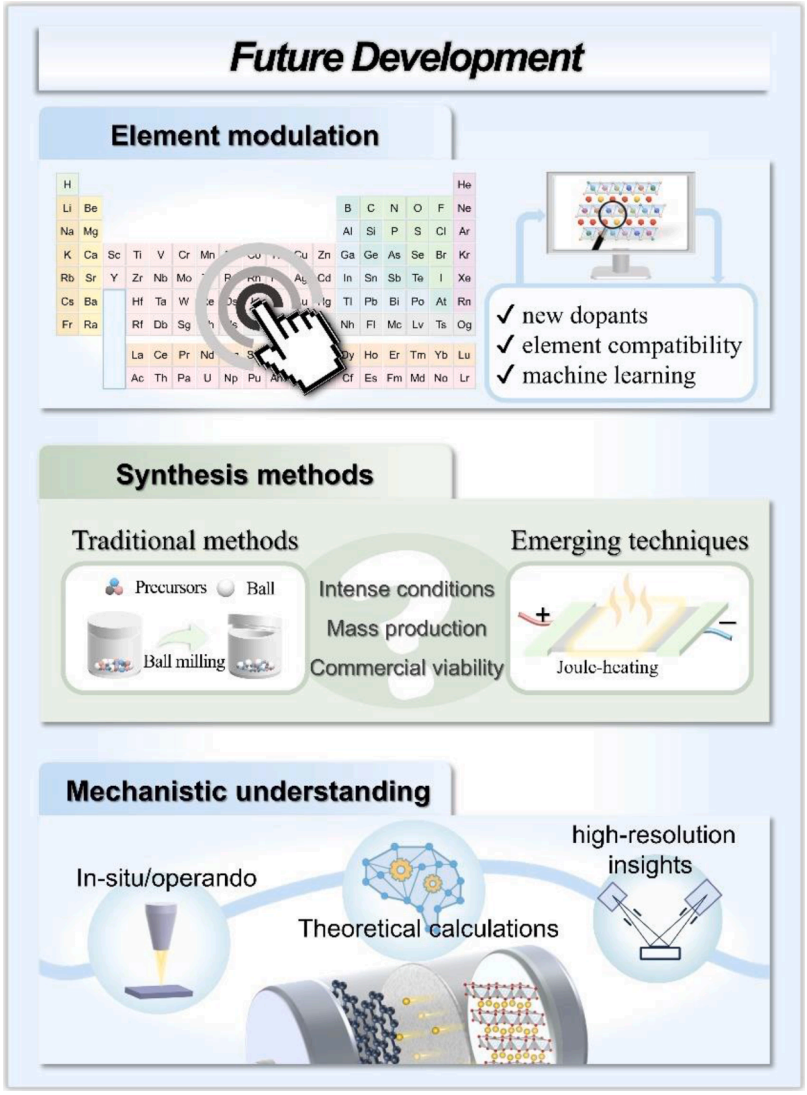

Fig. 13. Future development of high-entropy approaches.

participate in redox reactions but instead help stabilize the host structure. Moreover, even when the same elemental combination is used, variations in elemental concentration can significantly impact material performance. Under the premise that the total concentration of doped sites remains constant, increasing the concentration of a specific element enhances its corresponding functional characteristics, often requiring a compensatory adjustment of other components' functionalities.

Additionally, elemental concentration plays a critical role in determining the configurational entropy of the system. When components are present in equimolar (or nearly equimolar) ratios, the configurational entropy reaches its theoretical maximum, which may facilitate the formation of homogeneous solid solutions. Beyond these fundamental compositional design principles, future research could focus on exploring novel dopants and assessing elemental compatibility. In this regard, high-throughput computation and machine learning can be leveraged for element screening, facilitating the establishment of more efficient and rational design guidelines.

For traditional doping, future directions may include co-doping strategies using well-studied elements or the introduction of new dopants such as high-valence Mo^{6+},[284–286] W^{6+},[287] Ta^{5+},[288,289] Sb^{5+},[290] and Zr^{4+},[291] which, even in small amounts, can stabilize structures and enhance performance without directly contributing to capacity or acting as redox centers. High-entropy approaches can benefit from the established knowledge of traditional doping strategies and should place greater emphasis on studying element compatibility, particularly in the design of high-entropy layered materials. For example, the extensive research on compatibility in rock-salt, high-entropy materials provides a solid foundation that can be applied to layered structures,[292] as demonstrated by Hu's group,[261] whose studies on element compatibility in layered structures can significantly inform the design of high-entropy materials. To overcome the design complexity associated with high-entropy materials, advanced computational tools are expected to play a crucial role. High-throughput computation and machine learning models can rapidly screen potential doping combinations and high-entropy materials, significantly reducing design complexity and time costs [293,294]. Leveraging large material databases can provide valuable insights into element interactions and guide the selection of optimal combinations, streamlining the design process [295,296]. Additionally, phase diagrams and thermodynamic stability screening can help avoid unstable design options by predicting the Gibbs free energy and formation energy of various combinations [297,298].

6.2.2. *Synthesis methods*

On the synthesis front, emerging techniques such as carbothermal shock synthesis [299,300] and Joule-heating synthesis [301–303] offer

potential breakthroughs in reducing energy consumption and achieving uniform, small-sized precursors. For instance, carbothermal shock synthesis has been successfully used to create high-entropy alloy nanoparticles containing up to eight different metal elements,[299] while Joule-heating synthesis has rapidly produced high-entropy rock-salt oxides and spinel oxides [301]. Traditional methods like ball milling also play a crucial role in the synthesis of high-entropy materials. Ball milling is an efficient method for producing uniform and small-sized precursors by mixing pure composite powders in specific ratios, facilitating the formation of solid solution powders through continuous lattice distortions, dislocations, and vacancies [304]. Looking ahead, scaling up these synthesis methods for large-scale production remains a significant challenge, particularly for high-entropy materials. However, innovations in high-throughput synthesis could pave the way for more efficient, cost-effective manufacturing processes. The development of scalable synthesis techniques will be crucial for the commercial viability of high-entropy materials, enabling their broader application in advanced energy storage and other technologies. The commercialization of high-entropy materials presents significant potential but also faces key challenges such as high production costs and complex synthesis protocols [243]. The synthesis of these materials often requires precise control over multiple elements and their distribution, which can increase production time and costs. Additionally, the reliance on specialized equipment and facilities adds to the economic burden, making large-scale manufacturing challenging in the short term. However, with continued advancements in synthesis techniques, we expect more efficient methods to emerge, reducing production time and costs. Furthermore, innovations in cost-effective and environmentally friendly manufacturing processes—such as simplifying synthesis methods, reducing energy consumption, and minimizing hazardous chemicals—will likely make large-scale production more feasible. Developing scalable synthesis techniques that retain the unique properties of high-entropy materials will be critical for their broader adoption [305]. Additionally, phase separation and compositional control during the synthesis process remain significant challenges hindering the large-scale production of high-entropy layered oxides. In the future, rational element modulation will be crucial for mitigating these issues, thereby enhancing their commercial viability.

While challenges remain, the trajectory for high-entropy materials remains promising. As synthesis efficiency, manufacturing processes, and material design continue to improve,[306] high-entropy materials are expected to play a pivotal role in various industries, driving innovation and contributing to the development of more sustainable technologies in the near future.

6.2.3. *Mechanistic understanding*

Mechanistic analysis remains a critical area for future exploration, particularly in understanding the fundamental effects of layered high-entropy materials, which extend into five key effects: structure stabilization, high disorder characteristics, entropy extension effect, cocktail effect, and entropy-enhanced local regulation effect. Refining the understanding of these effects will be essential for advancing the field. The use of advanced characterization techniques, such as synchrotron X-ray diffraction and neutron diffraction, will be instrumental in providing high-resolution insights into the structural evolution, phase transitions, and electronic structures of these complex materials [307,308]. *In-situ* and *operando* techniques, combined with machine learning-assisted data analysis, can offer real-time monitoring of dynamic changes in high-entropy nanomaterials during electrochemical reactions, providing deeper insights into the underlying mechanisms [309]. Additionally, DFT calculations serve as powerful tools for identifying optimal ion diffusion pathways, and calculating migration energy barriers. These calculations offer intuitive insights into high-entropy mechanisms and provide essential theoretical support for experimental research. In practical material design, combining DFT with other advanced computational tools, such as high-throughput computation,[310] machine learning,[311]. Cluster-Expansion Monte Carlo simulations,[292] and the Special Quasi-Random Structure method,[312] will further enhance prediction efficiency and accelerate the discovery of new materials.

As research progresses, the goal will be to develop a more comprehensive understanding of the relationships between element combinations, structural features, and electrochemical performance in both doping and high-entropy materials, ultimately guiding the design of next-generation materials for advanced energy storage applications.

CRediT authorship contribution statement

Yanjiao Ma: Writing – review & editing, Writing – original draft, Supervision, Funding acquisition, Conceptualization. **Han Du:** Writing – review & editing, Writing – original draft, Formal analysis. **Siyuan Zheng:** Writing – review & editing, Writing – original draft, Data curation. **Zihao Zhou:** Writing – review & editing, Visualization, Methodology. **Hehe Zhang:** Writing – review & editing, Methodology, Formal analysis. **Yuan Ma:** Writing – review & editing, Funding acquisition. **Stefano Passerini:** Writing – review & editing, Supervision. **Yuping Wu:** Writing – review & editing, Supervision, Project administration.

Declaration of competing interest

The authors declare that they have no known competing financial interests or personal relationships that could have appeared to influence the work reported in this paper.

Acknowledgements

This work is supported by the National Natural Science Foundation of China (Key Project No. 52131306), the Project on Carbon Emission Peak and Neutrality of Jiangsu Province (No. BE2022031-4) and Research Start-up Fund of Nanjing Normal University (184080H201B41). The basic funding of the Helmholtz Association is also acknowledged.

Data availability

No data was used for the research described in the article.

References

[1] Y.-J. Guo, R.-X. Jin, M. Fan, W.-P. Wang, S. Xin, L.-J. Wan, Y.-G. Guo, Sodium layered oxide cathodes: properties, practicality and prospects, Chem. Soc. Rev. 53 (2024) 7828–7874.
[2] M.H. Han, E. Gonzalo, G. Singh, T. Rojo, A comprehensive review of sodium layered oxides: powerful cathodes for Na-ion batteries, Energy Environ. Sci. 8 (2015) 81–102.
[3] S. Wang, C. Sun, N. Wang, Q. Zhang, Ni- and/or Mn-based layered transition metal oxides as cathode materials for sodium ion batteries: status, challenges and countermeasures, J. Mater. Chem. A 7 (2019) 10138–10158.
[4] Q. Liu, Z. Hu, M. Chen, C. Zou, H. Jin, S. Wang, S. Chou, S. Dou, Recent Progress of Layered Transition Metal Oxide Cathodes for Sodium-Ion Batteries, Small 15 (2019) 1805381.
[5] K. Wang, H. Zhuo, J. Wang, F. Poon, X. Sun, B. Xiao, Recent Advances in Mn-Rich Layered Materials for Sodium-Ion Batteries, Adv. Funct. Mater. 33 (2023) 2212607.
[6] M. Zarrabeitia, J. Carretero-González, M. Leskes, H. Adenusi, B. Iliev, T.J. S. Schubert, S. Passerini, E. Castillo-Martinez, Could potassium-ion batteries become a competitive technology? Energy Mater. 3 (2023).
[7] Y.-M. Yin, C. Pei, W. Xia, X. Luo, D.-S. Li, Recent Advances and Perspectives on the Promising High-Voltage Cathode Material of $Na_3(VO)_2(PO_4)_2F$, Small 19 (2023) 2303666.
[8] R. Qiu, R. Fei, J.-Z. Guo, R. Wang, B. He, Y. Gong, X.-L. Wu, H. Wang, Encapsulation of $Na_3(VO)_2(PO_4)_2F$ into carbon nanofiber as an superior cathode material for flexible sodium-ion capacitors with high-energy-density and low-self-discharge, J. Power Sources 466 (2020) 228249.
[9] M. Zhou, X. Zhou, L. Li, X. Chen, Z. Qiao, S. Chou, Emerging high voltage V^{4+}/V^{5+} redox reactions in $Na_3V_2(PO_4)_3$-based cathodes for sodium-ion batteries, Chem. Sci. 15 (2024) 8651–8663.
[10] B. Zhang, Y. He, H. Gao, X. Wang, J. Liu, H. Xu, L. Wang, X. He, Unraveling the doping mechanisms in lithium iron phosphate, Energy Mater 2 (2022) 200013.

[11] J. Ge, L. Fan, A.M. Rao, J. Zhou, B. Lu, Surface-substituted Prussian blue analogue cathode for sustainable potassium-ion batteries, Nat. Sustain. 5 (2022) 225–234.
[12] J. Peng, W. Zhang, Q. Liu, J. Wang, S. Chou, H. Liu, S. Dou, Prussian Blue Analogues for Sodium-Ion Batteries: Past, Present, and Future, Adv. Mater. 34 (2022) 2108384.
[13] B. Xie, P. Zuo, L. Wang, J. Wang, H. Huo, M. He, J. Shu, H. Li, S. Lou, G. Yin, Achieving long-life Prussian blue analogue cathode for Na-ion batteries via triple-cation lattice substitution and coordinated water capture, Nano Energy 61 (2019) 201–210.
[14] W. Li, C. Han, G. Cheng, S. Chou, H. Liu, S. Dou, Chemical Properties, Structural Properties, and Energy Storage Applications of Prussian Blue Analogues, Small 15 (2019) 1900470.
[15] J. Zhang, J. Wan, M. Ou, S. Liu, B. Huang, J. Xu, J. Han, Enhanced all-climate sodium-ion batteries performance in a low-defect and Na-enriched Prussian blue analogue cathode by nickel substitution, Energy Mater 3 (2023) 300008.
[16] S. Fan, Y. Liu, Y. Gao, Y. Liu, Y. Qiao, L. Li, S. Chou, The design and synthesis of Prussian blue analogs as a sustainable cathode for sodium-ion batteries, SusMat 3 (2023) 749–780.
[17] H. Zhang, Y. Gao, X. Liu, Z. Yang, X. He, L. Li, Y. Qiao, W. Chen, R. Zeng, Y. Wang, S. Chou, Organic Cathode Materials for Sodium-Ion Batteries: From Fundamental Research to Potential Commercial Application, Adv. Funct. Mater. 32 (2022) 2107718.
[18] L. Fan, R. Ma, J. Wang, H. Yang, B. Lu, An Ultrafast and Highly Stable Potassium–Organic Battery, Adv. Mater. 30 (2018) 1805486.
[19] S. Wang, L. Wang, Z. Zhu, Z. Hu, Q. Zhao, J. Chen, All Organic Sodium-Ion Batteries with $Na_4C_8H_2O_6$, Angew. Chem. Int. Ed. 53 (2014) 5892–5896.
[20] Y. Deng, Z. Wu, R. Liang, Y. Jiang, D. Luo, A. Yu, Z. Chen, Layer-Based Heterostructured Cathodes for Lithium-Ion and Sodium-Ion Batteries, Adv. Funct. Mater. 29 (2019) 1808522.
[21] J. Liao, Y. Han, Z. Zhang, J. Xu, J. Li, X. Zhou, Recent Progress and Prospects of Layered Cathode Materials for Potassium-ion Batteries, Energy Environ. Mater. 4 (2021) 178–200.
[22] W. Zhong, X. Liu, Q. Cheng, T. Tan, Q. Huang, Q. Deng, J. Hu, C. Yang, Suppressing the interlayer-gliding of layered P3-type $K_{0.5}Mn_{0.7}Co_{0.2}Fe_{0.1}O_2$ cathode materials on electrochemical potassium-ion storage, Applied Phys. Rev. 8 (2021) 031412.
[23] Q. Zhang, C.R. Didier, W.K. Pang, Y. Liu, Z. Wang, S. Li, V.K. Peterson, J. Mao, Z. Guo, Structural Insight into Layer Gliding and Lattice Distortion in Layered Manganese Oxide Electrodes for Potassium-Ion Batteries, Adv. Energy Mater. 9 (2019) 1900568.
[24] P.K. Nayak, E.M. Erickson, F. Schipper, T.R. Penki, N. Munichandraiah, P. Adelhelm, H. Sclar, F. Amalraj, B. Markovsky, D. Aurbach, Review on Challenges and Recent Advances in the Electrochemical Performance of High Capacity Li- and Mn-Rich Cathode Materials for Li-Ion Batteries, Adv. Energy Mater. 8 (2018) 1702397.
[25] Y. Kim, W.M. Seong, A. Manthiram, Cobalt-free, high-nickel layered oxide cathodes for lithium-ion batteries: Progress, challenges, and perspectives, Energy Storage Mater 34 (2021) 250–259.
[26] Y.-L. Heng, Z.-Y. Gu, J.-Z. Guo, X.-T. Yang, X.-X. Zhao, X.-L. Wu, Research progress on the surface/interface modification of high-voltage lithium oxide cathode materials, Energy Mater 2 (2022) 200017.
[27] Z. Yang, C. Zheng, Z. Wei, J. Zhong, H. Liu, J. Feng, J. Li, F. Kang, Multi-dimensional correlation of layered Li-rich Mn-based cathode materials, Energy Mater 2 (2022) 200006.
[28] Z. Yu, Q. Tong, Y. Cheng, P. Yang, G. Zhao, H. Li, W. An, D. Yan, X. Lu, B. Tian, Enabling 4.6 V $LiNi_{0.6}Co_{0.2}Mn_{0.2}O_2$ cathodes with excellent structural stability: combining surface $LiLaO_2$ self-assembly and subsurface La-pillar engineering, Energy Mater 2 (2022) 37.
[29] J. Liu, W.H. Kan, C.D. Ling, Insights into the high voltage layered oxide cathode materials in sodium-ion batteries: Structural evolution and anion redox, J. Power Sources Sources 481 (2021) 229139.
[30] P. Wang, Y. You, Y. Yin, Y. Guo, Layered Oxide Cathodes for Sodium-Ion Batteries: Phase Transition, Air Stability, and Performance, Adv. Energy Mater. 8 (2018) 1701912.
[31] Y. Xiao, N.M. Abbasi, Y. Zhu, S. Li, S. Tan, W. Ling, L. Peng, T. Yang, L. Wang, X. Guo, Y. Yin, H. Zhang, Y. Guo, Layered Oxide Cathodes Promoted by Structure Modulation Technology for Sodium-Ion Batteries, Adv. Funct. Mater. 30 (2020) 2001334.
[32] A. Manthiram, A perspective on nickel-rich layered oxide cathodes for lithium-ion batteries, Energy Storage Mater 6 (2017) 125.
[33] X. Zhang, Z. Wei, K.N. Dinh, N. Chen, G. Chen, F. Du, Q. Yan, Layered Oxide Cathode for Potassium-Ion Battery: Recent Progress and Prospective, Small 16 (2020) 2002700.
[34] Z. Cui, X. Li, X. Bai, X. Ren, X. Ou, A comprehensive review of foreign-ion doping and recent achievements for nickel-rich cathode materials, Energy Storage Mater 57 (2023) 14–43.
[35] H. Tang, L. Duan, J. Liao, X. Sheng, J. Xu, X. Zhou, Magnesium ion-doped layered oxide cathodes for alkali-metal ion batteries: Recent research progress and outlook, Energy Storage Mater 62 (2023) 102935.
[36] Y. Guo, C. Zhang, S. Xin, J. Shi, W. Wang, M. Fan, Y. Chang, W. He, E. Wang, Y. Zou, X. Yang, F. Meng, Y. Zhang, Z. Lei, Y. Yin, Y. Guo, Competitive Doping Chemistry for Nickel-Rich Layered Oxide Cathode Materials, Angew. Chem. 134 (2022) e202116865.
[37] J. Li, M. Zhang, D. Zhang, Y. Yan, Z. Li, An effective doping strategy to improve the cyclic stability and rate capability of Ni-rich $LiNi_{0.8}Co_{0.1}Mn_{0.1}O_2$ cathode, Chem. Eng. J. 402 (2020) 126195.
[38] K. Wang, P. Yan, Z. Wang, J. Fu, Z. Zhang, X. Ke, M. Sui, Advancing layered cathode material's cycling stability from uniform doping to non-uniform doping, J. Mater. Chem. A 8 (2020) 16690–16697.
[39] R. Qing, J. Shi, D. Xiao, X. Zhang, Y. Yin, Y. Zhai, L. Gu, Y. Guo, Enhancing the Kinetics of Li-Rich Cathode Materials through the Pinning Effects of Gradient Surface Na^+ Doping, Adv. Energy Mater. 6 (2016) 1501914.
[40] H. Qian, H. Ren, Y. Zhang, X. He, W. Li, J. Wang, J. Hu, H. Yang, H.M.K. Sari, Y. Chen, X. Li, Surface Doping vs. Bulk Doping of Cathode Materials for Lithium-Ion Batteries: A Review, Electrochem. Energy Rev. 5 (2022) 2.
[41] F. Ding, C. Zhao, D. Xiao, X. Rong, H. Wang, Y. Li, Y. Yang, Y. Lu, Y.-S. Hu, Using High-Entropy Configuration Strategy to Design Na-Ion Layered Oxide Cathodes with Superior Electrochemical Performance and Thermal Stability, J. Am. Chem. Soc. 144 (2022) 8286–8295.
[42] Y. Pang, Y. Wang, X. Ding, Y. Xin, Q. Zhou, C. Jiang, B. Chen, H. Liu, F. Wu, H. Gao, A High-Entropy Approach to Activate the Oxygen Redox Activity and Suppress the Phase Transition of P2-Type Layered Cathode for Sodium-Ion Batteries, ACS Sustainable Chem. Eng. 12 (2024) 8203–8213.
[43] A. Bano, M. Noked, D.T. Major, Theoretical Insights into High-Entropy Ni-Rich Layered Oxide Cathodes for Low-Strain Li-Ion Batteries, Chem. Mater. 35 (2023) 8426–8439.
[44] S. Li, L. Wu, H. Fu, A.M. Rao, L. Cha, J. Zhou, B. Lu, Entropy-Tuned Layered Oxide Cathodes for Potassium-Ion Batteries, Small Methods 7 (2023) 2300893.
[45] Z. Zhou, Y. Ma, T. Brezesinski, B. Breitung, Y. Wu, Y. Ma, Improving upon rechargeable battery technologies: on the role of high-entropy effects, Energy Environ. Sci. 18 (2024) 19–52.
[46] C. Zhao, F. Ding, Y. Lu, L. Chen, Y.-S. Hu, High-Entropy Layered Oxide Cathodes for Sodium-Ion Batteries, Angew. Chem. Int. Ed. 59 (2020) 264–269.
[47] R. Zhang, C. Wang, P. Zou, R. Lin, L. Ma, L. Yin, T. Li, W. Xu, H. Jia, Q. Li, S. Sainio, K. Kisslinger, S.E. Trask, S.N. Ehrlich, Y. Yang, A.M. Kiss, M. Ge, B. J. Polzin, S.J. Lee, W. Xu, Y. Ren, H.L. Xin, Compositionally complex doping for zero-strain zero-cobalt layered cathodes, Nature 610 (2022) 67–73.
[48] F. Ding, Y. Lu, L. Chen, Y.-S. Hu, High-Entropy Strategy for Electrochemical Energy Storage Mater, Electrochem. Energy Rev. 7 (2024) 16.
[49] N.G. Garcia, J.M. Gonçalves, C. Real, B. Freitas, J.G. Ruiz-Montoya, H. Zanin, Medium- and high-entropy materials as positive electrodes for sodium-ion batteries: Quo Vadis? Energy Storage Mater 67 (2024) 103213.
[50] B. Ran, H. Li, R. Cheng, Z. Yang, Y. Zhong, Y. Qin, C. Yang, C. Fu, High-Entropy Oxides for Rechargeable Batteries, Adv. Sci. 11 (2024) 2401034.
[51] G.M. Tomboc, X. Zhang, S. Choi, D. Kim, L.Y.S. Lee, K. Lee, Stabilization, Characterization, and Electrochemical Applications of High-Entropy Oxides: Critical Assessment of Crystal Phase–Properties Relationship, Adv. Funct. Mater. 32 (2022) 2205142.
[52] F. Fu, X. Liu, X. Fu, H. Chen, L. Huang, J. Fan, J. Le, Q. Wang, W. Yang, Y. Ren, K. Amine, S.-G. Sun, G.-L. Xu, Entropy and crystal-facet modulation of P2-type layered cathodes for long-lasting sodium-based batteries, Nat. Commun. 13 (2022) 2826.
[53] S. Xu, L. Zhao, S. Li, S. Guo, Revealing the microstructure and mechanism of layered oxide cathodes for sodium-ion batteries by advanced TEM techniques, Chem. Commun. 61 (2025) 4147–4159.
[54] C. Zhao, Q. Wang, Z. Yao, J. Wang, B. Sánchez-Lengeling, F. Ding, X. Qi, Y. Lu, X. Bai, B. Li, H. Li, A. Aspuru-Guzik, X. Huang, C. Delmas, M. Wagemaker, L. Chen, Y.-S. Hu, Rational design of layered oxide materials for sodium-ion batteries, Science 370 (2020) 708–711.
[55] Y. Ding, D. Mu, B. Wu, R. Wang, Z. Zhao, F. Wu, Recent progresses on nickel-rich layered oxide positive electrode materials used in lithium-ion batteries for electric vehicles, Appl. Energy 195 (2017) 586–599.
[56] W. Lee, S. Muhammad, C. Sergey, H. Lee, J. Yoon, Y. Kang, W. Yoon, Advances in the Cathode Materials for Lithium Rechargeable Batteries, Angew. Chem. Int. Ed. 59 (2020) 2578–2605.
[57] R.J. Clément, P.G. Bruce, C.P. Grey, Review—Manganese-Based P2-Type Transition Metal Oxides as Sodium-Ion Battery Cathode Materials, J. Electrochem. Soc. 162 (2015) A2589–A2604.
[58] S. Cui, Y. Wei, T. Liu, W. Deng, Z. Hu, Y. Su, H. Li, M. Li, H. Guo, Y. Duan, W. Wang, M. Rao, J. Zheng, X. Wang, F. Pan, Optimized Temperature Effect of Li-Ion Diffusion with Layer Distance in $Li(Ni_xMn_yCo_z)O_2$ Cathode Materials for High Performance Li-Ion Battery, Adv. Energy Mater. 6 (2016) 1501309.
[59] M.G.T. Nathan, H. Yu, G.-T. Kim, J.-H. Kim, J.S. Cho, J. Kim, J.-K. Kim, Recent Advances in Layered Metal-Oxide Cathodes for Application in Potassium-Ion Batteries, Adv. Sci. 9 (2022) 2105882.
[60] C. Delmas, C. Fouassier, P. Hagenmuller, Structural classification and properties of the layered oxides, Physica B+C 99 (1980) 81–85.
[61] L. Liang, W. Zhang, F. Zhao, D.K. Denis, L. Hou, C. Yuan, Surface/Interface Structure Degradation of Ni-Rich Layered Oxide Cathodes toward Lithium-Ion Batteries: Fundamental Mechanisms and Remedying Strategies, Adv. Mater. Int. 7 (2020) 1901749.
[62] M. Zhang, W. Huang, J. Tang, Z. Liu, C. Sheng, X. Sun, H. Zhong, S. Xu, W. Ning, X. Xiao, T. Liu, S. Guo, H. Zhou, Precise Synthesis of 4.75 V-Tolerant $LiCoO_2$ with Homogeneous Delithiation and Reduced Internal Strain, J. Am. Chem. Soc. 147 (2025) 1563–1573.
[63] M.M. Thackeray, K. Amine, Layered Li–Ni–Mn–Co oxide cathodes, Nat Energy 6 (2021) 933. –933.
[64] A. Manthiram, J.B. Goodenough, Layered lithium cobalt oxide cathodes, Nat. Energy 6 (2021) 323. –323.
[65] W. Li, E.M. Erickson, A. Manthiram, High-nickel layered oxide cathodes for lithium-based automotive batteries, Nat. Energy 5 (2020) 26–34.

[66] P. Oh, J. Yun, S. Park, G. Nam, M. Liu, J. Cho, Recent Advances and Prospects of Atomic Substitution on Layered Positive Materials for Lithium-Ion Battery, Adv. Energy Mater. 11 (2021) 2003197.

[67] S. Zhao, Z. Guo, K. Yan, S. Wan, F. He, B. Sun, G. Wang, Towards high-energy-density lithium-ion batteries: Strategies for developing high-capacity lithium-rich cathode materials, Energy Storage Mater 34 (2021) 716–734.

[68] Y. Gao, Z. Pan, J. Sun, Z. Liu, J. Wang, High-Energy Batteries: Beyond Lithium-Ion and Their Long Road to Commercialisation, Nano-Micro Lett 14 (2022) 94.

[69] X. Ji, Q. Xia, Y. Xu, H. Feng, P. Wang, Q. Tan, A review on progress of lithium-rich manganese-based cathodes for lithium ion batteries, J. Power Sources 487 (2021) 229362.

[70] A. Manthiram, J.C. Knight, S. Myung, S. Oh, Y. Sun, Nickel-Rich and Lithium-Rich Layered Oxide Cathodes: Progress and Perspectives, Adv. Energy Mater. 6 (2016) 1501010.

[71] H. Ge, Z. Shen, Y. Wang, Z. Sun, X. Cao, C. Wang, X. Fan, J. Bai, R. Li, T. Yang, G. Wu, Design of high-performance and sustainable Co-free Ni-rich cathodes for next-generation lithium-ion batteries, SusMat 4 (2024) 48–71.

[72] L. Zeng, H. Liang, B. Qiu, Z. Shi, S. Cheng, K. Shi, Q. Liu, Z. Liu, Voltage Decay of Li-Rich Layered Oxides: Mechanism, Modification Strategies, and Perspectives, Adv. Funct. Mater. 33 (2023) 2213260.

[73] T. Liu, J. Liu, L. Li, L. Yu, J. Diao, T. Zhou, S. Li, A. Dai, W. Zhao, S. Xu, Y. Ren, L. Wang, T. Wu, R. Qi, Y. Xiao, J. Zheng, W. Cha, R. Harder, I. Robinson, J. Wen, J. Lu, F. Pan, K. Amine, Origin of structural degradation in Li-rich layered oxide cathode, Nature 606 (2022) 305–312.

[74] G. Xu, X. Liu, A. Daali, R. Amine, Z. Chen, K. Amine, Challenges and Strategies to Advance High-Energy Nickel-Rich Layered Lithium Transition Metal Oxide Cathodes for Harsh Operation, Adv. Funct. Mater. 30 (2020) 2004748.

[75] J. Liu, J. Wang, Y. Ni, K. Zhang, F. Cheng, J. Chen, Recent breakthroughs and perspectives of high-energy layered oxide cathode materials for lithium ion batteries, Materials Today 43 (2021) 132–165.

[76] D. Ko, J. Park, B.Y. Yu, D. Ahn, K. Kim, H.N. Han, W.S. Jeon, C. Jung, A. Manthiram, Degradation of High-Nickel-Layered Oxide Cathodes from Surface to Bulk: A Comprehensive Structural, Chemical, and Electrical Analysis, Adv. Energy Mater. 10 (2020) 2001035.

[77] Y. Luo, Q. Pan, H. Wei, Y. Huang, L. Tang, Z. Wang, C. Yan, J. Mao, K. Dai, Q. Wu, X. Zhang, J. Zheng, Fundamentals of Ion-Exchange Synthesis and Its Implications in Layered Oxide Cathodes: Recent Advances and Perspective, Adv. Energy Mater. 13 (2023) 2300125.

[78] Z. Xu, K. Song, X. Chang, L. Li, W. Zhang, Y. Xue, J. Zhang, D. Lin, Z. Liu, Q. Wang, Y. Yu, C. Yang, Layered oxide cathodes: A comprehensive review of characteristics, research, and development in lithium and sodium ion batteries, Carbon Neutralization 3 (2024) 832–856.

[79] S. Komaba, N. Yabuuchi, T. Nakayama, A. Ogata, T. Ishikawa, I. Nakai, Study on the Reversible Electrode Reaction of $Na_{1-x}Ni_{0.5}Mn_{0.5}O_2$ for a Rechargeable Sodium-Ion Battery, Inorg. Chem. 51 (2012) 6211–6220.

[80] X. Li, Y. Wang, D. Wu, L. Liu, S.-H. Bo, G. Ceder, Jahn–Teller Assisted Na Diffusion for High Performance Na Ion Batteries, Chem. Mater. 28 (2016) 6575–6583.

[81] C. Luo, A. Langrock, X. Fan, Y. Liang, C. Wang, P2-type transition metal oxides for high performance Na-ion battery cathodes, J. Mater. Chem. A 5 (2017) 18214–18220.

[82] Y. Yang, Z. Wang, C. Du, B. Wang, X. Li, S. Wu, X. Li, X. Zhang, X. Wang, Y. Niu, F. Ding, X. Rong, Y. Lu, N. Zhang, J. Xu, R. Xiao, Q. Zhang, X. Wang, W. Yin, J. Zhao, L. Chen, J. Huang, Y.-S. Hu, Decoupling the air sensitivity of Na-layered oxides, Science 385 (2024) 744–752.

[83] Z. Liu, Advances and perspectives on transitional metal layered oxides for potassium-ion battery, Energy Storage Mater 34 (2021) 211–228.

[84] Z. Xiao, F. Xia, L. Xu, X. Wang, J. Meng, H. Wang, X. Zhang, L. Geng, J. Wu, L. Mai, Suppressing the Jahn–Teller Effect in Mn-Based Layered Oxide Cathode toward Long-Life Potassium-Ion Batteries, Adv. Funct. Mater. 32 (2022) 2108244.

[85] R.-J. Luo, X.-L. Li, J.-Y. Ding, J. Bao, C. Ma, C.-Y. Du, X.-Y. Cai, X.-J. Wu, Y.-N. Zhou, Suppressing Jahn-Teller distortion and phase transition of $K_{0.5}MnO_2$ by K-site Mg substitution for potassium-ion batteries, Energy Storage Mater 47 (2022) 408–414.

[86] Y. Hironaka, K. Kubota, S. Komaba, P2- and P3-K_xCoO_2 as an electrochemical potassium intercalation host, Chem. Commun. 53 (2017) 3693–3696.

[87] H.-H. Ryu, H.H. Sun, S.-T. Myung, C.S. Yoon, Y.-K. Sun, Reducing cobalt from lithium-ion batteries for the electric vehicle era, Energy Environ. Sci. 14 (2021) 844–852.

[88] X. Xu, X.-L. Li, M.M. Rahman, J. Bao, R.-J. Luo, C. Ma, C.-Y. Du, J. Zeng, Z. Mei, Z. Qian, E. Hu, Y.-N. Zhou, Promoting reversibility of layered potassium cathode through interstitial doping, Chem. Eng. J. 477 (2023) 147021.

[89] Y.-S. Xu, M.-Y. Qi, Q.-H. Zhang, F.-Q. Meng, Y.-N. Zhou, S.-J. Guo, Y.-G. Sun, L. Gu, B.-B. Chang, C.-T. Liu, A.-M. Cao, L.-J. Wan, Anion Doping for Layered Oxides with a Solid-Solution Reaction for Potassium-Ion Battery Cathodes, ACS Appl. Mater. Interfaces 14 (2022) 13379–13387.

[90] A. Choi, J. Lim, H. Kim, S.C. Jung, H. Lim, H. Kim, M. Kwon, Y.K. Han, S.M. Oh, K.T. Lee, Site-Selective In Situ Electrochemical Doping for Mn-Rich Layered Oxide Cathode Materials in Lithium-Ion Batteries, Adv. Energy Mater. 8 (2018) 1702514.

[91] Y. Huang, Y. Zhu, A. Nie, H. Fu, Z. Hu, X. Sun, S.-C. Haw, J.-M. Chen, T.-S. Chan, S. Yu, G. Sun, G. Jiang, J. Han, W. Luo, Y. Huang, Enabling Anionic Redox Stability of P2-$Na_{5/6}Li_{1/4}Mn_{3/4}O_2$ by Mg Substitution, Adv. Mater. 34 (2022) 2105404.

[92] R. Huang, Q. Xue, J. Lin, X. Zhang, J. Zhou, F. Wu, L. Li, R. Chen, Layered K0.54Mn0.78Mg0.22O2 as a high-performance cathode material for potassium-ion batteries, Nano Res 15 (2022) 3143–3149.

[93] Z. Zhang, Y. Liu, Z. Liu, H. Li, Y. Huang, W. Liu, D. Ruan, X. Cai, X. Yu, Dual-strategy of Cu-doping and O3 biphasic structure enables Fe/Mn-based layered oxide for high-performance sodium-ion batteries cathode, J. Power Sources 567 (2023) 232930.

[94] W. Kang, Z. Zhang, P.-K. Lee, T.-W. Ng, W. Li, Y. Tang, W. Zhang, C.-S. Lee, D. Y. Wai Yu, Copper substituted P2-type $Na_{0.67}Cu_xMn_{1-x}O_2$: a stable high-power sodium-ion battery cathode, J. Mater. Chem. A 3 (2015) 22846–22852.

[95] L. Wang, Y.-G. Sun, L.-L. Hu, J.-Y. Piao, J. Guo, A. Manthiram, J. Ma, A.-M. Cao, Copper-substituted $Na_{0.67}Ni_{0.3-x}Cu_xMn_{0.7}O_2$ cathode materials for sodium-ion batteries with suppressed P2–O2 phase transition, J. Mater. Chem. A 5 (2017) 8752–8761.

[96] H. Liu, X. Gao, J. Chen, J. Gao, H. Wang, Y. Mei, H. Liu, W. Deng, G. Zou, H. Hou, X. Ji, Cu-substitution P2-$Na_{0.66}Mn_{1-x}Cu_xO_2$ sodium-ion cathode with enhanced interlayer stability, J. Energy Chem. 75 (2022) 478–485.

[97] T. Chen, W. Liu, Y. Zhuo, H. Hu, M. Zhu, R. Cai, X. Chen, J. Yan, K. Liu, Single-phase P2-type layered oxide with Cu-substitution for sodium ion batteries, J. Energy Chem. 43 (2020) 148–154.

[98] X. Bai, M. Sathiya, B. Mendoza-Sánchez, A. Iadecola, J. Vergnet, R. Dedryvère, M. Saubanère, A.M. Abakumov, P. Rozier, J. Tarascon, Anionic Redox Activity in a Newly Zn-Doped Sodium Layered Oxide P2-$Na_{2/3}Mn_{1-y}Zn_yO_2$ ($0<y<0.23$), Adv. Energy Mater. 8 (2018) 1802379.

[99] K. Zhang, D. Kim, Z. Hu, M. Park, G. Noh, Y. Yang, J. Zhang, V.W. Lau, S.-L. Chou, M. Cho, S.-Y. Choi, Y.-M. Kang, Manganese based layered oxides with modulated electronic and thermodynamic properties for sodium ion batteries, Nat. Commun. 10 (2019) 5203.

[100] W. Cheng, J. Ding, Z. Liu, J. Zhang, Q. Liu, X. Wang, L. Wang, Z. Sun, Y. Cheng, Z. Xu, Y. Lei, J. Wang, Y. Huang, Zn/Ti dual concentration-gradients surface doping to improve the stability and kinetics for Li-rich layered oxides cathode, Chem. Eng. J. 451 (2023) 138678.

[101] Y. Lu, M. Song, J. Huang, L. Zhang, B. Zhao, W. Wu, X. Wu, K/Zn dual-site doping toward ultralow-strain P2-type Ni/Mn-based cathode materials for sodium-ion batteries, J. Energy Storage 77 (2024) 109933.

[102] Z. Feng, S. Zhang, R. Rajagopalan, X. Huang, Y. Ren, D. Sun, H. Wang, Y. Tang, Dual-Element-Modified Single-Crystal $LiNi_{0.6}Co_{0.2}Mn_{0.2}O_2$ as a Highly Stable Cathode for Lithium-Ion Batteries, ACS Appl. Mater. Interfaces 13 (2021) 43039–43050.

[103] R. Dang, N. Li, Y. Yang, K. Wu, Q. Li, Y.L. Lee, X. Liu, Z. Hu, X. Xiao, Designing advanced P3-type $K_{0.45}Ni_{0.1}Co_{0.1}Mn_{0.8}O_2$ and improving electrochemical performance via Al/Mg doping as a new cathode Material for potassium-ion batteries, J. Power Sources 464 (2020) 228190.

[104] B. Hu, F. Geng, C. Zhao, B. Doumert, J. Trébosc, O. Lafon, C. Li, M. Shen, B. Hu, Deciphering the Origin of High Electrochemical Performance in a Novel Ti-Substituted P2/O3 Biphasic Cathode for Sodium-Ion Batteries, ACS Appl. Mater. Interfaces 12 (2020) 41485–41494.

[105] H.-H. Ryu, N.-Y. Park, J.H. Seo, Y.-S. Yu, M. Sharma, R. Mücke, P. Kaghazchi, C. S. Yoon, Y.-K. Sun, A highly stabilized Ni-rich NCA cathode for high-energy lithium-ion batteries, Materials Today 36 (2020) 73–82.

[106] Y.-J. Guo, P.-F. Wang, Y.-B. Niu, X.-D. Zhang, Q. Li, X. Yu, M. Fan, W.-P. Chen, Y. Yu, X. Liu, Q. Meng, S. Xin, Y.-X. Yin, Y.-G. Guo, Boron-doped sodium layered oxide for reversible oxygen redox reaction in Na-ion battery cathodes, Nat. Commun. 12 (2021) 5267.

[107] X. Wang, X. Dong, X. Feng, Q. Shi, J. Wang, X. Yin, J. Zhang, Y. Zhao, In-Plane BO_3 Configuration in P2 Layered Oxide Enables Outstanding Long Cycle Performance for Sodium Ion Batteries, Small Methods 7 (2023) 2201201.

[108] M.S. Chae, H.J. Kim, J. Lyoo, R. Attias, Y. Gofer, S. Hong, D. Aurbach, Anomalous Sodium Storage Behavior in Al/F Dual-Doped P2-Type Sodium Manganese Oxide Cathode for Sodium-Ion Batteries, Adv. Energy Mater. 10 (2020) 2002205.

[109] H. Chen, Z. Wu, Y. Zhong, T. Chen, X. Liu, J. Qu, W. Xiang, J. Li, X. Chen, X. Guo, B. Zhong, Boosting the reactivity of Ni^{2+}/Ni^{3+} redox couple via fluorine doping of high performance $Na_{0.6}Mn_{0.95}Ni_{0.05}O_{2-x}F_x$ cathode, Electrochim. Acta 308 (2019) 64–73.

[110] H. Wang, A.M. Hashem, A.E. Abdel-Ghany, S.M. Abbas, R.S. El-Tawil, T. Li, X. Li, H. El-Mounayri, A. Tovar, L. Zhu, A. Mauger, C.M. Julien, Effect of Cationic (Na^+) and Anionic (F^-) Co-Doping on the Structural and Electrochemical Properties of $LiNi_{1/3}Mn_{1/3}Co_{1/3}O_2$ Cathode Material for Lithium-Ion Batteries, Int. J. Mol. Sci. 23 (2022) 6755.

[111] Q. Zhang, Y. Huang, Y. Liu, S. Sun, K. Wang, Y. Li, X. Li, J. Han, Y. Huang, F-doped O3-$NaNi_{1/3}Fe_{1/3}Mn_{1/3}O_2$ as high-performance cathode materials for sodium-ion batteries, Sci. China Mater. 60 (2017) 629–636.

[112] W.-J. Shi, Y.-W. Yan, C. Chi, X.-T. Ma, D. Zhang, S.-D. Xu, L. Chen, X.-M. Wang, S.-B. Liu, Fluorine anion doped $Na_{0.44}MnO_2$ with layer-tunnel hybrid structure as advanced cathode for sodium ion batteries, J. Power Sources 427 (2019) 129–137.

[113] X. Cui, S. Wang, X. Ye, X. Fan, C. Gao, Y. Quan, S. Wen, X. Cai, J. Huang, S. Li, Insights into the improved cycle and rate performance by ex-situ F and in-situ Mg dual doping of layered oxide cathodes for sodium-ion batteries, Energy Storage Mater 45 (2022) 1153–1164.

[114] J.O. Binder, S.P. Culver, R. Pinedo, D.A. Weber, M.S. Friedrich, K.I. Gries, K. Volz, W.G. Zeier, J. Janek, Investigation of Fluorine and Nitrogen as Anionic Dopants in Nickel-Rich Cathode Materials for Lithium-Ion Batteries, ACS Appl. Mater. Interfaces 10 (2018) 44452–44462.

[115] Q. Mao, Y. Yu, J. Wang, L. Zheng, Z. Wang, Y. Qiu, Y. Hao, X. Liu, Mitigating the P2–O2 transition and Na^+ /vacancy ordering in $Na_{2/3}Ni_{1/3}Mn_{2/3}O_2$ by anion/

cation dual-doping for fast and stable Na $^{+}$ insertion/extraction, J. Mater. Chem. A 9 (2021) 10803–10811.
[116] X.-Y. Zhang, H.-Y. Hu, X.-Y. Liu, J. Wang, Y.-F. Liu, Y.-F. Zhu, L.-Y. Kong, Z.-C. Jian, S.-L. Chou, Y. Xiao, Expediting layered oxide cathodes based on electronic structure engineering for sodium-ion batteries: Reversible phase transformation, abnormal structural regulation, and stable anionic redox, Nano Energy 128 (2024) 109905.
[117] Q. Wang, S. Mariyappan, G. Rousse, A.V. Morozov, B. Porcheron, R. Dedryvère, J. Wu, W. Yang, L. Zhang, M. Chakir, M. Avdeev, M. Deschamps, Y.-S. Yu, J. Cabana, M.-L. Doublet, A.M. Abakumov, J.-M. Tarascon, Unlocking anionic redox activity in O3-type sodium 3d layered oxides via Li substitution, Nat. Mater. 20 (2021) 353–361.
[118] J.E. Wang, W.H. Han, K.J. Chang, Y.H. Jung, D.K. Kim, New insight into Na intercalation with Li substitution on alkali site and high performance of O3-type layered cathode material for sodium ion batteries, J. Mater. Chem. A 6 (2018) 22731–22740.
[119] Z. Wu, Y. Ni, S. Tan, E. Hu, L. He, J. Liu, M. Hou, P. Jiao, K. Zhang, F. Cheng, J. Chen, Realizing High Capacity and Zero Strain in Layered Oxide Cathodes via Lithium Dual-Site Substitution for Sodium-Ion Batteries, J. Am. Chem. Soc. 145 (2023) 9596–9606.
[120] J. Zhang, T. Cao, Y. Lei, J. Li, W. Fan, B. Zhang, X. Liu, Y. Si, H. Wang, Nickel-rich layered cathode LiNi0.8Co0.1Mn0.1O2 mediated by a selective lattice doping towards high-performance lithium ion battery, J. Alloys Compd. 957 (2023) 170400.
[121] A. Ma, Z. Yin, J. Wang, Z. Wang, H. Guo, G. Yan, Al-doped $NaNi_{1/3}Mn_{1/3}Fe_{1/3}O_2$ for high performance of sodium ion batteries, Ionics 26 (2020) 1797–1804.
[122] M. Matsui, F. Mizukoshi, H. Hasegawa, N. Imanishi, Ca-substituted P3-type $NaxNi_{1/3}Mn_{1/3}Co_{1/3}O_2$ as a potential high voltage cathode active material for sodium-ion batteries, J. Power Sources 485 (2021) 229346.
[123] C. Lv, J. Yang, Y. Peng, X. Duan, J. Ma, Q. Li, T. Wang, 1D Nb-doped $LiNi_{1/3}Co_{1/3}Mn_{1/3}O_2$ nanostructures as excellent cathodes for Li-ion battery, Electrochim. Acta 297 (2019) 258–266.
[124] Z. Yan, L. Tang, Y. Huang, W. Hua, Y. Wang, R. Liu, Q. Gu, S. Indris, S. Chou, Y. Huang, M. Wu, S. Dou, A Hydrostable Cathode Material Based on the Layered P2@P3 Composite that Shows Redox Behavior for Copper in High-Rate and Long-Cycling Sodium-Ion Batteries, Angew. Chem. Int. Ed. 58 (2019) 1412–1416.
[125] Q. Yang, P.-F. Wang, J.-Z. Guo, Z.-M. Chen, W.-L. Pang, K.-C. Huang, Y.-G. Guo, X.-L. Wu, J.-P. Zhang, Advanced P2-$Na_{2/3}Ni_{1/3}Mn_{7/12}Fe_{1/12}O_2$ Cathode Material with Suppressed P2–O2 Phase Transition toward High-Performance Sodium-Ion Battery, ACS Appl. Mater. Interfaces 10 (2018) 34272–34282.
[126] S.C. Han, H. Lim, J. Jeong, D. Ahn, W.B. Park, K.-S. Sohn, M. Pyo, Ca-doped Na_xCoO_2 for improved cyclability in sodium ion batteries, J. Power Sources 277 (2015) 9–16.
[127] J. Feng, Y. Liu, D. Fang, J. Li, Reusing the steel slag to design a gradient-doped high-entropy oxide for high-performance sodium ion batteries, Nano Energy 118 (2023) 109030.
[128] T. Yang, Y. Huang, J. Zhang, H. Zhu, J. Ren, T. Li, L.C. Gallington, S. Lan, L. Yang, Q. Liu, Insights into Ti doping for stabilizing the $Na_{2/3}Fe_{1/3}Mn_{2/3}O_2$ cathode in sodium ion battery, J. Energy Chem. 73 (2022) 542–548.
[129] R. Li, Y. Liu, Z. Wang, J. Li, A P2/O3 biphasic cathode material with highly reversibility synthesized by Sn-substitution for Na-ion batteries, Electrochim. Acta 318 (2019) 14–22.
[130] L. Wang, J. Liang, X. Zhang, S. Li, T. Wang, F. Ma, J. Han, Y. Huang, Q. Li, An effective dual-modification strategy to enhance the performance of $LiNi_{0.6}Co_{0.2}Mn_{0.2}O_2$ cathode for Li-ion batteries, Nanoscale 13 (2021) 4670–4677.
[131] M. Sathiya, Q. Jacquet, M. Doublet, O.M. Karakulina, J. Hadermann, J. Tarascon, A Chemical Approach to Raise Cell Voltage and Suppress Phase Transition in O3 Sodium Layered Oxide Electrodes, Adv. Energy Mater. 8 (2018) 1702599.
[132] D. Gao, Y. Huang, H. Dong, C. Li, C. Chang, Atomic Horizons Interpretation on Enhancing Electrochemical Performance of Ni-Rich NCM Cathode via W Doping: Dual Improvements in Electronic and Ionic Conductivities from DFT Calculations and Experimental Confirmation, Small 19 (2023) 2205122.
[133] W. Han, X. Gao, Y. Song, X. Wang, G. Gao, H. Chen, Q. Gu, W. Luo, Synergistic Effect of Co-Mo Pinning in Lay-Structured Oxide Cathode for Enhancing Stability toward Potassium-Ion Batteries, Small 20 (2024) 2400252.
[134] H.H. Sun, U.-H. Kim, J.-H. Park, S.-W. Park, D.-H. Seo, A. Heller, C.B. Mullins, C. S. Yoon, Y.-K. Sun, Transition metal-doped Ni-rich layered cathode materials for durable Li-ion batteries, Nat. Commun. 12 (2021) 6552.
[135] L. Bao, Z. Yang, L. Chen, Y. Su, Y. Lu, W. Li, F. Yuan, J. Dong, Y. Fang, Z. Ji, C. Shi, W. Feng, The Effects of Trace Yb Doping on the Electrochemical Performance of Li-Rich Layered Oxides, ChemSusChem 12 (2019) 2294–2301.
[136] Y. Cheng, Y. Sun, C. Chu, L. Chang, Z. Wang, D. Zhang, W. Liu, Z. Zhuang, L. Wang, Stabilizing effects of atomic Ti doping on high-voltage high-nickel layered oxide cathode for lithium-ion rechargeable batteries, Nano Res 15 (2022) 4091–4099.
[137] A. Gomez-Martin, F. Reissig, L. Frankenstein, M. Heidbüchel, M. Winter, T. Placke, R. Schmuch, Magnesium Substitution in Ni-Rich NMC Layered Cathodes for High-Energy Lithium Ion Batteries, Adv. Energy Mater. 12 (2022) 2103045.
[138] K. Mathiyalagan, K. Karuppiah, A. Ponnaiah, S. Rengapillai, S. Marimuthu, Significant role of magnesium substitution in improved performance of layered O3-Na-Mn-Ni-Mg-O cathode material for developing sodium-ion batteries, Int. J. Energy Res. 46 (2022) 10656–10667.
[139] R.J. Clément, J. Billaud, A. Robert Armstrong, G. Singh, T. Rojo, P.G. Bruce, C. P. Grey, Structurally stable Mg-doped P2-$Na_{2/3}Mn_{1-y}Mg_yO_2$ sodium-ion battery cathodes with high rate performance: insights from electrochemical, NMR and diffraction studies, Energy Environ. Sci. 9 (2016) 3240–3251.
[140] M. Chandra, R. Shukla, R. Saroha, A.K. Panwar, A. Gupta, S. Basu, R.S. Dhaka, Physical properties and electrochemical performance of Zn-substituted $Na_{0.44}Mn_{1-x}Zn_xO_2$ nanostructures as cathode in Na-ion batteries, Ceram. Int. 44 (2018) 21127–21131.
[141] X. Gao, J. Chen, H. Liu, S. Yin, Y. Tian, X. Cao, G. Zou, H. Hou, W. Wei, L. Chen, X. Ji, Copper-substituted Na_xMO_2 (M=Fe, Mn) cathodes for sodium ion batteries: Enhanced cycling stability through suppression of Mn(III) formation, Chem. Eng. J. 406 (2021) 126830.
[142] Z. Chen, R. Jiao, H. Liu, H. Wang, X. Liu, X. Zhang, M. Jia, Y. Chen, X. Yan, Coupling the Electronic Distribution and Oxygen Redox Potential via Cu Substitution of Layered Oxide Cathodes for Sodium-Ion Batteries, ACS Sustainable Chem. Eng. 12 (2024) 816–825.
[143] X. Rong, E. Hu, Y. Lu, F. Meng, C. Zhao, X. Wang, Q. Zhang, X. Yu, L. Gu, Y.-S. Hu, H. Li, X. Huang, X.-Q. Yang, C. Delmas, L. Chen, Anionic Redox Reaction-Induced High-Capacity and Low-Strain Cathode with Suppressed Phase Transition, Joule 3 (2019) 503–517.
[144] X. Rong, J. Liu, E. Hu, Y. Liu, Y. Wang, J. Wu, X. Yu, K. Page, Y.-S. Hu, W. Yang, H. Li, X.-Q. Yang, L. Chen, X. Huang, Structure-Induced Reversible Anionic Redox Activity in Na Layered Oxide Cathode, Joule 2 (2018) 125–140.
[145] U. Maitra, R.A. House, J.W. Somerville, N. Tapia-Ruiz, J.G. Lozano, N. Guerrini, R. Hao, K. Luo, L. Jin, M.A. Pérez-Osorio, F. Massel, D.M. Pickup, S. Ramos, X. Lu, D.E. McNally, A.V. Chadwick, F. Giustino, T. Schmitt, L.C. Duda, M.R. Roberts, P. G. Bruce, Oxygen redox chemistry without excess alkali-metal ions in $Na_{2/3}[Mg_{0.28}Mn_{0.72}]O_2$, Nat. Chem. 10 (2018) 288–295.
[146] K. Wang, H. Wan, P. Yan, X. Chen, J. Fu, Z. Liu, H. Deng, F. Gao, M. Sui, Dopant Segregation Boosting High-Voltage Cyclability of Layered Cathode for Sodium Ion Batteries, Adv. Mater. 31 (2019) 1904816.
[147] Y. Wang, L. Wang, H. Zhu, J. Chu, Y. Fang, L. Wu, L. Huang, Y. Ren, C. Sun, Q. Liu, X. Ai, H. Yang, Y. Cao, Ultralow-Strain Zn-Substituted Layered Oxide Cathode with Suppressed P2–O2 Transition for Stable Sodium Ion Storage, Adv. Funct. Mater. 30 (2020) 1910327.
[148] E. De La Llave, E. Talaie, E. Levi, P.K. Nayak, M. Dixit, P.T. Rao, P. Hartmann, F. Chesneau, D.T. Major, M. Greenstein, D. Aurbach, L.F. Nazar, Improving Energy Density and Structural Stability of Manganese Oxide Cathodes for Na-Ion Batteries by Structural Lithium Substitution, Chem. Mater. 28 (2016) 9064–9076.
[149] Q.-C. Wang, J.-K. Meng, X.-Y. Yue, Q.-Q. Qiu, Y. Song, X.-J. Wu, Z.-W. Fu, Y.-Y. Xia, Z. Shadike, J. Wu, X.-Q. Yang, Y.-N. Zhou, Tuning P2-Structured Cathode Material by Na-Site Mg Substitution for Na-Ion Batteries, J. Am. Chem. Soc. 141 (2019) 840–848.
[150] J. Liu, W. Huang, R. Liu, J. Lang, Y. Li, T. Liu, K. Amine, H. Li, Entropy Tuning Stabilizing P2-Type Layered Cathodes for Sodium-Ion Batteries, Adv. Funct. Mater. 34 (2024) 2315437.
[151] L. Sun, Y. Xie, X. Liao, H. Wang, G. Tan, Z. Chen, Y. Ren, J. Gim, W. Tang, Y. He, K. Amine, Z. Ma, Insight into Ca-Substitution Effects on O3-Type $NaNi_{1/3}Fe_{1/3}Mn_{1/3}O_2$ Cathode Materials for Sodium-Ion Batteries Application, Small 14 (2018) 1704523.
[152] B. Peng, Y. Chen, F. Wang, Z. Sun, L. Zhao, X. Zhang, W. Wang, G. Zhang, Unusual Site-Selective Doping in Layered Cathode Strengthens Electrostatic Cohesion of Alkali-Metal Layer for Practicable Sodium-Ion Full Cell, Adv. Mater. 34 (2022) 2103210.
[153] M. Shen, J. Wang, Z. Ren, T. Wu, X. Liu, L. Chen, W. Li, A. Lu, Quasi-Zero Volume Strain Cathode Materials for Sodium Ion Battery through Synergetic Substitution Effect of Li and Mg, Adv. Funct. Mater. 33 (2023) 2303812.
[154] Y. Wang, G. Hu, Z. Peng, Y. Cao, X. Lai, X. Qi, Z. Gan, W. Li, Z. Luo, K. Du, Influence of Li substitution on the structure and electrochemical performance of P2-type $Na_{0.67}Ni_{0.2}Fe_{0.15}Mn_{0.65}O_2$ cathode materials for sodium ion batteries, J. Power Sources 396 (2018) 639–647.
[155] C. Wang, L. Liu, S. Zhao, Y. Liu, Y. Yang, H. Yu, S. Lee, G.-H. Lee, Y.-M. Kang, R. Liu, F. Li, J. Chen, Tuning local chemistry of P2 layered-oxide cathode for high energy and long cycles of sodium-ion battery, Nat. Commun. 12 (2021) 2256.
[156] R. Saroha, Synergetic effects of cation (K^{+}) and anion (S^{2-}) doping on the structural integrity of Li/Mn-rich layered cathode material with considerable cyclability and high-rate capability for Li-ion batteries, Electrochim. Acta 366 (2021) 137471.
[157] C.-F. Li, L.-D. Chen, L. Wu, Y. Liu, Z.-Y. Hu, W.-J. Cui, W.-D. Dong, X. Liu, W.-B. Yu, Y. Li, G. Van Tendeloo, B.-L. Su, Directly revealing the structure-property correlation in Na^{+}-doped cathode materials, Appl. Surf. Sci. 612 (2023) 155810.
[158] P. Vanaphuti, Y. Liu, X. Ma, J. Fu, Y. Lin, J. Wen, Z. Yang, Y. Wang, Stabilized Lithium, Manganese-Rich Layered Cathode Materials Enabled by Integrating Co-Doping and Nanocoating, ACS Appl. Mater. Interfaces 13 (2021) 22597–22607.
[159] Y. Liu, W.-B. Yu, B.-X. Xu, Impedance modelling of all-solid-state thin film batteries: influence of the reaction kinetics, J. Mater. Chem. A 10 (2022) 313–325.
[160] Q. Li, G. Li, C. Fu, D. Luo, J. Fan, L. Li, K^{+}-Doped $Li_{1.2}Mn_{0.54}Co_{0.13}Ni_{0.13}O_2$: A Novel Cathode Material with an Enhanced Cycling Stability for Lithium-Ion Batteries, ACS Appl. Mater. Interfaces 6 (2014) 10330–10341.
[161] F. Kong, C. Liang, R.C. Longo, D.-H. Yeon, Y. Zheng, J.-H. Park, S.-G. Doo, K. Cho, Conflicting Roles of Anion Doping on the Electrochemical Performance of Li-Ion Battery Cathode Materials, Chem. Mater. 28 (2016) 6942–6952.
[162] Q. Wang, A. Sarkar, D. Wang, L. Velasco, R. Azmi, S.S. Bhattacharya, T. Bergfeldt, A. Düvel, P. Heitjans, T. Brezesinski, H. Hahn, B. Breitung, Multi-anionic and -cationic compounds: new high entropy materials for advanced Li-ion batteries, Energy Environ. Sci. 12 (2019) 2433–2442.

[163] J. Wang, C. Liu, G. Xu, C. Miao, M. Wen, M. Xu, C. Wang, W. Xiao, Strengthened the structural stability of in-situ F^- doping Ni-rich $LiNi_{0.8}Co_{0.15}Al_{0.05}O_2$ cathode materials for lithium-ion batteries, Chem. Eng. J. 438 (2022) 135537.
[164] U.-H. Kim, G.-T. Park, P. Conlin, N. Ashburn, K. Cho, Y.-S. Yu, D.A. Shapiro, F. Maglia, S.-J. Kim, P. Lamp, C.S. Yoon, Y.-K. Sun, Cation ordered Ni-rich layered cathode for ultra-long battery life, Energy Environ. Sci. 14 (2021) 1573–1583.
[165] J. Wang, X. Lei, S. Guo, L. Gu, X. Wang, A. Yu, D. Su, Doping Strategy in Nickel-Rich Layered Oxide Cathode for Lithium-Ion Battery, Renewables 1 (2023) 316–340.
[166] A.V. Radhamani, C. Karthik, R. Ubic, M.S. Ramachandra Rao, C. Sudakar, Suppression of antisite defects in fluorine-doped $LiFePO_4$, Scr. Mater. 69 (2013) 96–99.
[167] Z. Ahaliabadeh, X. Kong, E. Fedorovskaya, T. Kallio, Extensive comparison of doping and coating strategies for Ni-rich positive electrode materials, J. Power Sources 540 (2022) 231633.
[168] J. Wang, X. Lei, S. Guo, L. Gu, X. Wang, A. Yu, D. Su, Doping Strategy in Nickel-Rich Layered Oxide Cathode for Lithium-Ion Battery, Renewables 1 (2023) 316–340.
[169] C. Tian, F. Lin, M.M. Doeff, Electrochemical Characteristics of Layered Transition Metal Oxide Cathode Materials for Lithium Ion Batteries: Surface, Bulk Behavior, and Thermal Properties, Acc. Chem. Res. 51 (2018) 89–96.
[170] C. Wang, L. Han, R. Zhang, H. Cheng, L. Mu, K. Kisslinger, P. Zou, Y. Ren, P. Cao, F. Lin, H.L. Xin, Resolving atomic-scale phase transformation and oxygen loss mechanism in ultrahigh-nickel layered cathodes for cobalt-free lithium-ion batteries, Matter 4 (2021) 2013–2026.
[171] J.-N. Zhang, Q. Li, C. Ouyang, X. Yu, M. Ge, X. Huang, E. Hu, C. Ma, S. Li, R. Xiao, W. Yang, Y. Chu, Y. Liu, H. Yu, X.-Q. Yang, X. Huang, L. Chen, H. Li, Trace doping of multiple elements enables stable battery cycling of $LiCoO_2$ at 4.6 V, Nat. Energy 4 (2019) 594–603.
[172] H. Fu, Y.-P. Wang, G. Fan, S. Guo, X. Xie, X. Cao, B. Lu, M. Long, J. Zhou, S. Liang, Synergetic stability enhancement with magnesium and calcium ion substitution for Ni/Mn-based P2-type sodium-ion battery cathodes, Chem. Sci. 13 (2022) 726–736.
[173] A. Anilkumar, N. Nair, S.V. Nair, S. Baskar, Tailoring high Na content in P2-type layered oxide cathodes via Cu Li dual doping for sodium-ion batteries, J. Energy Storage 72 (2023) 108291.
[174] B. Guo, Aluminum and fluorine co-doping for promotion of stability and safety of lithium-rich layered cathode material, Electrochim. Acta 236 (2017) 171–179.
[175] W. Yan, S. Yang, Y. Huang, Y. Yang, Guohui Yuan, A review on doping/coating of nickel-rich cathode materials for lithium-ion batteries, J. Alloys Compd. 819 (2020) 153048.
[176] H. Yu, Y. Cao, L. Chen, Y. Hu, X. Duan, S. Dai, C. Li, H. Jiang, Surface enrichment and diffusion enabling gradient-doping and coating of Ni-rich cathode toward Li-ion batteries, Nat. Commun. 12 (2021) 4564.
[177] D. Kong, J. Hu, Z. Chen, K. Song, C. Li, M. Weng, M. Li, R. Wang, T. Liu, J. Liu, M. Zhang, Y. Xiao, F. Pan, Ti-Gradient Doping to Stabilize Layered Surface Structure for High Performance High-Ni Oxide Cathode of Li-Ion Battery, Adv. Energy Mater. 9 (2019) 1901756.
[178] K. Park, H. Jung, L. Kuo, P. Kaghazchi, C.S. Yoon, Y. Sun, Improved Cycling Stability of $Li[Ni_{0.90}Co_{0.05}Mn_{0.05}]O_2$ Through Microstructure Modification by Boron Doping for Li-Ion Batteries, Adv. Energy Mater. 8 (2018) 1801202.
[179] S. Liu, Z. Liu, X. Shen, W. Li, Y. Gao, M.N. Banis, M. Li, K. Chen, L. Zhu, R. Yu, Z. Wang, X. Sun, G. Lu, Q. Kong, X. Bai, L. Chen, Surface Doping to Enhance Structural Integrity and Performance of Li-Rich Layered Oxide, Adv. Energy Mater. 8 (2018) 1802105.
[180] S. Schweidler, M. Botros, F. Strauss, Q. Wang, Y. Ma, L. Velasco, G. Cadilha Marques, A. Sarkar, C. Kübel, H. Hahn, J. Aghassi-Hagmann, T. Brezesinski, B. Breitung, High-entropy materials for energy and electronic applications, Nat. Rev. Mater. 9 (2024) 266–281.
[181] J. Zhao, S. Gao, H. Wei, Z. Wei, F. Du, High Entropy Materials for Reversible Electrochemical Energy Storage Systems, ChemElectroChem 11 (2024) e202300606.
[182] J.W. Sturman, E.A. Baranova, Y. Abu-Lebdeh, Review: High-Entropy Materials for Lithium-Ion Battery Electrodes, Front. Energy Res. 10 (2022) 862551.
[183] Y. Ma, Y. Ma, S.L. Dreyer, Q. Wang, K. Wang, D. Goonetilleke, A. Omar, D. Mikhailova, H. Hahn, B. Breitung, T. Brezesinski, High-Entropy Metal–Organic Frameworks for Highly Reversible Sodium Storage, Adv. Mater. 33 (2021) 2101342.
[184] A. Sarkar, B. Breitung, H. Hahn, High entropy oxides: The role of entropy, enthalpy and synergy, Scr. Mater. 187 (2020) 43–48.
[185] J.-W. Yeh, S.-K. Chen, S.-J. Lin, J.-Y. Gan, T.-S. Chin, T.-T. Shun, C.-H. Tsau, S.-Y. Chang, Nanostructured High-Entropy Alloys with Multiple Principal Elements: Novel Alloy Design Concepts and Outcomes, Adv. Eng. Mater. 6 (2004) 299–303.
[186] B. Cantor, I.T.H. Chang, P. Knight, A.J.B. Vincent, Microstructural development in equiatomic multicomponent alloys, Mater. Sci. Eng. A 375–377 (2004) 213–218.
[187] D. Lu, X. Fu, D. Guo, W. Ma, S. Sun, G. Shao, Z. Zhou, Challenges and opportunities in 2D high-entropy alloy electrocatalysts for sustainable energy conversion, SusMat 3 (2023) 730–748.
[188] W. Shi, H. Liu, Z. Li, C. Li, J. Zhou, Y. Yuan, F. Jiang, (Kelvin) Kun Fu, Y. Yao, High-entropy alloy stabilized and activated Pt clusters for highly efficient electrocatalysis, SusMat 2 (2022) 186–196.
[189] C.M. Rost, E. Sachet, T. Borman, A. Moballegh, E.C. Dickey, D. Hou, J.L. Jones, S. Curtarolo, J.-P. Maria, Entropy-stabilized oxides, Nat. Commun. 6 (2015) 8485.
[190] Y. Ma, Y. Ma, Q. Wang, S. Schweidler, M. Botros, T. Fu, H. Hahn, T. Brezesinski, B. Breitung, High-entropy energy materials: challenges and new opportunities, Energy Environ. Sci. 14 (2021) 2883–2905.
[191] D. Liu, P. Guo, H. Pan, R. Wu, Emerging high-entropy compounds for electrochemical energy storage and conversion, Prog. Mater. Sci. 145 (2024) 101300.
[192] A. Sarkar, R. Djenadic, N.J. Usharani, K.P. Sanghvi, V.S.K. Chakravadhanula, A. S. Gandhi, H. Hahn, S.S. Bhattacharya, Nanocrystalline multicomponent entropy stabilised transition metal oxides, J. Eur. Ceram. Soc. 37 (2017) 747–754.
[193] H. Gao, J. Li, F. Zhang, C. Li, J. Xiao, X. Nie, G. Zhang, Y. Xiao, D. Zhang, X. Guo, Y. Wang, Y. Kang, G. Wang, H. Liu, Revealing the Potential and Challenges of High-Entropy Layered Cathodes for Sodium-Based Energy Storage, Adv. Energy Mater. 14 (2024) 2304529.
[194] F. Wu, S. Wu, X. Ye, Y. Ren, P. Wei, Research progress of high-entropy cathode materials for sodium-ion batteries, Chin. Chem. Lett. (2024) 109851.
[195] X. Gao, X. Zhang, X. Liu, Y. Tian, Q. Cai, M. Jia, X. Yan, Recent Advances for High-Entropy based Layered Cathodes for Sodium Ion Batteries, Small Methods 7 (2023) 2300152.
[196] B.S. Murty, J.-W. Yeh, S. Ranganathan, High-entropy alloys, Elsevier Inc, Londres, 2014.
[197] D.B. Miracle, O.N. Senkov, A critical review of high entropy alloys and related concepts, Acta Materialia 122 (2017) 448–511.
[198] R. Carroll, C. Lee, C.-W. Tsai, J.-W. Yeh, J. Antonaglia, B.A.W. Brinkman, M. LeBlanc, X. Xie, S. Chen, P.K. Liaw, K.A. Dahmen, Experiments and Model for Serration Statistics in Low-Entropy, Medium-Entropy and High-Entropy Alloys, Sci. Rep. 5 (2015) 16997.
[199] W. Zheng, G. Liang, Q. Liu, J. Li, J.A. Yuwono, S. Zhang, V.K. Peterson, Z. Guo, The promise of high-entropy materials for high-performance rechargeable Li-ion and Na-ion batteries, Joule 7 (2023) 2732–2748.
[200] B. Wang, J. Ma, K. Wang, D. Wang, G. Xu, X. Wang, Z. Hu, C. Pao, J. Chen, L. Du, X. Du, G. Cui, High-Entropy Phase Stabilization Engineering Enables High-Performance Layered Cathode for Sodium-Ion Batteries, Adv. Energy Mater. (2024) 2401090.
[201] A. Sarkar, L. Velasco, D. Wang, Q. Wang, G. Talasila, L. De Biasi, C. Kübel, T. Brezesinski, S.S. Bhattacharya, H. Hahn, B. Breitung, High entropy oxides for reversible energy storage, Nat. Commun. 9 (2018) 3400.
[202] L. Feng, W.G. Fahrenholtz, G.E. Hilmas, Two-step synthesis process for high-entropy diboride powders, J. Am. Ceram. Soc. 103 (2020) 724–730.
[203] Y. Zhang, W.-M. Guo, Z.-B. Jiang, Q.-Q. Zhu, S.-K. Sun, Y. You, K. Plucknett, H.-T. Lin, Dense high-entropy boride ceramics with ultra-high hardness, Scr. Mater. 164 (2019) 135–139.
[204] T.J. Harrington, J. Gild, P. Sarker, C. Toher, C.M. Rost, O.F. Dippo, C. McElfresh, K. Kaufmann, E. Marin, L. Borowski, P.E. Hopkins, J. Luo, S. Curtarolo, D. W. Brenner, K.S. Vecchio, Phase stability and mechanical properties of novel high entropy transition metal carbides, Acta Mater 166 (2019) 271–280.
[205] L. Feng, W.G. Fahrenholtz, G.E. Hilmas, Low-temperature sintering of single-phase, high-entropy carbide ceramics, J. Am. Ceram. Soc. 102 (2019) 7217–7224.
[206] E. Lewin, Multi-component and high-entropy nitride coatings—A promising field in need of a novel approach, J. Appl. Phys. 127 (2020) 160901.
[207] A. Kretschmer, D. Holec, K. Yalamanchili, H. Rudigier, M. Hans, J.M. Schneider, P.H. Mayrhofer, Strain-stabilized Al-containing high-entropy sublattice nitrides, Acta Mater 224 (2022) 117483.
[208] L. Lin, K. Wang, A. Sarkar, C. Njel, G. Karkera, Q. Wang, R. Azmi, M. Fichtner, H. Hahn, S. Schweidler, B. Breitung, High-Entropy Sulfides as Electrode Materials for Li-Ion Batteries, Adv. Energy Mater. 12 (2022) 2103090.
[209] Y. Ma, Y. Hu, Y. Pramudya, T. Diemant, Q. Wang, D. Goonetilleke, Y. Tang, B. Zhou, H. Hahn, W. Wenzel, M. Fichtner, Y. Ma, B. Breitung, T. Brezesinski, Resolving the Role of Configurational Entropy in Improving Cycling Performance of Multicomponent Hexacyanoferrate Cathodes for Sodium-Ion Batteries, Adv. Funct. Mater. 32 (2022) 2202372.
[210] Z.-Y. Gu, J.-Z. Guo, J.-M. Cao, X.-T. Wang, X.-X. Zhao, X.-Y. Zheng, W.-H. Li, Z.-H. Sun, H.-J. Liang, X.-L. Wu, An Advanced High-Entropy Fluorophosphate Cathode for Sodium-Ion Batteries with Increased Working Voltage and Energy Density, Adv. Mater. 34 (2022) 2110108.
[211] Y. Ma, T. Brezesinski, B. Breitung, Y. Ma, High-entropy hexacyanoferrates as robust cathode active materials for sodium storage, Matter 6 (2023) 313–315.
[212] J. Hu, L. Cao, Z. Wang, J. Liu, J. Zhang, Y. Cao, Z. Lu, H. Cheng, Hollow high-entropy metal organic framework derived nanocomposite as efficient electrocatalyst for oxygen reduction reaction, Compos. Commun. 27 (2021) 100866.
[213] X. Li, Z. Qiang, G. Han, S. Guan, Y. Zhao, S. Lou, Y. Zhu, Enhanced Redox Electrocatalysis in High-Entropy Perovskite Fluorides by Tailoring d–p Hybridization, Nano-Micro Lett. 16 (2024) 55.
[214] Y. Yao, Q. Dong, A. Brozena, J. Luo, J. Miao, M. Chi, C. Wang, I.G. Kevrekidis, Z. J. Ren, J. Greeley, G. Wang, A. Anapolsky, L. Hu, High-entropy nanoparticles: Synthesis-structure-property relationships and data-driven discovery, Science 376 (2022) eabn3103.
[215] W.-L. Hsu, C.-W. Tsai, A.-C. Yeh, J.-W. Yeh, Clarifying the four core effects of high-entropy materials, Nat. Rev. Chem. 8 (2024) 471–485.
[216] Y. Chen, H. Fu, Y. Huang, L. Huang, X. Zheng, Y. Dai, Y. Huang, W. Luo, Opportunities for High-Entropy Materials in Rechargeable Batteries, ACS Mater. Lett. 3 (2021) 160–170.
[217] A. Roy, J. Munshi, G. Balasubramanian, Low energy atomic traps sluggardize the diffusion in compositionally complex refractory alloys, Intermetallics 131 (2021) 107106.
[218] L. Liu, Y. Zhang, J. Han, X. Wang, W. Jiang, C. Liu, Z. Zhang, P.K. Liaw, Nanoprecipitate-Strengthened High-Entropy Alloys, Adv. Sci. 8 (2021) 2100870.
[219] J. Song, F. Ning, Y. Zuo, A. Li, H. Wang, K. Zhang, T. Yang, Y. Yang, C. Gao, W. Xiao, Z. Jiang, T. Chen, G. Feng, D. Xia, Entropy Stabilization Strategy for

Enhancing the Local Structural Adaptability of Li-Rich Cathode Materials, Adv. Mater. 35 (2023) 2208726.
[220] R. Zhang, C. Wang, P. Zou, R. Lin, L. Ma, T. Li, I. Hwang, W. Xu, C. Sun, S. Trask, H.L. Xin, Long-life lithium-ion batteries realized by low-Ni, Co-free cathode chemistry, Nat. Energy 8 (2023) 695–702.
[221] L. Liang, M. Su, Z. Sun, L. Wang, L. Hou, H. Liu, Q. Zhang, C. Yuan, High-entropy doping promising ultrahigh-Ni Co-free single-crystalline cathode toward commercializable high-energy lithium-ion batteries, Sci. Adv. 10 (2024) eado4472.
[222] X. Wang, Y. Zuo, Y. Qin, X. Zhu, S. Xu, Y. Guo, T. Yan, L. Zhang, Z. Gao, L. Yu, M. Liu, Y. Yin, Y. Cheng, P. Wang, Y. Guo, Fast Na^+ Kinetics and Suppressed Voltage Hysteresis Enabled by a High-Entropy Strategy for Sodium Oxide Cathodes, Adv. Mater. 36 (2024) 2312300.
[223] H. Xiang, Y. Xing, F. Dai, H. Wang, L. Su, L. Miao, G. Zhang, Y. Wang, X. Qi, L. Yao, H. Wang, B. Zhao, J. Li, Y. Zhou, High-entropy ceramics: Present status, challenges, and a look forward, J. Adv. Ceram. 10 (2021) 385–441.
[224] G. Zeng, B. Liu, U. Ali, Y. Li, H. Jia, M. Sun, Y. Li, Y. Hao, X. Yong, T. Wang, C. Wang, The local disorder induced by high-entropy doping results in highly stable cathode materials for aqueous potassium-ion batteries, Appl. Catal. B Environ. 351 (2024) 123996.
[225] S. Ma, P. Zou, H.L. Xin, Extending phase-variation voltage zones in P2-type sodium cathodes through high-entropy doping for enhanced cycling stability and rate capability, Mater. Today Energy 38 (2023) 101446.
[226] D.A. Anang, J.H Park, D.S. Bhange, M.K. Cho, W.Y. Yoon, K.Y. Chung, K.W. Nam, O3-type layer-structured $Na_{0.8}[Ni_{1/5}Fe_{1/5}Co_{1/5}Mn_{1/5}Ti_{1/5}]O_2$ as long life and high power cathode material for sodium-ion batteries, Ceram. Int. 45 (2019) 23164.
[227] L. Yao, P. Zou, C. Wang, J. Jiang, L. Ma, S. Tan, K.A. Beyer, F. Xu, E. Hu, H.L. Xin, High-Entropy and Superstructure-Stabilized Layered Oxide Cathodes for Sodium-Ion Batteries, Adv. Energy Mater. 12 (2022) 2201989.
[228] H. Wang, X. Gao, S. Zhang, Y. Mei, L. Ni, J. Gao, H. Liu, N. Hong, B. Zhang, F. Zhu, W. Deng, G. Zou, H. Hou, X.-Y. Cao, H. Chen, X. Ji, High-Entropy Na-Deficient Layered Oxides for Sodium-Ion Batteries, ACS Nano 17 (2023) 12530–12543.
[229] L. Yang, C. Chen, S. Xiong, C. Zheng, P. Liu, Y. Ma, W. Xu, Y. Tang, S.P. Ong, H. Chen, Multiprincipal Component P2-$Na_{0.6}(Ti_{0.2}Mn_{0.2}Co_{0.2}Ni_{0.2}Ru_{0.2})O_2$ as a High-Rate Cathode for Sodium-Ion Batteries, JACS Au 1 (2021) 98–107.
[230] Y. Cai, W. Liu, F. Chang, S. Jin, X. Yang, C. Zhang, L. Bai, T. Masese, Z. Li, Z.-D. Huang, Entropy-Stabilized Layered $K_{0.6}Ni_{0.05}Fe_{0.05}Mg_{0.05}Ti_{0.05}Mn_{0.725}O_2$ as a High-Rate and Stable Cathode for Potassium-Ion Batteries, ACS Appl. Mater. Interfaces 15 (2023) 48277–48286.
[231] Y. Ma, Z. Zhou, T. Brezesinski, Y. Ma, Y. Wu, Stabilizing Layered Cathodes by High-Entropy Doping, Research 7 (2024) 0503.
[232] P. Liang, K. Qi, S. Chen, X. Ding, X. Wu, C. Wu, Y. Zhu, Low-Electronegativity Cationic High-Entropy Doping to Trigger Stable Anion Redox Activity for High-Ni Co-Free Layered Cathodes in Li-Ion Batteries, Angew. Chem. 136 (2024) e202318186.
[233] Y. Wang, R. Xiao, Y.-S. Hu, M. Avdeev, L. Chen, P2-$Na_{0.6}[Cr_{0.6}Ti_{0.4}]O_2$ cation-disordered electrode for high-rate symmetric rechargeable sodium-ion batteries, Nat. Commun. 6 (2015) 6954.
[234] A. Joshi, S. Chakrabarty, S.H. Akella, A. Saha, A. Mukherjee, B. Schmerling, M. Ejgenberg, R. Sharma, M. Noked, High-Entropy Co-Free O3-Type Layered Oxyfluoride: A Promising Air-Stable Cathode for Sodium-Ion Batteries, Adv. Mater. 35 (2023) 2304440.
[235] Z. Liu, R. Liu, S. Xu, J. Tian, J. Li, H. Li, T. Yu, S. Chu, A.M. D'Angelo, W.K. Pang, L. Zhang, S. Guo, H. Zhou, Achieving a Deeply Desodiated Stabilized Cathode Material by the High Entropy Strategy for Sodium-ion Batteries, Angew. Chem. Int. Ed. (2024) e202405620.
[236] F. Ding, H. Wang, Q. Zhang, L. Zheng, H. Guo, P. Yu, N. Zhang, Q. Guo, F. Xie, R. Dang, X. Rong, Y. Lu, R. Xiao, L. Chen, Y.-S. Hu, Tailoring Electronic Structure to Achieve Maximum Utilization of Transition Metal Redox for High-Entropy Na Layered Oxide Cathodes, J. Am. Chem. Soc. 145 (2023) 13592–13602.
[237] Z. Wang, L. Fang, X. Fu, S. Zhang, H. Kong, H. Chen, F. Fu, A Ni/Co-free high-entropy layered cathode with suppressed phase transition and near-zero strain for high-voltage sodium-ion batteries, Chem. Eng. J. 480 (2024) 148130.
[238] Y. Jiang, W. Li, K. Luo, Solid-Solution Reaction and Ultrasmall Volume Change in High-Entropy P2-type Layered Oxide Cathode for All-Climate Sodium-Ion Batteries, ACS Sustainable Chem. Eng. 12 (2024) 8051–8060.
[239] Y.J. Zhao, J.W. Qiao, S.G. Ma, M.C. Gao, H.J. Yang, M.W. Chen, Y. Zhang, A hexagonal close-packed high-entropy alloy: The effect of entropy, Mater. Des. 96 (2016) 10–15.
[240] P.H. Mayrhofer, A. Kirnbauer, Ph. Ertelthaler, C.M. Koller, High-entropy ceramic thin films; A case study on transition metal diborides, Scr. Mater. 149 (2018) 93–97.
[241] H.W. Yao, J.W. Qiao, J.A. Hawk, H.F. Zhou, M.W. Chen, M.C. Gao, Mechanical properties of refractory high-entropy alloys: Experiments and modeling, J. Alloys Compd. 696 (2017) 1139–1150.
[242] A. Sarkar, R. Djenadic, D. Wang, C. Hein, R. Kautenburger, O. Clemens, H. Hahn, Rare earth and transition metal based entropy stabilised perovskite type oxides, J. Eur. Ceram. Soc. 38 (2018) 2318–2327.
[243] Y. Dong, Z. Zhou, Y. Ma, H. Zhang, F. Meng, Y. Wu, Y. Ma, Layered-Structured Sodium-Ion Cathode Materials: Advancements through High-Entropy Approaches, ACS Energy Lett. (2024) 5096–5119.
[244] A.J. Perez, D. Batuk, M. Saubanère, G. Rousse, D. Foix, E. McCalla, E.J. Berg, R. Dugas, K.H.W. Van Den Bos, M.-L. Doublet, D. Gonbeau, A.M. Abakumov, G. Van Tendeloo, J.-M. Tarascon, Strong Oxygen Participation in the Redox Governing the Structural and Electrochemical Properties of Na-Rich Layered Oxide Na_2IrO_3, Chem. Mater. 28 (2016) 8278–8288.
[245] H. Ren, Y. Li, Q. Ni, Y. Bai, H. Zhao, C. Wu, Unraveling Anionic Redox for Sodium Layered Oxide Cathodes: Breakthroughs and Perspectives, Adv. Mater. 34 (2022) 2106171.
[246] A. Gao, S. Shen, T. Shang, Y. Shi, H. Zhang, W. Lin, S. Wang, T. Lin, P. Ji, Y. Wang, Y. Chen, B. Yu, X. Lu, W. Zhong, Q. Zhang, L. Gu, Van der Waals phase transition investigation toward high-voltage layered cathodes, Sci. Adv. 10 (2024) eadp4906.
[247] P. Wang, H. Yao, X. Liu, J. Zhang, L. Gu, X. Yu, Y. Yin, Y. Guo, Ti-Substituted $NaNi_{0.5}Mn_{0.5-x}Ti_xO_2$ Cathodes with Reversible O3−P3 Phase Transition for High-Performance Sodium-Ion Batteries, Adv. Mater. 29 (2017) 1700210.
[248] H.-R. Yao, P.-F. Wang, Y. Gong, J. Zhang, X. Yu, L. Gu, C. OuYang, Y.-X. Yin, E. Hu, X.-Q. Yang, E. Stavitski, Y.-G. Guo, L.-J. Wan, Designing Air-Stable O3-Type Cathode Materials by Combined Structure Modulation for Na-Ion Batteries, J. Am. Chem. Soc. 139 (2017) 8440–8443.
[249] S. Majumder, R. Narasimman, S. Dhuruvan, P. Varatharajan, A. Raj Murugan, S. Sarojiniamma, I. Sinthai Appusamy, Solid-State Synthesis and Characterization of Mg-Substituted P2-$Na_{0.70}Ni_{0.45}Mn_{0.55}O_2$ Cathode Materials for Practical Sodium-Ion Batteries, Adv. Sustainable Syst. 7 (2023) 2200519.
[250] S. Kang, S. Lee, H. Lee, Y.-M. Kang, Manipulating disorder within cathodes of alkali-ion batteries, Nat. Rev. Chem. 8 (2024) 587–604.
[251] J. Maier, Review—Battery Materials: Why Defect Chemistry? J. Electrochem. Soc. 162 (2015) A2380–A2386.
[252] L. Wu, Y. Zhang, Z. Wu, J. Tian, H. Wang, H. Zhao, S. Xu, L. Chen, X. Duan, D. Zhang, H. Guo, Y. You, Z. Zhu, Stabilized O3-Type Layered Sodium Oxides with Enhanced Rate Performance and Cycling Stability by Dual-Site Ti^{4+}/K^+ Substitution, Adv. Sci. 10 (2023) 2304067.
[253] X. Tan, Y. Zhang, S. Xu, P. Yang, T. Liu, D. Mao, J. Qiu, Z. Chen, Z. Lu, F. Pan, W. Chu, High-Entropy Surface Complex Stabilized $LiCoO_2$ Cathode, Adv. Energy Mater. 13 (2023) 2300147.
[254] C. Zhao, C. Wang, X. Liu, I. Hwang, T. Li, X. Zhou, J. Diao, J. Deng, Y. Qin, Z. Yang, G. Wang, W. Xu, C. Sun, L. Wu, W. Cha, I. Robinson, R. Harder, Y. Jiang, T. Bicer, J.-T. Li, W. Lu, L. Li, Y. Liu, S.-G. Sun, G.-L. Xu, K. Amine, Suppressing strain propagation in ultrahigh-Ni cathodes during fast charging via epitaxial entropy-assisted coating, Nat. Energy 9 (2024) 345–356.
[255] Y. Yang, Enhancing the stability of Li-Rich Mn-based oxide cathodes through surface high-entropy strategy, Energy Storage Mater 71 (2024) 103587.
[256] J. Zhao, Regulating anionic redox reversibility in Li-rich layered cathodes via diffusion-induced entropy-assisted surface engineering, Energy Storage Mater 70 (2024) 103550.
[257] Z. Xu, X. Chen, W. Fan, M. Zhan, X. Mu, H. Cao, X. Wang, H. Xue, Z. Gao, Y. Liang, J. Liu, X. Tan, F. Pan, High-Entropy Rock-Salt Surface Layer Stabilizes the Ultrahigh-Ni Single-Crystal Cathode, ACS Nano 18 (2024) 33706.
[258] S. Sun, Y. Bai, High-entropy layer assisting quasi-zero-strain cathodes for P2-$Na_{2/3}Ni_{1/3}Mn_{2/3}O_2$, Appl. Phys. Lett. 124 (2024) 171602.
[259] J. Li, H. Yang, Q. Deng, W. Li, Q. Zhang, Z. Zhang, Y. Chu, C. Yang, Stabilizing Ni-rich Single-crystalline $LiNi_{0.83}Co_{0.07}Mn_{0.10}O_2$ Cathodes using Ce/Gd Co-doped High-entropy Composite Surfaces, Angew. Chem., Int. Ed. 63 (2024) e202318042.
[260] J.-W. Yeh, Recent progress in high-entropy alloys, Ann. Chim. Sci. Mat. 31 (2006) 633–648.
[261] F. Ding, P. Ji, Z. Han, X. Hou, Y. Yang, Z. Hu, Y. Niu, Y. Liu, J. Zhang, X. Rong, Y. Lu, H. Mao, D. Su, L. Chen, Y.-S. Hu, Tailoring planar strain for robust structural stability in high-entropy layered sodium oxide cathode materials, Nat. Energy 9 (2024) 1529.
[262] J. Zhou, J. Hu, X. Zhou, Z. Shang, Y. Yang, S. Xu, High-entropy doping for high-performance zero-cobalt high-nickel layered cathode materials, Energy Environ. Sci. 18 (2025) 347–353.
[263] J. Wang, Y. Cui, Q. Wang, K. Wang, X. Huang, D. Stenzel, A. Sarkar, R. Azmi, T. Bergfeldt, S.S. Bhattacharya, R. Kruk, H. Hahn, S. Schweidler, T. Brezesinski, B. Breitung, Lithium containing layered high entropy oxide structures, Sci. Rep. 10 (2020) 18430.
[264] Q. Zheng, Z. Ren, Y. Zhang, T. Qin, J. Qi, H. Jia, L. Jiang, L. Li, X. Liu, L. Chen, Surface Phase Conversion in a High-Entropy Layered Oxide Cathode Material, ACS Appl. Mater. Interfaces 15 (2023) 4643–4651.
[265] Q. Zheng, Z. Ren, Y. Zhang, X. Liu, J. Ma, L. Li, X. Liu, L. Chen, Surface-Stabilized High-Entropy Layered Oxyfluoride Cathode for Lithium-Ion Batteries, J. Phys. Chem. Lett. 14 (2023) 5553–5559.
[266] J. Sturman, C.-H. Yim, E.A. Baranova, Y. Abu-Lebdeh, Communication—Design of $LiNi_{0.2}Mn_{0.2}Co_{0.2}Fe_{0.2}Ti_{0.2}O_2$ as a High-Entropy Cathode for Lithium-Ion Batteries Guided by Machine Learning, J. Electrochem. Soc. 168 (2021) 050541.
[267] S. Choi, W. Feng, Y. Xia, High Entropy and Co-Free High Nickel Based Layered $LiNi_{0.9}Mn_{0.1}O_2$ Cathode for Li-Ion Batteries, ACS Appl. Energy Mater. 7 (2024) 3339.
[268] K. Walczak, A. Plewa, C. Ghica, W. Zając, A. Trenczek-Zając, M. Zając, J. Toboła, J. Molenda, $NaMn_{0.2}Fe_{0.2}Co_{0.2}Ni_{0.2}Ti_{0.2}O_2$ high-entropy layered oxide – experimental and theoretical evidence of high electrochemical performance in sodium batteries, Energy Storage Mater 47 (2022) 500–514.
[269] C.-C. Lin, H.-Y. Liu, J.-W. Kang, C.-C. Yang, C.-H. Li, H.-Y.T. Chen, S.-C. Huang, C.-S. Ni, Y.-C. Chuang, B.-H. Chen, C.-K. Chang, H.-Y. Chen, In-situ X-ray studies of high-entropy layered oxide cathode for sodium-ion batteries, Energy Storage Mater 51 (2022) 159–171.
[270] Y. Dang, Z. Xu, H. Yang, K. Tian, Z. Wang, R. Zheng, H. Sun, Y. Liu, D. Wang, Designing water/air-stable Co-free high-entropy oxide cathodes with suppressed

irreversible phase transition for sodium-ion batteries, Appl. Surf. Sci. 636 (2023) 157856.
[271] A. Ghosh, R. Hegde, P. Senguttuvan, A high entropy O3-$Na_{1.0}Li_{0.1}Ni_{0.3}Fe_{0.1}Mn_{0.25}Ti_{0.25}O_2$ cathode with reversible phase transitions and superior electrochemical performances for sodium-ion batteries, J. Mater. Chem. A 12 (2024) 14583.
[272] K. Tian, H. He, X. Li, D. Wang, Z. Wang, R. Zheng, H. Sun, Y. Liu, Q. Wang, Boosting electrochemical reaction and suppressing phase transition with a high-entropy O3-type layered oxide for sodium-ion batteries, J. Mater. Chem. A 10 (2022) 14943–14953.
[273] X. Liu, Y. Wan, M. Jia, H. Zhang, W. Xie, H. Hu, X. Yan, X. Zhang, Facilitating the high voltage stability of NFM via transition metal slabs high-entropy configuration strategy, Energy Storage Mater 67 (2024) 103313.
[274] H. Guo, M. Avdeev, K. Sun, X. Ma, H. Wang, Y. Hu, D. Chen, Pentanary transition-metals Na-ion layered oxide cathode with highly reversible O3-P3 phase transition, Chem. Eng. J. 412 (2021) 128704.
[275] X.-Y. Du, Y. Meng, H. Yuan, D. Xiao, High-entropy substitution: A strategy for advanced sodium-ion cathodes with high structural stability and superior mechanical properties, Energy Storage Mater 56 (2023) 132–140.
[276] Z.-Y. Li, Zr-doped P2-$Na_{0.75}Mn_{0.55}Ni_{0.25}Co_{0.05}Fe_{0.10}Zr_{0.05}O_2$ as high-rate performance cathode material for sodium ion batteries, Electrochim. Acta 223 (2017) 92–99.
[277] J. Wang, S.L. Dreyer, K. Wang, Z. Ding, T. Diemant, G. Karkera, Y. Ma, A. Sarkar, B. Zhou, M.V. Gorbunov, A. Omar, D. Mikhailova, V. Presser, M. Fichtner, H. Hahn, T. Brezesinski, B. Breitung, Q. Wang, P2-type layered high-entropy oxides as sodium-ion cathode materials, Mater. Futures 1 (2022) 035104.
[278] P. Zhou, Z. Che, J. Liu, J. Zhou, X. Wu, J. Weng, J. Zhao, H. Cao, J. Zhou, F. Cheng, High-entropy P2/O3 biphasic cathode materials for wide-temperature rechargeable sodium-ion batteries, Energy Storage Mater 57 (2023) 618–627.
[279] R. Li, X. Qin, X. Li, J. Zhu, L. Zheng, Z. Li, W. Zhou, High-Entropy and Multiphase Cathode Materials for Sodium-Ion Batteries, Adv. Energy Mater. 14 (2024).
[280] J. Mu, T. Cai, W. Dong, C. Zhou, Z. Han, F. Huang, Biphasic high-entropy layered oxide as a stable and high-rate cathode for sodium-ion batteries, Chem. Eng. J. 471 (2023) 144403.
[281] S. Chu, C. Shao, J. Tian, J. Wang, Y. Rao, C. Xu, H. Zhou, S. Guo, High Entropy-Induced Kinetics Improvement and Phase Transition Suppression in K-Ion Battery Layered Cathodes, ACS Nano 18 (2024) 337–346.
[282] J. Sturman, C.-H. Yim, E.A. Baranova, Y. Abu-Lebdeh, Communication—Design of $LiNi_{0.2}Mn_{0.2}Co_{0.2}Fe_{0.2}Ti_{0.2}O_2$ as a High-Entropy Cathode for Lithium-Ion Batteries Guided by Machine Learning, J. Electrochem. Soc. 168 (2021) 050541.
[283] B. Zhang, Y. Zhang, X. Wang, H. Liu, Y. Yan, S. Zhou, Y. Tang, G. Zeng, X. Wu, H.-G. Liao, Y. Qiu, H. Huang, L. Zheng, J. Xu, W. Yin, Z. Huang, Y. Xiao, Q. Xie, D.-L. Peng, C. Li, Y. Qiao, S.-G. Sun, Role of Substitution Elements in Enhancing the Structural Stability of Li-Rich Layered Cathodes, J. Am. Chem. Soc. 145 (2023) 8700–8713.
[284] G.-T. Park, B. Namkoong, S.-B. Kim, J. Liu, C.S. Yoon, Y.-K. Sun, Introducing high-valence elements into cobalt-free layered cathodes for practical lithium-ion batteries, Nat. Energy 7 (2022) 946–954.
[285] W. Li, Q. Chen, D. Zhang, C. Fang, S. Nian, W. Wang, C. Xu, C. Chang, High stability of Mo-F dual-doped O3-type $NaNi_{1/3}Fe_{1/3}Mn_{1/3}O_2$ cathode material for sodium-ion battery, Mater. Today Commun. 32 (2022) 103839.
[286] G.-T. Park, D.R. Yoon, U.-H. Kim, B. Namkoong, J. Lee, M.M. Wang, A.C. Lee, X. W. Gu, W.C. Chueh, C.S. Yoon, Y.-K. Sun, Ultrafine-grained Ni-rich layered cathode for advanced Li-ion batteries, Energy Environ. Sci. 14 (2021) 6616–6626.
[287] U.-H. Kim, D.-W. Jun, K.-J. Park, Q. Zhang, P. Kaghazchi, D. Aurbach, D.T. Major, G. Goobes, M. Dixit, N. Leifer, C.M. Wang, P. Yan, D. Ahn, K.-H. Kim, C.S. Yoon, Y.-K. Sun, Pushing the limit of layered transition metal oxide cathodes for high-energy density rechargeable Li ion batteries, Energy Environ. Sci. 11 (2018) 1271–1279.
[288] W. Wang, Y. Sun, P. Wen, Y. Zhou, D. Zhang, Enhanced conduction and phase transition reversibility of O3-type $NaNi_{1/3}Fe_{1/3}Mn_{1/3}O_2$ cathode via Ta doping for high-performance sodium-ion battery, J. Energy Storage 79 (2024) 110177.
[289] U.-H. Kim, G.-T. Park, B.-K. Son, G.W. Nam, J. Liu, L.-Y. Kuo, P. Kaghazchi, C. S. Yoon, Y.-K. Sun, Heuristic solution for achieving long-term cycle stability for Ni-rich layered cathodes at full depth of discharge, Nat. Energy 5 (2020) 860–869.
[290] T. Yuan, S. Li, Y. Sun, J.-H. Wang, A.-J. Chen, Q. Zheng, Y. Zhang, L. Chen, G. Nam, H. Che, J. Yang, S. Zheng, Z.-F. Ma, M. Liu, A. High-Rate, Durable Cathode for Sodium-Ion Batteries: Sb-Doped O3-Type Ni/Mn-Based Layered Oxides, ACS Nano 16 (2022) 18058–18070.
[291] L. Zhu, J. Tian, H. Miao, Y. Liu, Tailored synthesis and characterization of Zr-doped $NaNi_{1/3}Fe_{1/3}Mn_{1/3}O_2$ cathode materials for advanced energy storage, Materials Today Communications 40 (2024) 109552.
[292] Z. Lun, B. Ouyang, D.-H. Kwon, Y. Ha, E.E. Foley, T.-Y. Huang, Z. Cai, H. Kim, M. Balasubramanian, Y. Sun, J. Huang, Y. Tian, H. Kim, B.D. McCloskey, W. Yang, R.J. Clément, H. Ji, G. Ceder, Cation-disordered rocksalt-type high-entropy cathodes for Li-ion batteries, Nat. Mater. 20 (2021) 214–221.
[293] J. Fish, Mesoscopic and multiscale modelling in materials, Nat. Mater. 20 (2021) 774–786.
[294] K.T. Butler, Machine learning for molecular and materials science, Nature 559 (2018) 547–555.
[295] A. Jain, S.P. Ong, G. Hautier, W. Chen, W.D. Richards, S. Dacek, S. Cholia, D. Gunter, D. Skinner, G. Ceder, K.A. Persson, Commentary: The Materials Project: A materials genome approach to accelerating materials innovation, APL Mater 1 (2013) 011002.
[296] D. Xue, P.V. Balachandran, J. Hogden, J. Theiler, D. Xue, T. Lookman, Accelerated search for materials with targeted properties by adaptive design, Nat. commun. 7 (2016) 1–9.
[297] R. Feng, First-principles prediction of high-entropy-alloy stability, Npj Comput. Mater. 3 (2017) 50.
[298] M. de Jong, W. Chen, T. Angsten, A. Jain, R. Notestine, A. Gamst, M. Sluiter, C. K. Ande, J.J. Plata, C. Toher, S. Curtarolo, G. Ceder, K.A. Persson, M. Asta, Charting the complete elastic properties of inorganic crystalline compounds, Scientific data 2 (2015) 1–13.
[299] Y. Yao, Z. Huang, P. Xie, S.D. Lacey, R.J. Jacob, H. Xie, F. Chen, A. Nie, T. Pu, M. Rehwoldt, D. Yu, M.R. Zachariah, C. Wang, R. Shahbazian-Yassar, J. Li, L. Hu, Carbothermal shock synthesis of high-entropy-alloy nanoparticles, Science 359 (2018) 1489–1494.
[300] A. Abdelhafiz, B. Wang, A.R. Harutyunyan, J. Li, Carbothermal Shock Synthesis of High Entropy Oxide Catalysts: Dynamic Structural and Chemical Reconstruction Boosting the Catalytic Activity and Stability toward Oxygen Evolution Reaction, Adv. Energy Mater. 12 (2022) 2200742.
[301] H. Wu, Q. Lu, Y. Li, J. Wang, Y. Li, R. Jiang, J. Zhang, X. Zheng, X. Han, N. Zhao, J. Li, Y. Deng, W. Hu, Rapid Joule-Heating Synthesis for Manufacturing High-Entropy Oxides as Efficient Electrocatalysts, Nano Lett. 22 (2022) 6492–6500.
[302] T. Li, Y. Yao, Z. Huang, P. Xie, Z. Liu, M. Yang, J. Gao, K. Zeng, A.H. Brozena, G. Pastel, M. Jiao, Q. Dong, J. Dai, S. Li, H. Zong, M. Chi, J. Luo, Y. Mo, G. Wang, C. Wang, R. Shahbazian-Yassar, L. Hu, Denary oxide nanoparticles as highly stable catalysts for methane combustion, Nat. Catal. 4 (2021) 62–70.
[303] Y. Feng, L. Yang, Z. Yan, D. Zuo, Z. Zhu, L. Zeng, Y. Zhu, J. Wan, Discovery of high entropy garnet solid-state electrolytes via ultrafast synthesis, Energy Storage Mater 63 (2023) 103053.
[304] M. Vaidya, G.M. Muralikrishna, B.S. Murty, High-entropy alloys by mechanical alloying: A review, J. Mater. Res. 34 (2019) 664–686.
[305] W. Bao, H. Shen, Y. Zhang, C. Qian, G. Zeng, K. Jing, D. Cui, J. Xia, H. Liu, C. Guo, F. Yu, K. Sun, J. Li, High-entropy oxides for energy storage and conversion, J. Mater. Chem. A 12 (2024) 23179–23201.
[306] Y. Zheng, Y. Meng, X. Hu, H. Peng, L. Feng, Y. Wang, B. Li, Synthesis-Structure-Property of High-Entropy Layered Oxide Cathode for Li/Na/K-Ion Batteries, Adv. Mater. 37 (2025) 2413202.
[307] X. Liu, W. Zuo, B. Zheng, Y. Xiang, K. Zhou, Z. Xiao, P. Shan, J. Shi, Q. Li, G. Zhong, R. Fu, Y. Yang, P2-$Na_{0.67}Al_xMn_{1-x}O_2$: Cost-Effective, Stable and High-Rate Sodium Electrodes by Suppressing Phase Transitions and Enhancing Sodium Cation Mobility, Angew. Chem. Int. Ed. 58 (2019) 18086–18095.
[308] B. Cao, T. Li, W. Zhao, L. Yin, H. Cao, D. Chen, L. Li, F. Pan, M. Zhang, Correlating Rate-Dependent Transition Metal Dissolution between Structure Degradation in Li-Rich Layered Oxides, Small 19 (2023) 2301834.
[309] Y. Yao, Q. Dong, A. Brozena, J. Luo, J. Miao, M. Chi, C. Wang, I.G. Kevrekidis, Z. J. Ren, J. Greeley, G. Wang, A. Anapolsky, L. Hu, High-entropy nanoparticles: Synthesis-structure-property relationships and data-driven discovery, Science 376 (2022) 6589.
[310] M. Aykol, S. Kim, V.I. Hegde, D. Snydacker, Z. Lu, S. Hao, S. Kirklin, D. Morgan, C. Wolverton, High-throughput computational design of cathode coatings for Li-ion batteries, Nat. Commun. 7 (2016) 13779.
[311] R. Machaka, Machine learning-based prediction of phases in high-entropy alloys, Computational Materials Science 188 (2021) 110244.
[312] T. Zuo, M.C. Gao, L. Ouyang, X. Yang, Y. Cheng, R. Feng, S. Chen, P.K. Liaw, J. A. Hawk, Y. Zhang, Tailoring magnetic behavior of CoFeMnNi$_x$ (x = Al, Cr, Ga, and Sn) high entropy alloys by metal doping, Acta Materialia 130 (2017) 10–18.